DEFECT LOCATION IN STRUCTURES BY A VIBRATION
TECHNIQUE

by

Peter Cawley

CONTENTSPage

Memorandum   (i)

Acknowledgments   (ii)

Summary   (iii)

List of Tables   (v)

List of Figures   (vi)

Nomenclature   (viii)

CHAPTER 1   INTRODUCTION   1

    1.1   The role of non-destructive testing   1

    1.2   Existing NDT techniques   2

    1.3   The use of vibration response measurements in NDT   3

    1.4   The location of defects within a structure using
           vibration measurements   4

    1.5   Research programme   6

CHAPTER 2   DYNAMIC ANALYSIS AND THEORY OF DAMAGE LOCATION   8

    2.1   The dynamic analysis   8

    2.1.1 The choice of element   8

    2.1.2 The formation of the element stiffness and mass matrices   9

    2.1.3 The eigenvalue solution system   11

    2.1.4 The solution of free-free problems   13

    2.2   The method of damage location   14

    2.3   The use of sensitivity analysis   14

    2.4   Presentation of the results of the location scheme   17

    2.5   The problem of directional damage   18

    2.6   The problem of erroneous frequency measurements   20

    2.7   The estimation of the magnitude of the damage   21

    2.8   The final location scheme   21

CHAPTER 3   PRINCIPLES OF THE EXPERIMENTAL DETERMINATION OF THE   22
             STRUCTURAL NATURAL FREQUENCIES

    3.1   Requirements   22

    3.2   Steady-state methods   22

    3.3   The transient method   23

    3.3.1 Introduction   23

    3.3.2 Theoretical background   25

    3.3.3 The choice of error function   26

    3.3.4 The expected accuracy of the method   27

MEMORANDUM

The accompanying dissertation entitled "Defect location in structures by a vibration technique" is submitted in support of an application for the Degree of Doctor of Philosophy at the University of Bristol.

Except where indicated in the text by reference to other work, the content of this dissertation is original. The supervisor's contribution was that normally made in a British university. None of the work described has been, or is being, submitted for any other degree or diploma to this or any other university.

The work has formed the basis of the following papers:

"The predicted and experimental natural modes of free-free CFRP plates", J. Composite Materials, 1978.

"The location of defects in structures by a vibration technique", accepted for publication in J. Strain Analysis.

"A vibration technique for non-destructive testing of fibre composite structures". Submitted for publication.

"Improved frequency resolution from transient tests with short record lengths". Submitted for publication

"Defect location in structures by a vibration technique". Submitted for 1979 ASME Vibrations Conference.

P. Cawley
November 1978

(ii)

ACKNOWLEDGMENTS

I would like to thank Dr. Bob Adams for his guidance and encouragement throughout this research work. I am indebted to Mr. John Skinner for the manufacture of the carbon fibre reinforced plastic plates and to the staff of the University Computer Centre for their assistance in guiding my programs through the vagaries of the South West Universities Computer Network. I also gratefully acknowledge the assistance of the academic and technical staff of the Faculty of Engineering. Finally, I would like to thank Miss Barbara Tremlin for typing this thesis.

SUMMARY

A vibration technique for non-destructively assessing the integrity of structures has been described. The method uses measurements of changes in the lower structural natural frequencies, which can be made at a single point in the structure, in conjunction with a dynamic analysis of the system to detect, locate and roughly to quantify damage. It has been shown that the mathematical model of the structure need not be sophisticated and only one full analysis is required for each type of structure to be tested.

The dynamic analysis was carried out using the finite element method as this is applicable to all structures. The dynamic finite element program written for this work has been described and the natural frequency and nodal pattern predictions made using this program have been compared with experimental results from an aluminium plate and from carbon fibre reinforced plastic plates with a variety of ply orientations. Excellent agreement was shown between the theoretical and experimental results.

A program has been developed which enables the location of the damage site and the estimation of the severity of the damage from the results of the dynamic analysis and the measured changes in the structural natural frequencies. The computational requirements of the location routine are small and the program could readily be adapted to run on a micro-computer.

The measurement of natural frequencies from the Fourier transform of the structural response to an impulse has been investigated and a method for improving the frequency resolution obtained from this type of test developed. Preliminary tests have shown that it is possible to obtain frequency resolution of one-tenth of the spacing between the frequency points produced by the Fourier transform at a low cost in terms of computer time and store. The results indicate that this technique would be the most suitable method of frequency measurement for the proposed non-destructive test since it combines accuracy with a short test time. However, because of the unreliability of the available transient recording equipment, the main test programme was carried out using steady-state frequency measurement.

Results have been presented from tests of the non-destructive testing technique on an aluminium plate and a variety of carbon fibre reinforced plastic structures, including two honeycomb panels obtained from the aerospace industry. Five different forms of damage have been used and it has

been shown that the method can successfully be used to detect and locate each type of damage.

LIST OF TABLES

LIST OF FIGURES

(vii)

NOMENCLATURE

a	plate side length
A	area of damage
b	$1 - \nu_{xy}^2 \, E_y/E_x$
B	matrix of derivatives of element shape functions
c	damping ratio = proportion of critical damping = $\xi/2\sqrt{km}$
C	inverse of elasticity matrix, i.e. matrix relating strain to stress
D	elasticity matrix, i.e. matrix relating stress to strain
D*	elasticity matrix for damaged volume
D^e	mean elasticity matrix for layered material
e	error
E	total normalised error in location routine
E	error function in transient test technique
E_x	longitudinal Young's modulus
E_y	transverse Young's modulus
f	natural frequency
F	Fourier transform
g	function
G_{xy}	longitudinal shear modulus
G_{yz}	transverse shear modulus
h_k	z co-ordinate of top of kth layer of layered material
i	$\sqrt{-1}$
k	spring stiffness
K	global stiffness matrix
K^e	element stiffness matrix
ℓ	function
L	lower triangular matrix formed by Choleski decomposition of K
m	mass
M	global mass matrix
M^e	element mass matrix
n	number of points used in computation of Fourier transform
N	matrix of element shape functions
P	magnitude of response function
$\underline{r}$	position vector
$s_{\underline{r}i}$	sensitivity of mode i to damage at $\underline{r}$
S	strain energy
t	thickness

T	sample time
u	$\omega_n(1 - c^2)^{\frac{1}{2}}$
U	kinetic energy
V	volume
W	weighting factor
$\underline{x}$	mode shape vector
$x_1, x_2 \ldots x_n$	elements of mode shape vector
$\left.\begin{array}{c} x \\ y \\ z \end{array}\right\}$	Cartesian co-ordinates
α	constant
γ	shear strain
δX	small change in quantity X
$\underline{\varepsilon}$	strain vector
λ	ω^2
μ	$1/\omega^2$
ν	$c\omega_n$
ν_{xy}	major Poisson's ratio
ν_{yz}	transverse Poisson's ratio
ξ	damping coefficient
ρ	density
$\underline{\sigma}$	stress vector
τ	shear stress
ϕ	amplitude factor
χ_1, χ_2, χ_3	noise levels
ψ	natural frequency parameter
ω	frequency
ω_n	natural frequency of structure
ω_p	natural frequency of single degree of freedom model

Subscripts

exp	experimental
i,j	modes i, j respectively
k	layer number
min	minimum
$\underline{r}$	position given by vector $\underline{r}$
theor	theoretical
$\left.\begin{array}{c} x \\ y \\ z \end{array}\right\}$	co-ordinate directions

- 1 -

CHAPTER 1

INTRODUCTION

1.1 The role of non-destructive testing

Engineering designs are limited by the quality of the available materials. In situations where failure in service could have grave social or economic consequences, the quality of the material used assumes a major importance. This is particularly true where the need for higher working stresses leads to the adoption of stronger but more brittle materials, which are usually more sensitive to the presence of any flaws. To ensure reliability, it has become essential to include non-destructive examination of the material quality in many production procedures.

Improved understanding of the mechanisms of flaw propagation has made it possible to predict the effect of a given defect on structural performance. If non-destructive testing (NDT) methods can reliably be used to locate defects before they are sufficiently severe to propagate catastrophically, it is possible to design structures on the assumption that they will be subject to periodical in-service inspections. This philosophy is incorporated into the design of most modern aircraft, the design criterion being that a component must remain serviceable for at least one interval between inspections with a defect just large enough to be detected by the NDT technique which is to be used. Considerable savings in weight, with consequent improvements in the economy of operation, are therefore achieved without sacrificing reliability. Similarly, the escalating cost of replacement has encouraged the use of in-service inspection techniques in many industries in an attempt to ensure that the maximum useful component life is obtained.

High-performance glass and carbon fibre reinforced plastics (GFRP and CFRP) using epoxy resin matrices are selected for applications which exploit their specific strength and directional properties and where the use of expensive materials is economically justified. The need for reliable defect identification is greater with composites than with many metals because composites can only be inspected after moulding which corresponds to virtually a finished metal part. Rejection at this stage is particularly costly since the materials cannot be recycled. High material costs also mean that premature replacement of components in service can produce very significant increases in life cycle costs.

1.2 Existing NDT techniques

The potential benefits from non-destructive testing, both before and during service, can only be fully realised if quick and reliable testing methods are available. Recent years have seen the advent of many new NDT techniques without the appearance of any universally applicable method.

X-radiography is probably the most widely used NDT technique. It has been used successfully in many industries and has the advantage that an overall inspection can rapidly be made with the structure *in situ*. Areas of particular interest may then be examined in detail using X-ray microscopy or other NDT techniques. However, in common with the other radiographic methods using gamma ray or neutron sources, X-radiography suffers from serious health hazards and expensive safety precautions must be taken when these methods are used.

Ultrasonic inspection has also found extensive application and can be used successfully to locate a wide variety of defects. This method suffers from the disadvantage that the component under inspection must be investigated in a piecewise manner. With the C-scan system, this process has been automated to produce a map of the area scanned with regions of defective material being indicated by one of a range of shades of grey, but the test still takes a considerable time and cannot usually be performed with the structure *in situ*.

Dye penetrants have been widely used but are subject to the limitation that the damage must be open to the surface, which itself must be relatively smooth and uncontaminated. Testing can also take a considerable time.

The above methods have all been used extensively with composite materials. In contrast, eddy current testing which has been very successful with some metal components has not been generally applied to composites, though it might be possible to use it with CFRP in spite of the fact that the conducting phase, the fibres, are embedded in an insulating matrix. Again, however, this technique suffers from the disadvantage that piecewise inspection is required.

Among the "new" NDT techniques being investigated are several thermal methods using temperature sensitive coatings or infra-red scanning to examine defects in laminates heated from the reverse side or to locate hot spots during fatigue loading or large amplitude vibration. These techniques are applicable to laminates with low thermal conductivity but problems must be expected with many metals since the surface temperature

would tend to equalise. Several holographic techniques have been developed but these tend to be difficult to set up and generally require a vibration-free environment.

Although not strictly a non-destructive test, a considerable amount of work has been done on stress wave (or acoustic) emission. Stress waves are generated both by highly localised areas of plastic deformation and by microscopic or macroscopic crack growth; they are usually detected by a piezoelectric crystal. This method can only be used to detect damage when it is actually propagating and the results are readily confused by the presence of other noise sources. For these reasons, the technique finds application mainly in the laboratory and in proof testing procedures.

There is no currently available test which dispenses with the need for piecewise examination of the whole structure, which can be performed *in situ* and does not involve serious health risks. If such a test could be developed and combined reliability with ease of operation, it would be applicable to a wide range of industries.

1.3 The use of vibration response measurements in NDT

Adams et al.[1,2] found that damage in specimens fabricated from fibre reinforced plastics could be detected by a reduction in stiffness and an increase in damping, whether this damage were localised, as in a crack, or distributed through the bulk of the specimen as many microcracks. This change in stiffness resulted in a decrease in the natural frequencies of the specimen. Similar findings are also reported in References 3-5.

Measurements of the dynamic characteristics, that is the natural frequencies and damping, of a structure is potentially a very attractive form of non-destructive test since these properties can be measured at a single point of the structure and are independent of the position chosen. A test based on these measurements would therefore not require access to the whole of the structure and would not involve time-consuming scanning of the whole surface. The test could also potentially be carried out *in situ* and the time required to take the measurements would be small, particularly if a transient test technique[6,7] were employed.

There have been several reports[8-10] concerning the use of measurements of the natural frequencies and damping of components as a means of quality control. The use of natural frequency measurements as a pre-service non-destructive evaluation tool is possible where there are large numbers of the same component produced to good dimensional accuracy, any

components whose natural frequencies fall outside a given band being
rejected.   Structural damping is not so dependent on the precise
dimensions of the object but is more difficult to measure accurately.
Measurements of either natural frequencies or damping could be used as an
in-service test, changes in these properties at different stages of the
life of the component being related to structural degradation.

1.4   The location of damage within a structure using vibration measurements

The stress distribution through a vibrating structure is non-uniform
and is different for each natural frequency (mode).   This means that any
localised damage would affect each mode differently, depending on the
particular location of the damage.   The damage may be modelled as a local
decrease in the stiffness of the structure so, if it is situated at a
point of zero stress in a given mode, it will have no effect on the
natural frequency of that mode.   On the other hand, if it is at a point
of maximum stress, it will have the greatest effect.

Consider, for example, the first three axial modes of a uniform,
free-free bar, whose stress distributions are sketched in Fig. 1.   Damage
at the middle of the bar would have a negligible effect on the second mode
but would induce a maximum change in the natural frequencies of the first
and third modes.   However, if the damage were situated at site A, it
would have a smaller effect on the first and third modes but would cause a
relatively large change in the second mode frequency.   It would therefore
be possible to use measurements of the changes in the natural frequencies
of the bar to locate the position of the damage.   Changes in damping
could be used in exactly the same manner for locating defects.

Owing to symmetry, damage at site B would have an identical effect to
damage at site A so the two sites could not be distinguished by this simple
test.   If, however, the bar were asymmetrical due to, for example, the
addition of a mass at one end, it would be possible to define the damage
site uniquely.   Again, the test could be used as a pre-service quality
control procedure or for in-service inspection.   However, since the
location of damage is dependent on comparing small changes in the dynamic
characteristics of the structure in different modes rather than merely
observing the changes, as is the case with the simple detection of the
presence of damage, the test is probably more suited to in-service
inspection where changes can be related to previous measurements on the
same component.

The location of the damage site requires the computation of the
relative effect on several modes of damage at different sites within the

structure. The experimentally measured changes may then be compared with the theoretically calculated changes for damage at different sites and the position of the damage deduced. If natural frequency measurements are to be carried out, the effect of damage may be determined by modelling the damage as a local decrease in the stiffness of the structure and carrying out a dynamic analysis of the system. Since the effect of damage is dependent on the stress distribution, which is in turn dependent on the mode shapes, the requirement of the dynamic analysis is that a reasonable approximation to the mode shapes be obtained.

The frequency measurement principle has been successfully tested on structures which could be treated as one-dimensional and which were therefore capable of solution by closed-form analytical techniques.[11,12] It was found to be possible to detect damage equivalent to the removal of one per cent of the cross-sectional area of the structure at a single location from measurements of the lower axial or torsional natural frequencies. Excellent agreement was also obtained between the predicted and actual damage sites.

Loland et al.[13-16] have applied the principle to off-shore oil rigs using measurements of the natural frequencies of the framework obtained from the Fourier transform of the structural response to wave excitation. Their analysis did not attempt to locate the position of damage within a structural member but merely to predict whether a given member was fractured.

The Central Electricity Generating Board[17] have used measurements of the changes in the flexural natural frequencies of turbine rotors to locate the position of transverse cracks in rotors which were suspected to be damaged because of unusually high levels of vibration during the running of the turbine. The natural frequency measurements were carried out with the rotor removed from the machine and supported on flexible slings. The location of the position of the crack was approached in a different manner to that used in References 11-16. The effect of a transverse crack at various axial positions on the first four flexural natural frequencies of the rotor was derived in terms of the stress intensity factor for a circum-ferentially notched bar and the mode shapes of the undamaged rotor. The mode shapes were determined experimentally. Since the results of References 11 and 12 indicated that the effect of damage at a point of the structure may be found to sufficient accuracy with a fairly unsophisticated analysis and without the need to measure the mode shapes, the approach adopted there[11,12] was followed in this investigation.

This dissertation describes the extension of the method of References 11 and 12 to two-dimensional and, potentially, to three-dimensional structures. The analysis of the one-dimensional structures described in References 11 and 12 was carried out using receptance techniques.[18] There is no two-dimensional equivalent of receptance techniques, so another method had to be used. Finite element analysis was chosen as it is well documented,[19] accurate, and can be used to analyse any structure. The method developed here is therefore applicable to all structures and the proposed technique can be used with any type of structural vibration, that is torsional, axial, flexural or combinations of these. When testing one-dimensional structures, it was convenient to use axial or torsional modes, but this is not practicable with shell-type structures so the results presented here were obtained using flexural vibration.

Earlier work in the department[20,21] had been concerned with high-performance composite materials and this investigation was initially designed to develop a non-destructive test for structures fabricated from fibre reinforced materials. Accordingly, most of the tests have been carried out on composite structures. However, the method is equally applicable to metal structures. Indeed, the natural frequencies of metal components can usually be found to greater accuracy than those of composite structures, so the method would be more sensitive with metals.

At this stage, no attempt was made to apply the method to structures *in situ* since this would have added unnecessary complications to this initial investigation of the technique. There is, however, no reason why the test should not be applied to structures *in situ*, provided that the boundary conditions applied to the structure do not vary significantly between successive sets of measurements.

Structural damping was not monitored in the tests described here, though the results of References 1-5 indicate that the damping would increase with damage. It was felt that changes in dynamic stiffness would be easier to measure than the associated changes in damping.

1.5 Research programme

The main object of the work was to develop the non-destructive test described in References 11 and 12 for use with multi-dimensional structures.

The major theoretical aspects of the programme involved the development of a dynamic finite element program and the production of a routine for the location of damage from measured frequency changes. It was

decided to write a dynamic finite element program rather than to modify an existing program because, at the start of the work, it was not clear how much the basic program would have to be amended for the purposes of the damage location routine and it is often difficult to carry out major alterations on programs written in other contexts.

The transient method for measuring structural natural frequencies described by, for example, White[6,7] was to be investigated as a possible alternative to the conventional steady state techniques. Having developed a method for the experimental determination of structural natural frequencies, the frequency and mode shape predictions made using the finite element program were to be compared with experimental results.

The feasibility of the non-destructive testing technique and the accuracy of the damage location routine with different forms of damage were then to be investigated on a variety of shell-type structures including two obtained from the aerospace industry.

CHAPTER 2

DYNAMIC ANALYSIS AND THEORY OF DAMAGE LOCATION

2.1 The dynamic analysis

2.1.1 The choice of element

The requirements for the element to be used in this work were that it should be capable of the analysis of shell-type structures fabricated from composite materials and that it should be able to accommodate irregularly shaped boundaries without the need to use large numbers of elements which would be costly in terms of computer time and store.

The element chosen was the 8-node, 40 degree of freedom configuration described by Zienkiewicz et al.[22,23] The element is formulated from the equations of three-dimensional elasticity, making the assumption that the stress normal to the mid-plane is zero. This means that the problems[19] with element conformity normally associated with elements derived using standard plate theory are avoided. The element can accommodate irregularly shaped boundaries and may be deformed to represent a curved shell structure by means of readily implemented co-ordinate transformations.

Five degrees of freedom, three displacements of the middle plane and two rotations of the normal about axes parallel to the middle plane are retained at each node. The retention of the two rotations as independent variables means that the formulation retains the assumption that plane sections remain plane but does not make the Kirchoff assumption that normals to the middle surface remain normal. Transverse shear deformation, which can be significant with highly anisotropic materials at much higher length to thickness ratios than with isotropic materials,[24] is therefore allowed for in a manner similar to that of Mindlin.[25] Sun and Whitney[26] have shown that this approach gives accurate results for the lower flexural modes of vibration with laminates of, for example, CFRP where the transverse shear moduli do not vary drastically from layer to layer.

These factors meant that the element appeared to be ideal for the proposed work and all the results presented here have been computed using this element. None of the analysis for the location of damage, however, is specifically dependent on this particular element, but can be applied to any, suitable, type of element.

2.1.2 The formation of the element stiffness and mass matrices

The element stiffness matrix, K^e, is computed from the matrix of the derivatives of the element shape functions, B, and the elasticity matrix, D, according to the equation, [19]

$$K^e = \int_V B^T \, D \, B \, dV \tag{1}$$

The elasticity matrix is derived from the relations of three-dimensional elasticity by setting the stress normal to the mid-plane equal to zero. This is a reasonable assumption to make in shell situations since the stress normal to the mid-plane is negligible by comparison with the in-plane stresses. The nine stress and strain components of three-dimensional elasticity may be reduced to six by including only one of each pair of complementary shear components in the equations. Stress, $\underline{\sigma}$, and strain, $\underline{\varepsilon}$, are then related according to an equation of the form

$$\underline{\varepsilon} = C \, \underline{\sigma} \tag{2}$$

where $\underline{\varepsilon} = \left[\varepsilon_x, \, \varepsilon_y, \, \varepsilon_z, \, \gamma_{yz}, \, \gamma_{zx}, \, \gamma_{xy} \right]^T$,

and $\underline{\sigma} = \left[\sigma_x, \, \sigma_y, \, \sigma_z, \, \tau_{yz}, \, \tau_{zx}, \, \tau_{xy} \right]^T$.

For a transversely isotropic material such as unidirectional CFRP with axes as shown in Fig. 2, the matrix, C, is given by [27]

$$C = \begin{bmatrix}
1/E_x & -\nu_{xy}/E_x & -\nu_{xy}/E_x & 0 & 0 & 0 \\
-\nu_{xy}/E_x & 1/E_y & -\nu_{yz}/E_y & 0 & 0 & 0 \\
-\nu_{xy}/E_x & -\nu_{yz}/E_y & 1/E_y & 0 & 0 & 0 \\
0 & 0 & 0 & 1/G_{yz} & 0 & 0 \\
0 & 0 & 0 & 0 & 1/G_{xy} & 0 \\
0 & 0 & 0 & 0 & 0 & 1/G_{xy}
\end{bmatrix} \tag{3}$$

Upon setting $\sigma_z = 0$, Equation (2) reduces to

$$\begin{bmatrix} \varepsilon_x \\ \varepsilon_y \\ \gamma_{yz} \\ \gamma_{zx} \\ \gamma_{xy} \end{bmatrix} = \begin{bmatrix}
1/E_x & -\nu_{xy}/E_x & 0 & 0 & 0 \\
-\nu_{xy}/E_x & 1/E_y & 0 & 0 & 0 \\
0 & 0 & 1/G_{yz} & 0 & 0 \\
0 & 0 & 0 & 1/G_{xy} & 0 \\
0 & 0 & 0 & 0 & 1/G_{xy}
\end{bmatrix} \begin{bmatrix} \sigma_x \\ \sigma_y \\ \tau_{yz} \\ \tau_{zx} \\ \tau_{xy} \end{bmatrix} \tag{4}$$

Inversion of Equation (4) yields

$$
\begin{bmatrix} \sigma_x \\ \sigma_y \\ \tau_{yz} \\ \tau_{zx} \\ \tau_{xy} \end{bmatrix} = D \begin{bmatrix} \epsilon_x \\ \epsilon_y \\ \gamma_{yz} \\ \gamma_{zx} \\ \gamma_{xy} \end{bmatrix} \quad , \tag{5}
$$

where D is the elasticity matrix for the material and is given by

$$
D = \begin{bmatrix} E_x/b & \nu_{xy} E_y/b & 0 & 0 & 0 \\ \nu_{xy} E_y/b & E_y/b & 0 & 0 & 0 \\ 0 & 0 & G_{yz} & 0 & 0 \\ 0 & 0 & 0 & G_{xy} & 0 \\ 0 & 0 & 0 & 0 & G_{xy} \end{bmatrix} \quad , \tag{6}
$$

where $b = 1 - \nu_{xy}^2 E_y/E_x$.

The matrix may be transformed to a different axis system corresponding to the case, for example, of a CFRP lamina in which the fibres are not aligned to the plate axes, by means of the standard relations given by, for example, Lekhnitskii.[27]

The integration required to form the element stiffness matrix indicated in Equation (1) was performed numerically using a Gaussian quadrature scheme. It has been shown[23,28] that, in thin shell situations, it is essential to use two-point integration in the directions parallel to the mid-plane. If a higher order of integration is used, the element becomes too stiff as the ratio of side length to thickness increases. The formulation assumes a linear displacement variation through the thickness of the element so two-point integration in this direction gave exact results.

When the element was used to analyse a layered structure, it was necessary to split up the integration of Equation (1) so that the contribution to the integral from each layer was evaluated separately. Two-point Gaussian integration across each layer was used in this case.

The element mass matrix, M^e, is computed from the material density, ρ, and the matrix of the element shape functions, N, according to the equation[19]

$$
M^e = \int_V N^T \rho N \, dV \tag{7}
$$

This form of the mass matrix neglects the effect of rotary inertia. It would be possible to include this effect but it was felt that, for the thin

structures used in this investigation, the error caused by neglecting rotary inertia would be negligible. The implementation of the element therefore included the effect of transverse shear deformation but not that of rotary inertia. This is reasonable with composite materials because transverse shear effects are significant at much higher length to thickness ratios than with isotropic materials[24] whereas the rotary inertia effects are similar in the two cases and are negligible with thin structures.

The integration of Equation (7) was carried out using the same procedure as that used for the stiffness matrix.

2.1.3 The eigenvalue solution system

The routine implemented for the extraction of the natural frequencies from the stiffness and mass matrices was largely derived from that of Anderson.[29] Assembly of the global stiffness and mass matrices[19] yields the eigenvalue equation

$$(K - M \omega^2) \underline{x} = \underline{0} \tag{8}$$

where ω is the frequency and $\underline{x}$ is the mode shape vector.*

This problem may be reduced to standard form by performing a Choleski decomposition of the stiffness matrix,

$$K = LL^T$$

where L is a lower triangular matrix.

Substituting in (8), setting $\mu = 1/\omega^2$ and multiplying by L^{-1}, the inverse of L yields

$$(L^{-1} M(L^{-1})^T - \mu)L^T \underline{x} = \underline{0} \tag{9}$$

The equation is now in the standard form

$$(H - \mu) \underline{\zeta} = \underline{0} \tag{10}$$

with $H = L^{-1} M(L^{-1})^T$ and $\underline{\zeta} = L^T \underline{x}$

This equation may be solved for the highest eigenvalue, μ, corresponding to the lowest natural frequency using vector iteration. The rate of convergence using simple iteration is very slow, particularly for eigenvalues which are close together. This problem is particularly severe in

---

* In this dissertation, the vector, $\underline{x}$, with elements x_1, x_2, ...x_n represents the mode shape vector while the symbol, x, without subscripts represents a co-ordinate direction.

the free-free case because there are six rigid body modes. The conver-
gence rate is much improved by the use of an accelerator of the type
suggested by Irons and Tuck.[30] This was implemented in the program
used to compute the results presented here. The higher natural
frequencies are obtained by deflating the matrix H so that the highest
eigenvalue in the system becomes zero without the other eigenvalues being
changed.

The cost in terms of computer time and storage of a solution of
Equation (9) can be very high. The number of operations is roughly pro-
portional to n^3 where n is the number of degrees of freedom. It is
therefore highly desirable to reduce the value of n. This may
conveniently be done by using the eigenvalue economiser technique described
by Irons.[31] This method retains only a small proportion of the nodal
deflections. These 'master' deflections appear in the eigenvalue
equation (8) while the remaining 'slave' deflections take values which
minimise the strain energy. The number of master deflections may be as
small as 5 per cent of the total, yet the natural frequencies obtained for
the lower structural modes of vibration are within one or two per cent of
those computed without the elimination process. This is due to Rayleigh's
principle, which states that a first order error in mode shape gives only
a second order error in estimated frequency.

The strain energy, S, of an n degree of freedom system is given by

$$S = \tfrac{1}{2}\, \underline{x}^T\, K\underline{x} = \tfrac{1}{2}\begin{bmatrix} x_1, & x_2, & \dots & x_n \end{bmatrix} K \begin{bmatrix} x_1 \\ x_2 \\ \vdots \\ x_n \end{bmatrix} . \tag{11}$$

Likewise, the kinetic energy, U, is given by

$$U = \frac{\omega^2}{2}\, \underline{x}^T\, M\underline{x} . \tag{12}$$

Suppose that the sth deflection is to be eliminated. Differentiating
equation (11) with respect to x_s and setting the result equal to zero in
order to minimise the strain energy with respect to x_s gives

$$K_{s1}\, x_1 + K_{s2}\, x_2 + \ldots + K_{ss}\, x_s + \ldots + K_{sn}\, x_n = 0. \tag{13}$$

Substituting for x_s in Equation (11) gives

$$K_{ij}{}^* = K_{ij} - K_{is}(K_{js}/K_{ss}) \qquad\qquad , i,j = 1,n \tag{14}$$

where K^* is a modified stiffness matrix such that the strain energy is the

minimum obtainable by varying x_s. Similarly,

$$M_{ij}^* = M_{ij} - M_{is}(K_{js}/K_{ss}) - M_{js}(K_{is}/K_{ss})$$

$$+ M_{ss}(K_{is}/K_{ss})(K_{js}/K_{ss}) \qquad , i,j = 1,n \qquad (15)$$

Clearly,

$$K_{is} = K_{si} = M_{is} = M_{si} = 0, \text{ all } i.$$

Thus, row and column s of the stiffness and mass matrices may be deleted giving the desired reduction in matrix size.

The master deflections should be selected to be chiefly in the direction of the motion which is to be investigated. The work described here was concerned mainly with the flexural modes of shell structures so the master variables were selected to be mainly the lateral deflections of the mid-plane.

2.1.4 The solution of free-free problems

Consider a free-free structure in which it is desired to eliminate all the degrees of freedom in, for example, the x direction. There is a rigid body mode in this direction, that is, one which makes no contribution to the strain energy. When all but one of the deflections in this direction have been eliminated, the last one will make no contribution to the strain energy. It is therefore meaningless to minimise the strain energy with respect to this deflection so the elimination process cannot be carried out. This means that, in a free-free problem, it is necessary to retain sufficient deflections in each direction to overcome this difficulty. The results presented here are all from free-free structures and were computed using a 6 x 6 mesh which gives 133 nodes and 665 degrees of freedom. This was reduced to 53 master variables, comprising the lateral deflection at each corner node plus four other variables selected so that the singularity problems were avoided.

For a free-free problem, the global stiffness matrix, K, is singular. The Choleski decomposition and inversion to form Equation (9) from Equation (8) cannot, therefore, be performed. The simplest way to overcome this difficulty is to add a constant times the mass matrix to each term of Equation (8). This yields

$$\left[(K + \alpha M) - M(\omega^2 + \alpha)\right] \underline{x} = 0 \qquad (16)$$

The matrix $(K + \alpha M)$ will, in general, be non-singular so the method can proceed as before. For the vector iteration process to converge rapidly to the eigenvalues, the value of α should be as small as possible. If α

is too small, however, the matrix $(K + \alpha M)$ approximates to K and the inversion process becomes ill-conditioned. Experience suggests that the optimum value of α is approximately $2\omega_1^2$ where ω_1 is the first non-zero natural frequency.

2.2 The method of damage location

The change in the natural frequency of mode i of a structure due to localised damage is a function of the position vector of the damage, $\underline{r}$, and the reduction in stiffness caused by the damage, δK. Thus,

$$\delta\omega_i = g(\delta K, \underline{r}) . \tag{17}$$

Expanding this function about the undamaged state ($\delta K = 0$) and ignoring second order terms yields

$$\delta\omega_i = g(0, \underline{r}) + \delta K \frac{\partial g}{\partial(\delta K)} (0, \underline{r}) . \tag{18}$$

But $g(0, \underline{r}) = 0$, for all $\underline{r}$ since there is no frequency change without damage. Hence,

$$\delta\omega_i = \delta K \, h_i(\underline{r}) . \tag{19}$$

Similarly,

$$\delta\omega_j = \delta K \, h_j(\underline{r}) . \tag{20}$$

Thus, provided that the change in stiffness is independent of frequency,

$$\frac{\delta\omega_i}{\delta\omega_j} = \frac{h_i(\underline{r})}{h_j(\underline{r})} = \ell(\underline{r}) . \tag{21}$$

The ratio of the frequency changes in two modes is therefore only a function of the damage location. Positions where the theoretically determined ratio $\delta\omega_i/\delta\omega_j$ equals the experimentally measured value are therefore possible damage sites.

It is now necessary to compute the change in the natural frequencies of the structure due to damage at a given site. The basis of the method is to consider damage as a local decrease in the stiffness of the structure. One way of computing the changes in the natural frequencies due to damage in a given element of the finite element mesh would be to reduce the stiffness of that element and to repeat the dynamic analysis. This could be done for each element in turn so that the theoretical changes in frequency for damage at a number of sites would be found. The problem with this method is that the amount of computer time involved would be prohibitive.

2.3 The use of sensitivity analysis

A very attractive alternative to repeating the full dynamic analysis in order to compute the changes in the natural frequencies due to localised

damage is to use a sensitivity analysis. By this method, the sensitivities of the natural frequencies of a system to small changes in the stiffness are calculated from the mode shapes of the undamaged structure produced by the initial full dynamic analysis.

From Section 2.1.3, the basic eigenvalue equation which is solved in the dynamic analysis is

$$(K - M\lambda)\underline{x} = \underline{0} \quad , \tag{22}$$

where $\lambda = \omega^2$.

Consider the effect of a small change, δK, in the stiffness matrix with similarly denoted changes in the other parameters. Equation (22) then becomes

$$\{(K + \delta K) - (M + \delta M)(\lambda + \delta\lambda)\}(\underline{x} + \delta\underline{x}) = \underline{0}. \tag{23}$$

Multiplying out and neglecting second order terms yields

$$K \underline{x} - \lambda M \underline{x} - \lambda \delta M \underline{x} + \delta K \underline{x} - \delta\lambda M \underline{x} + K \delta\underline{x} - \lambda M \delta\underline{x} = \underline{0}. \tag{24}$$

But $K \underline{x} - \lambda M \underline{x} = 0$ from Equation (22) and the model of damage used does not include a change in mass so $\delta M = 0$. Equation (24) therefore reduces to

$$\delta K \underline{x} - \delta\lambda M \underline{x} + K \delta\underline{x} - \lambda M \delta\underline{x} = \underline{0}. \tag{25}$$

Multiplying through by $\underline{x}^T$ gives

$$\underline{x}^T \delta K \underline{x} - \delta\lambda \underline{x}^T M \underline{x} + (\underline{x}^T K - \lambda \underline{x}^T M)\delta\underline{x} = 0. \tag{26}$$

Since K and M are symmetric matrices,[19] the transpose of Equation (22) is

$$\underline{x}^T(K - \lambda M) = \underline{0}.$$

Post-multiplying by $\delta\underline{x}$ gives

$$(\underline{x}^T K - \lambda \underline{x}^T M)\delta\underline{x} = 0.$$

Hence, Equation (26) reduces to

$$\underline{x}^T \delta K \underline{x} - \delta\lambda \underline{x}^T M \underline{x} = 0 \quad ,$$

or $$\delta\lambda = \frac{\underline{x}^T \delta K \underline{x}}{\underline{x}^T M \underline{x}} \quad . \tag{27}$$

The sensitivities of the natural frequencies to changes in stiffness, δK, may therefore readily be computed from the mode shape vectors and the mass matrix of the undamaged system.

Equation (27) requires the full mode shape vector to be computed whereas the dynamic analysis described in Section 2.1 only computes the values of the master deflections left after the procedure to reduce the number of variables in the eigenvalue problem has been carried out. When the slave deflection, x_s, is being eliminated, the condition which

- 16 -

minimises the strain energy with respect to x_s is (Equation (13) of Section 2.1.3)

$$K_{s1}x_1 + K_{s2}x_2 + \ldots + K_{ss}x_s \ldots + K_{sn}x_n = 0$$

where K_{si}, $i = 1,n$ is the sth row of the stiffness matrix. Thus, if the values of K_{si}, $i = 1,n$ at this stage of the elimination process are stored, x_s may be computed from the values of the master deflections. This was accomplished by writing the relevant row of the stiffness matrix to backing store for retrieval at the appropriate stage.

The denominator of Equation (27) is ~~equal~~ proportional to twice the kinetic energy of the structure. This may be estimated from the mass matrix of the structure after the elimination process and the vector of the master deflections computed during the eigenvalue solution. It is therefore not necessary to use the full mass matrix, which results in a considerable saving of computer store.

It is now necessary to compute the change in stiffness, δK, due to damage at a point in the structure. From Section 2.1.2, the element stiffness matrix is given by

$$K^e = \int_V B^T DB \, dV \quad . \tag{28}$$

Consider a change in the stiffness of the element over some volume R, denoted by a new elasticity matrix for this region, D^*. Then the change in the stiffness matrix is given by

$$\delta K = \int_R B^T(D^* - D)B \, dV \quad . \tag{29}$$

In two-dimensional structures, the damage is modelled as being of constant severity through the thickness and affecting an area A. If the damaged area is small then

$$\delta K \approx \int_t \left[B^T(D^* - D)B \right]_r A \, dz \quad , \tag{30}$$

where $\left[B^T(D^* - D)B \right]_r$ denotes that the expression within the brackets is evaluated at the position of the damage site, $\underline{r}$. For a three-dimensional structure, the corresponding expression would be

$$\delta K \approx R \left[B^T(D^* - D)B \right]_r \quad .$$

If it is assumed that the damage affects the stiffness by the same proportion in all directions then $(D^* - D) \propto D$. If the damage is equivalent to a hole, then $D^* = 0$ and Equation (30) reduces to

$$\delta K \approx - \int_t \left[B^T DB \right]_r A \, dz \quad . \tag{31}$$

This expression may readily be evaluated using the routines which calculate the stiffness matrix in the dynamic analysis. Equation (27) may then be used to output the sensitivities of the natural frequencies to damage at any point of the structure.

The results of the sensitivity analysis when the damage has been taken to be the equivalent of removing a whole element have been compared with those obtained by setting the stiffness of the element to zero and repeating the dynamic analysis. Excellent agreement was obtained, so the sensitivity analysis method was adopted for all the tests carried out in this investigation.

2.4 Presentation of the results of the location scheme

Measurement of the frequency changes in one pair of modes will yield a locus of possible damage sites, that is points where the ratio of the experimentally determined changes equals the theoretical ratio. The loci for several pairs of modes may be superimposed, the actual damage site being given by the intersection of the curves. With symmetrical structures, two or more sites will be predicted, the number depending on the degree of geometric symmetry and the elastic symmetry of the structural material. At least two mode pairs must be used in order to define the damage site uniquely or to reduce the number of possible sites to the minimum dictated by symmetry. However, because the frequency changes tend to be small and the model of damage is unsophisticated, it is desirable to use a larger number of mode pairs so that some averaging of the results is obtained. This scheme has been implemented, but it was found to be difficult to automate the plotting of the loci which meant that they had to be plotted manually. This procedure was very tedious, particularly when a large number of mode pairs was used.

An alternative was to output the sensitivities at a series of grid points and to compute an error function at each point which was a measure of the error in assuming the damage to be at that point. The point at which the error was a minimum gave approximately the position of the damage.

Define the error in assuming the damage to be at position $\underline{r}$, given frequency changes $\delta\omega_i$ and $\delta\omega_j$ in modes i and j respectively, as

$$
\left.
\begin{aligned}
e_{\underline{r}ij} &= \frac{s_{\underline{r}i}/s_{\underline{r}j}}{\delta\omega_i/\delta\omega_j} - 1 \quad, \quad \frac{s_{\underline{r}i}}{s_{\underline{r}j}} > \frac{\delta\omega_i}{\delta\omega_j} \\[2ex]
e_{\underline{r}ij} &= \frac{\delta\omega_i/\delta\omega_j}{s_{\underline{r}i}/s_{\underline{r}j}} - 1 \quad, \quad \frac{s_{\underline{r}i}}{s_{\underline{r}j}} < \frac{\delta\omega_i}{\delta\omega_j}
\end{aligned}
\right\}
\qquad (32)
$$

In Equation (32), $\delta\omega_i$ and $\delta\omega_j$ are the *experimentally* measured frequency changes in modes i and j due to the actual damage, which is at some unknown position. On the other hand, s_{ri} and s_{rj} are the *theoretical* frequency changes due to damage at site $\underline{r}$ in modes i and j respectively, computed from equations (27) and (31).

The value of the error function, $e_{\underline{r}ij}$, is computed for each mode pair according to Equation (32). These values are then summed to give a measure, $e_{\underline{r}}$, of the total error in assuming the damage to be at position $\underline{r}$, given the experimentally measured frequency changes. Thus,

$$e_{\underline{r}} = \sum_{\substack{\text{all pairs} \\ i \quad j}} e_{\underline{r}ij} \tag{33}$$

The most probable damage site is taken to be the one at which the value of $e_{\underline{r}}$ is a minimum. Let this minimum value be e_{min}. It might be thought that e_{min} would be zero at the damage site. However, due to errors in the experimental measurements, the use of an unsophisticated model of damage in the determination of the theoretical frequency changes and the fact that only a finite number of possible positions, $\underline{r}$, are considered, this is unlikely to be the case. If more than the minimum requirement of two mode pairs for the determination of the damage site are used, some averaging of the results is obtained and the position at which $e_{\underline{r}}$ is a minimum can confidently be predicted to be close to the damage site.

To aid interpretation, the final number output to the damage location chart, $E_{\underline{r}}$, is the reciprocal of $e_{\underline{r}}$ normalised with respect to e_{min}. Thus,

$$E_{\underline{r}} = \frac{100 \ e_{min}}{e_{\underline{r}}} \tag{34}$$

The most probable damage site(s) is therefore that (or those) where

$E_{\underline{r}} = 100$ (i.e. $e_{\underline{r}} = e_{min}$).

It remains to decide how many grid points should be used. The finite element described in Section 2.1 gives a quadratic displacement variation across it which allows for a linear stress variation. The effect of damage at a point in the structure is dependent on the stress at that point, so it would be wasteful of computer time to use more than two grid points along one side of the element. Values between the points could be computed by interpolation. The results presented here have been computed using a 6 x 6 finite element mesh with two grid points per element side giving 144 points in all. The accuracy obtained has not warranted the use of interpolation between the points.

An example of the chart output is given in Fig. 3, the hole shown being the actual damage in this case. The dotted lines show the finite element mesh. In this case, four possible sites are indicated because of symmetry.

2.5 The problem of directional damage

The model of damage used in the preceding sections has assumed that the local stiffness of the structure is reduced by the same proportion in all directions. This would be approximately true with a hole in an isotropic material but the assumption is no longer valid with a crack or with a hole in an anisotropic material.

Consider the situation shown in Fig. 4. The crack shown will have a negligible effect on mode B since there is little stress across it, whereas it will have a relatively large effect on modes A and C. However, a hole at the same site would have a significant effect on all three modes. The model of damage used in the damage location scheme described in the preceding sections was a hole, so erroneous results would be expected with

mode pairs A,B and B,C. However, with mode pair A,C, because the stress direction at the damage is the same in each mode, the ratio of the frequency changes produced by the crack would be the same as the ratio of the changes given by a hole. The damage location scheme would therefore give the correct result with mode pair A,C.

This suggests that the damage location scheme could be improved by giving high weight to modes in which the directions of the stress vectors at the point of interest are similar, and low weight to modes where there is low similarity. This is readily achieved by weighting the error according to the scalar product of the normalised stress vectors for the two modes. Thus, Equation (33) becomes

$$\underline{e}_r = \sum_{\substack{\text{all pairs} \\ i, j}} \underline{e}_{rij} \, \underline{W}_{rij} \quad , \tag{35}$$

where

$$\underline{W}_{rij} = \left| \frac{\underline{\sigma}_{ri} \cdot \underline{\sigma}_{rj}}{|\underline{\sigma}_{ri}||\underline{\sigma}_{rj}|} \right| \quad . \tag{36}$$

Thus, for the example shown in Fig. 4, $\underline{W}_{rAB} \simeq 0$; $\underline{W}_{rAC} \simeq 1$.

The values of stress at the grid points may be computed during the dynamic analysis using standard techniques.[19] The values of the stresses obtained depends on the position through the thickness at which they are calculated. In flexural vibration, the direct stresses would be zero at the mid-plane. The stresses are therefore calculated at a point away from the mid-plane, the precise position being immaterial since only the direction of the stress vector is required, not the magnitude. The transverse shear stresses were sufficiently small to be neglected in all the structures tested.

Many of the structures used in this investigation were fabricated from layered materials which results in the direction of the stress vector at a given point through the thickness being dependent on the orientation of the material at that point. Therefore, if the stress weighting procedure is to be used, an average stress vector must be computed. This has been achieved by defining a mean elasticity matrix for the ply configuration of the structure and using this matrix in the stress computation rather than one of the elasticity matrices of the individual layers which were used in the formation of the element stiffness matrix described in Section 2.1.2. The derivation of the mean elasticity matrix is given in Appendix A. An alternative to this procedure would be to weight the error according to the

direction of the moment vector at the relevant point.

In practice, in order to reduce the amount of data required to be output from the dynamic analysis and hence to save on the amount of disc space required, the stresses were computed at the mid-points of the elements. These values were then assigned to all the grid points within the element. This procedure is sufficiently accurate provided the stress directions do not change rapidly with position (rapid change of magnitude does not matter as the stresses are normalised). This is the case with the lower modes of vibration such as those used in this investigation.

The stress weighting procedure has been adopted in all the results presented here. The results obtained without weighting were fairly similar to those presented, particularly in cases where more modes were used. This is probably because the results tend to average out to give the correct solution. The results with stress weighting tended to be better defined and there was a marked improvement in some cases where only a few modes were used.

2.6 The problem of erroneous frequency measurements

Occasionally, it was found that the results using the damage location scheme described in the preceding sections were incorrect but that the errors were rectified if the results were computed without using the readings from one mode. This could be due to an error in the frequency measurements, the appearance of a double resonance which was not noticed, a relatively large change in mode shape due to the damage (the location scheme assumes that the mode shape is essentially unchanged) or the model of damage not being good enough to predict the frequency change accurately. A method was therefore sought to automate the procedure of checking whether one mode was causing the final result to be incorrect.

The technique developed uses the fact that if one mode is causing errors in the final results while the other modes give correct results, removing this mode will tend to make the damage site more clearly defined on the location chart. The sum of the numbers on the location chart will therefore be reduced.

The modified location scheme computes the results with all the modes included and with each mode neglected in turn. The final solution is taken as the one with the lowest sum of numbers on the chart. When more than six modes are used, a facility is incorporated for neglecting two modes but this was found to be rarely necessary. If less than five modes are measured, then all the readings must be used.

2.7 The estimation of the magnitude of the damage

The sensitivity analysis uses Equations (27) and (31) to output the frequency change in each mode due to a hole of area A centred on each of the grid points in turn. Comparison of the measured frequency change in a given mode with that given by the sensitivity analysis for a hole of area A at the predicted damage site therefore gives an indication of the severity of the damage in terms of the size of a hole equivalent to the damage. The result varies considerably between the modes, particularly if the damage is directional, so an average value is taken.

The method gives a rough indication of the magnitude of the damage but is clearly not accurate. The calculation is performed at the grid point where the error is a minimum, but the damaged area may be between grid points. This can introduce a substantial error into the calculation. The model of damage used does not take into account the mass of material removed by a hole. This is reasonable with most types of damage since damage does not usually reduce the mass of the structure. An error is, however, introduced in the case of a hole. The sensitivity analysis is probably only accurate for relatively small changes in the local stiffness since it does not take account of the effect of stress concentrations around the damage. This means that the effect of a hole is underestimated, resulting in the area predicted from the measured frequency changes being larger than the actual size of the hole. Nevertheless, the method gives a useful indication of the severity of the damage. The results show that the predicted severity always increases as the amount of damage is increased.

2.8 The final damage location scheme

The method implemented for these tests involved performing the dynamic analysis, the sensitivity analysis and the stress calculations on the University ICL 4 - 70 computer, the results being output to disc or tape. The time taken by this program was approximately 50 per cent higher than that required for a single dynamic analysis, so the saving in computer time over repeating the dynamic analysis with each element damaged in turn was very large.

These results, together with the experimental measurements, were then used as input to the program which computed the relative errors and produced the location chart. This program could readily be adapted to run on a micro-computer. The major computational effort is in performing the original analysis. However, this need only be performed once for a given type of structure.

CHAPTER 3

PRINCIPLES OF THE EXPERIMENTAL DETERMINATION OF THE
STRUCTURAL NATURAL FREQUENCIES

3.1 Requirements

The proposed NDT technique requires the reproducible determination of several of the lower natural frequencies of the structure under investigation. The degree to which the frequencies are reproducible directly determines the minimum size of defect which can be detected. In the work on one-dimensional structures described in References 11 and 12, it was possible to resolve the frequencies of small metal structures to about ± 0.01 per cent while, for composite components, the resolution was of the order of ± 0.05 per cent. The structures available for this investigation had their lower natural frequencies in the range 50-2000 Hz, most of the modes of interest having frequencies below 1000 Hz. A reproducibility of ± 0.2 Hz represents an accuracy of ± 0.05 per cent at 400 Hz so this was the order of resolution required.

Structural natural frequencies may be measured either by conventional steady-state methods or by a transient test from the Fourier transform of the response of the structure to an impulse. The application of these two methods to the present work is discussed in this chapter.

3.2 Steady-state methods

The steady-state method for structural dynamic testing is well established[32] and involves tuning the frequency of the excitation applied to the structure until the criterion for resonance is satisfied. The usual criterion to use with lightly damped structures is that of minimum impedance (force/response). This may be simplified to maximum response if the force is frequency independent over the range of interest. The problem with this method is that it is slow, requiring the manual tuning of an oscillator. It is possible to automate the process and use a steady sweep but, if high resolution is required or if the structural damping is low, the sweep rate must be very slow in order to allow the response to stabilise. Automation is considerably simplified if a programmable digital synthesiser and a micro-computer are available. It is then readily possible to adjust the sweep rate according to the rate of change of response with frequency and hence to use a very slow sweep rate only around resonance. This results in a large reduction in test time.

3.3 The transient method

3.3.1 Introduction

The determination of the dynamic characteristics of structures from the Fourier transform of their response to a force of very short duration is increasingly preferred to the conventional steady-state methods. This trend seems likely to continue as the cost of the digital equipment required is reduced. The transient method is attractive because the test time is very short, the measurements are simple to perform and there is the possibility of very rapid results output if on-line computing facilities are available. The basic method has been described by White[6,7] who has also discussed the choice of forcing function.

The spacing between the frequency points produced by the Fourier transform is 1/T where T is the time record length. If the resonant frequency is taken to be that of the frequency point at which the response magnitude is a maximum, the uncertainty in the value of the natural frequency obtained is 1/2T. This means that, if improved frequency resolution is required, the response must be recorded for a longer time. The amount of store required and the time taken for the transform are therefore increased. Even with low damping structures, however, the amplitude of the motion is considerably reduced after a few hundred cycles, so there is a limit to the time for which the response can be recorded with an acceptable degree of accuracy. These factors effectively limit the frequency resolution which can be obtained from the type of test described in References 6 and 7.

Several techniques have been used to overcome these problems. One possibility is to use white noise excitation which is applied continuously to the structure for the duration of the test, thereby removing the difficulty of the motion being damped out and making it possible to record the response for a longer time. This has the disadvantage that several records must be averaged in order to ensure that the mean spectrum of the excitation is flat over the frequency range of interest. This averaging can be expensive in terms of computer time and also increases the duration of the test.

Another possible way of decreasing the spacing between the frequency points is to add zeros to the end of the data records, hence increasing the record length. This does not mean that more information is obtained from the test, but merely that the spectrum is effectively computed at more points which makes it easier to define the position of the resonant peaks.

Both the above methods involve increasing the number of data points, n, used in the computation of the Fourier transform. The time taken for the transform is proportional to $n \log_{10} n$ and the store required is proportional to n, so it can be seen that the computation requirements increase rapidly with n. In practice, however, high frequency resolution is usually only required in the region of the resonant peaks, whereas the standard transform gives the same resolution throughout the spectrum. It is possible to take advantage of this fact by recording the response for a sufficiently long time to give the required resolution at a sample rate which is high enough to prevent aliasing.* This data is then fed through a digital bandpass filter centred on the region of interest which outputs a smaller number of points on which the transform is performed. This produces the spectrum over the bandwidth of the filter with the desired frequency resolution. The filtering process can then be repeated for other parts of the spectrum. This method gives large savings in time over performing the Fourier transform on the whole of the original data but a considerable quantity of store is required. It is possible to perform the filtering on-line and so to economise on store, but this means that, if several frequency ranges are to be investigated, the test must be repeated for each one. This filtering technique has been implemented by several digital equipment manufacturers and is known as 'zoom' or 'band-selectable frequency analysis'.

The store available on the transient capture unit in the department was 2048 points on each of two channels and is fairly typical of currently available systems. If the range 0-1 kHz were to be investigated, a sample rate of at least 2 kHz would have to be used in order to prevent aliasing. The response could therefore be recorded for about one second giving a spacing between the frequency points produced by the Fourier transform of 1 Hz and a resolution of $\pm$ 0.5 Hz if the natural frequency were to be taken as the point of maximum response. It would be possible to add zeros to the end of the record and hence to compute the transform on more points, but insufficient store was available on the computer for this to be practicable. The 'zoom' equipment would have been ideal for the proposed test but is extremely expensive, costing upwards of £30,000. If the proposed non-destructive test were to be widely applied in industry

---

* Shannon's sampling theorem states that, for a signal to be faithfully reconstituted from a set of samples, the sampling frequency must be at least twice the frequency of the signal. If the sample rate is less than this, frequencies above half the sampling frequency are misinterpreted as lower ones. This effect is known as aliasing.

using the transient method for measuring frequencies, it would be essential to develop a cheaper method for improving the resolution. Accordingly, an alternative technique was developed which attempts to resolve the natural frequencies to better accuracy than the spacing between the frequency points produced by the Fourier transform.

3.3.2 Theoretical background

The frequency response function of a lightly damped structure may accurately be modelled as the sum of the response functions of a series of single degree of freedom mass, spring and viscous damper systems. The Fourier transform of the impulse response recorded for time T of such a system has been derived by Clarkson and Mercer[33] and is given by

$$F(w) = \phi(X + iY) \tag{37}$$

where

$$X = (\omega_n^2 - \omega^2)\gamma - (e^{i\nu t}\gamma/u)\left[\alpha(\omega_n^2 - \omega^2) - 2\beta c\omega_n\omega\right]$$

$$Y = -2c\omega_n\omega\gamma + (e^{i\nu T}\gamma/u)\left[\beta(\omega_n^2 - \omega^2) + 2\alpha c\omega_n\omega\right]$$

ω_n = undamped natural frequency = $\sqrt{k/m}$

ω = frequency

k = spring stiffness

m = mass

ξ = damping coefficient

c = damping ratio = $\xi/2\sqrt{km}$ = proportion of critical damping

$\gamma = 1/\left[(\omega_n^2 - \omega^2)^2 + 4c^2\omega_n^2\omega^2\right]$

$u = \omega_n(1 - c^2)^{\frac{1}{2}}$

$\nu = c\omega_n$

T = record length

$i = \sqrt{-1}$

$\alpha = u \cos uT \cos \omega T + \omega \sin uT \sin \omega T + \nu \sin uT \cos \omega T$

$\beta = u \cos uT \sin \omega T - \omega \sin uT \cos \omega T + \nu \sin uT \sin \omega T$

ϕ = amplitude factor

The magnitude of the response is therefore given by

$$P(\omega) = \phi(X^2 + Y^2)^{\frac{1}{2}} \tag{38}$$

Using these equations, it is possible to compute the magnitude of the response at any frequency due to a system of damping ratio c and undamped natural frequency ω_n assuming the impulse response of the system to have been recorded for time T. The relative values of the response magnitude at given points around the resonant peak are dependent on the position of the peak in relation to these points. The Fourier transform algorithm

computes the value of the transform at points spaced $1/T$ Hz apart. Using the above equations, the relative values of the response magnitude at these points for a peak at any frequency can be calculated. A comparison of the values computed from the experimental data with those from Equations (37) and (38) for the resonant peak at different frequencies can be used to estimate the natural frequency with better accuracy. This is conveniently achieved by defining an error function which is to be minimised with respect to the frequency of the resonant peak.

3.3.3 The choice of error function

The approximate frequencies of the resonant peaks can be found by locating the local maxima of the response magnitude derived from the Fourier transform of the data from an impulse test on the structure. Let there be a local maximum, P_1, at frequency ω_1, the adjacent points being P_0 at frequency $\omega_1 - \Delta\omega$ and P_2 at frequency $\omega_1 + \Delta\omega$ where $\Delta\omega$ is the spacing between the frequency points and is equal to $1/T$. The more accurate value of the resonant frequency is to be computed from the relative values of P_0, P_1 and P_2.

It is desirable to choose a function which is independent of the absolute values of the response because the response function is modelled locally as that of a single degree of freedom system whereas practical structures are multi-degree of freedom systems so there are contributions to the response from other modes. Away from their respective resonant peaks, however, the rate of change with frequency of the levels of the other modes is small so they make an approximately equal (unknown) contribution to the values of P_0, P_1 and P_2. The presence of noise will tend to have a similar, though less predictable, effect.

Define $g_1(\omega_p)$ as the theoretical value of the response magnitude at frequency ω_1 computed from equations (37) and (38) for a single degree of freedom system of natural frequency ω_p and damping ratio equal to that of the relevant mode of the structure under test, when the impulse response is recorded for time T. $g_0(\omega_p)$ is therefore the theoretical value of the response magnitude at frequency $\omega_1 - \Delta\omega$, while $g_2(\omega_p)$ is the theoretical value of the response magnitude at frequency $\omega_1 + \Delta\omega$. Then, when ω_p equals the natural frequency of the relevant mode of the structure under test,

$$\left. \begin{aligned} \phi \; g_0(\omega_p) &= P_0 - \chi_0 \\ \phi \; g_1(\omega_p) &= P_1 - \chi_1 \\ \phi \; g_2(\omega_p) &= P_2 - \chi_2 \end{aligned} \right\} \tag{39}$$

where ϕ is a scaling factor and χ_i is the contribution from other modes plus any noise which is present at the frequency corresponding to P_i. Hence, if the values of χ_1, χ_2 and χ_3 are equal,

$$\frac{P_1 - P_0}{P_1 - P_2} = \frac{g_1(\omega_p) - g_0(\omega_p)}{g_1(\omega_p) - g_2(\omega_p)} \qquad . \qquad (40)$$

A suitable error function is therefore given by

$$E(\omega_p) = \left[\frac{P_1 - P_0}{P_1 - P_2} - \frac{g_1(\omega_p) - g_0(\omega_p)}{g_1(\omega_p) - g_2(\omega_p)}\right]^2 \qquad . \qquad (41)$$

The value of E may be calculated for a number of values of ω_p between $\omega_1 - \Delta\omega$ and $\omega_1 + \Delta\omega$, the frequency at which E is a minimum being taken as the resonant frequency of the structure. This frequency, in fact, corresponds to the undamped natural frequency, ω_n. The error will not be exactly zero at any value of ω_p because of numerical inaccuracies and because the values of χ_0, χ_1 and χ_2 will not, in fact, be equal.

This error function also has the advantage of being only a weak function of the damping ratio, c, so it is not necessary to measure the damping accurately before E is calculated. In the tests described in Section 6, the damping was computed from an estimate of the half power points made using the values of the response magnitude produced by the Fourier transform. Even with very low values of damping, this procedure was found to be sufficiently accurate.

3.3.4 The expected accuracy of the method

The method assumes that the frequency response function of the system under test can be expressed as the sum of a number of independent modes, each of which behaves like a single degree of freedom system with viscous damping. This is a reasonable approximation for lightly damped systems such as castings, rotor shafts or aircraft panels whose natural modes typically have damping ratios less than 0.05.

Given that the above assumption holds, the accuracy of the technique for a given mode depends on the damping ratio, c, the time for which the response is recorded, T, the accuracy of the analogue-to-digital conversion and the level of any other noise sources, the proximity of other modes and the level of the response in the mode of interest compared with the other modes. With most computer systems the inaccuracies introduced in the computation are sufficiently small to be neglected by comparison with the other errors. The accuracy of any of the techniques used to improve the frequency resolution is also dependent on the degree

to which the spectrum of the input force is flat over the range of interest. It is possible to compute the force spectrum and to find the frequency response function by dividing the response by the force spectrum, but this procedure adds considerably to the computation and instrumentation required.

As the damping is increased, the difference between P_0, P_1 and P_2 is reduced so that the peak becomes less well defined and the predicted position of the peak more sensitive to errors in the computed values of the response magnitudes. This is not too serious when comparing the method with steady-state measurements as, in this instance also, the accuracy obtainable decreases with increased damping.

The spacing between the spectral lines of the spectrum computed by the fast Fourier transform algorithm is 1/T and the proposed method will improve this resolution by a factor dependent on the other parameters. This factor is independent of T, so the resolution is still improved by increasing T, though with penalties in terms of computer time and storage.

Analogue-to-digital converters operate to a fixed number of levels, typically 2^{10} or 2^{12}. The conversion process effectively introduces noise into the signal which results in a decrease in the accuracy of the values of P_0, P_1 and P_2. The size of the possible error is independent of the values of the response magnitude which means that it is more significant when the differences between the values are small. If noise is a severe problem, the effect can be reduced by performing the Fourier transform not on the response itself but on the autocorrelation of the response as described by Kandianis.[34] This operation doubles the time taken to produce the frequency response function. If this is critical, the analogue-to-digital converters could be upgraded.

The method assumes that, within the region of interest, the response may accurately be modelled as that of a single degree of freedom system. This means that severe errors can be introduced if another peak is in close proximity, the magnitude of the error depending on the damping in each mode. The inaccuracies caused by this phenomenon are less serious with low damping systems as, in this case, the response decreases more quickly away from resonance. The choice of error function to be one which is unaffected by a constant added to the response magnitude helps to minimise this error since, away from the immediate vicinity of the peak, the absolute value of the response function may be significant while the rate of change with frequency is small; thus, the effect of this mode on the response at an adjacent peak approximates to the addition of a constant

to the response magnitude. This problem is not encountered if zeros are added to the response in order to achieve better frequency resolution since, with this method, no assumption is made as to the shape of the peak. If this procedure is adopted, however, the cost in terms of computer time and storage is high.

A perennial problem with impulse tests is that one mode tends to be excited much more strongly than the rest, which means that a poor signal to noise ratio is obtained in the other modes. This problem could be overcome by increasing the energy input at frequencies where the response was too low. However, this approach would require prior knowledge of the spectrum and would involve the computation of the force spectrum, the frequency response function being computed by the division of the response by the force spectrum. In most impact type tests, it is sufficiently accurate to assume that the force spectrum is constant over the region of interest. This solution could only be implemented if the forcing function were generated electrically as is the case with the swept sinewave discussed by White.[6,7] It would not be practicable if a mechanical impulse, such as the hammer blow employed in the tests reported in Section 6, were to be used. A more generally applicable solution to the problem would be to carry out the Fourier transform on the autocorrelation of the response as described by Kandianis,[34] and hence improve the effective signal to noise ratio.

Numerical tests performed using the proposed method indicate that with a single degree of freedom system the natural frequency can be found to an accuracy of $0.05/T$ assuming a 10 bit analogue-to-digital converter and a damping ratio, c, of less than 0.05. With more than one frequency present, the resolution at a given spacing between the peaks is strongly dependent on the damping. With a damping ratio of 0.001 it was possible to compute natural frequencies in the ratio of 1.02:1 to an accuracy of $0.1/T$, whereas with a damping ratio of 0.01, in order to achieve this order of accuracy, the ratio of the frequencies had to be 1.2:1. This still, however, represents a very considerable improvement in accuracy at a low cost in terms of computational effort.

CHAPTER 4

EXPERIMENTAL PROCEDURE

4.1 The choice between steady-state and transient testing

The numerical tests of the transient method for measuring natural
frequencies indicated that the technique would be ideal for the non-
destructive testing work since the frequencies would be found to the
required accuracy without the need for the tedious tuning of an oscillator.
This would result in a very short test time. The problem with the method
was that suitable equipment was not available. The department had
purchased a transient capture unit which enabled the acquisition and
storage of 2048 time data points on each of two channels at a pre-
selectable sample rate. These could then be written to tape for input to
a Prime 400 computer which was housed in the Faculty building. However,
preliminary tests of the equipment showed that there were major faults in
it which resulted in the data becoming corrupted. Problems were also
experienced with the computer interface which meant that the average time
from testing the structure to obtaining the frequencies was of the order
of three hours. These factors effectively ruled out the use of the
transient method of testing though, after the equipment was repaired, it
was possible to do a few tests to investigate the accuracy of the method
for improving the frequency resolution described in Section 3.3: these
tests are described in Section 6. The steady-state method was therefore
adopted for the investigation of the NDT technique.

The oscillator which was available for use in the test programme was
a sweep oscillator (B & K type 2010) which could be manually tuned to an
accuracy of ± 0.01 Hz over the frequency range of interest (50-2000 Hz).
It would have been fairly difficult to automate the determination of
natural frequencies using this instrument and it was decided not to
attempt to do so. This decision was influenced by the fact that only a
relatively small number of tests was proposed and, in real applications of
the NDT technique, the transient method of frequency measurement would
probably be used.

4.2 The support system

The method used for supporting the structure during the determination
of the natural frequencies should be simple to set up and must be repro-
ducible. Thus, the constraint applied to the structure must either be
the same each time the frequencies are determined or must be negligible.

Previous experience with one-dimensional structures[11,12] indicated that hanging the structure so that it was effectively free-free readily satisfied these requirements, the constraint applied to the structure being negligible. This procedure was therefore adopted for all the tests described here, the structure being suspended on nylon thread which was passed through small holes drilled near the edge of the structure, as shown in Fig. 5. For industrial applications of the test, it would probably be unacceptable to drill holes in the structure, so a method for clamping an attachment to the structure through which to pass the supporting strings would have to be developed. An arrangement which would probably be suitable has been described by Clary.[35]

The NDT method is not dependent on a free-free configuration being used, so there is no reason why, for example, the structure should not be firmly clamped. However, experience suggests that, in this case, it is difficult exactly to reproduce the constraint applied to the structure.

4.3 The excitation and monitoring of the structural response

4.3.1 Requirements

It is desirable that the number of additions to the structure be kept to a minimum in order to make the test easy to set up and also that the transducers should be small enough to have a negligible effect on the mode shapes of the structure. It would be possible to include the effect of the transducers in the dynamic analysis, but this would add unnecessary complications and uncertainties to the program.

It is essential to ensure that any additions which are made are rigidly attached to the structure so that the nature of the response is not affected by the additions. If the attachments are not rigid, the effect is similar to adding a spring-mass system to the structure which can have the effect of producing a double peak at one of the resonances, making it impossible to define a single resonant frequency.

4.3.2 Methods of excitation

Four possible methods of exciting the structure have been investigated: a proprietary electrodynamic shaker, a coil-magnet pair, a piezoelectric strain gauge and a moving coil loudspeaker.

The use of an electrodynamic shaker results in the addition of a sizeable electro-mechanical system to the structure. The vibration response of the combined system cannot, therefore, be assumed to be the same as that of the structure alone. The response of the structure itself

may, however, be deduced if the force input to it is monitored. This may conveniently be achieved by attaching the shaker to the structure via an impedance head which measures the force input to the structure and its acceleration. Resonance is then defined as the frequency at which the impedance (force/response) reaches a local minimum. The frequency analyser used in these tests incorporated a feedback circuit which could be used to keep the acceleration constant by controlling the current input to the shaker. Resonance was therefore located by tuning to the minimum force input to the structure. The method worked well but it was necessary to ensure that the attachment to the impedance head was aligned accurately. This proved to be a tedious procedure and, since the method involved monitoring the force input, it was more complicated than the other possible techniques in which the force input to the structure could be considered to be constant across a resonant peak of a structure with fairly low damping. Since the proposed non-destructive test only requires the determination of the frequency of the resonant peaks, and not the impedance at resonance or the structural damping, it was not necessary to measure the force input to the structure when the other methods of excitation were used.

The coil-magnet method was used successfully in the work on one-dimensional structures.[11,12] It involved bonding a horseshoe magnet to the structure and placing a current carrying coil between the poles of the magnet. This technique worked well with heavy structures, but the small CFRP plates used in this investigation tended to exhibit a very low frequency rigid body oscillation which caused the coil to collide with the poles of the magnet. The force required to generate this oscillation was probably produced by non-linearities in the excitation system or by air currents. The effect was not noticed with heavier structures because the force required to produce significant amplitudes would be greater.

The application of a voltage to a piezoelectric strain gauge causes deformation of the piezoelectric material. If the gauge is bonded to a structure at a point of non-zero strain in the modes of interest, it is possible to excite the required modes. This method was found to be very successful, the gauges weighing less than 0.5 gm, so their effect on the response of even the lightest structures used was negligible. The disadvantage of the method was that the gauges cost approximately £5 each and were difficult to remove from the structure after being bonded on.

The use of a moving coil loudspeaker for excitation involved placing the speaker in front of the structure and passing an alternating current

through the speaker coil. This technique had the advantage of being non-contacting and being simple to set up. The noise produced was not too severe since the structures used had fairly low damping and so required little exciting force for the low amplitudes which were required. Accordingly, this method was adopted for all the tests described here though, in other situations, it might be desirable to use one of the other methods.

4.3.3 Methods for monitoring the response

The structural response to the loudspeaker excitation has been successfully monitored using either an accelerometer or a piezoelectric strain gauge. The accelerometer was attached by screwing it on to a stud which was bonded to the structure at a point where the *displacement* was predicted to be non-zero in the modes of interest. The strain gauge was bonded direct to the structure at a point where the *strain* was predicted to be non-zero in the relevant modes. It was found that the accelerometers available represented a significant mass addition to the light, CFRP plates used in some of the tests so a strain gauge was preferable in these cases. However, when heavier structures, such as the aluminium plate described in Sections 6 and 7.1 were tested, the accelerometer was satisfactory and had the advantage that it could be re-used since only the stud was bonded to the structure. Strain gauges were used on all the CFRP components tested but it is probable that an accelerometer would have been satisfactory on the larger CFRP structures.

Resonance was located by tuning to the maximum output of the transducer. With fairly low damping materials, such as those used in this investigation, this is a reasonable criterion to use and is much easier to apply than that of the 90° phase shift between input force and displacement response. When an accelerometer was used, the peak which was located was, strictly speaking, the acceleration rather than the displacement resonance. However, with low damping structures the difference between the two is negligible and, in any case, the frequencies before and after damage were measured using the same transducer so the frequency change would be almost the same in both cases.

4.4 The effect of temperature on the natural frequencies

In order to obtain accurate measurements of the frequency changes due to damage, it is necessary to ensure either that the natural frequencies of the structure before and after damage are measured at the same ambient temperature or that the measurements are corrected for changes in temperature. With aluminium plates, the rate of change of natural frequency

with temperature was of the order of 0.03 per cent per degree Celsius while, with CFRP plates, the effect of temperature could be an order of magnitude greater than this, the size of the change being dependent on whether the stress was chiefly taken by the fibres or the matrix in the mode under consideration.

The tests described here were carried out in a constant temperature enclosure made from polythene sheeting on a metal framework. The air temperature was maintained at 25 ± 1 $^{\circ}$C by means of a thermostatically controlled relay connected to a set of light bulbs which acted as heaters. Due to thermal inertia, the temperature variation of the structures under test was probably less than ± 1 $^{\circ}$C. This was found to be sufficiently stable to enable accurate frequency changes to be recorded. In an industrial environment, the use of a constant temperature enclosure may be impracticable so it would be desirable to develop a method of correcting for ambient temperature changes. With metal structures, it was found to be possible to apply a correction factor based on the temperature coefficients of modulus and expansion, similar to that described in References 11 and 36. This approach would be difficult to apply to structures fabricated from composite materials since the different moduli have radically different temperature coefficients and the coefficients of expansion are direction dependent. It would, however, be a simple matter to determine experimentally the changes in each natural frequency of interest with temperature, and hence to derive the appropriate correction factors.

4.5 Frequency variations with time

With recently-fabricated composite materials, some long-term frequency drift was observed. This was probably due to chemical changes taking place in the matrix which affected the elastic moduli, particularly the transverse Young's modulus and the shear moduli which are strongly dependent on the matrix properties. The effect was also possibly due to slight warping of the structure caused by the relaxation of stresses induced during manufacture. Experience with structures which had been fabricated more than six months previously indicated that the time dependency was much reduced but, since the effect is dependent on the chemical nature of the matrix and the cure cycle, there was little point in trying accurately to quantify it at this stage. In industry, with the carefully controlled production of large quantities of the same material, it would readily be possible to produce data for the change in the material properties with time. This would be more difficult in the

laboratory where the cure cycle tends to be more variable and the material throughput is much smaller.

In the tests reported here, the effect of time on the natural frequencies was eliminated by carrying out all the tests on a given structure on the same day. In practical applications, there would be a much longer interval between tests so it would be necessary to correct for any time dependence of the frequencies. This could be done by deriving a correction factor based either on measured values of the time dependence of the elastic moduli or on measurements of the natural frequencies of a typical structure at regular intervals. It is probable that the latter method would be more satisfactory as the correction factor based on the time dependence of the elastic moduli would not take into account any warping which might occur.

4.6 The determination of the nodal patterns

The theoretical predictions of the mode shapes of the structures tested were checked roughly by determining the nodal patterns. The structure was placed on sponge rubber blocks and excited by an electro-mechanical shaker. Dry sand was spread lightly over the surface of the structure. When the system was tuned to resonance, the sand particles migrated to the nodal lines, giving a check on the theoretical predictions of their position. This system could not be used for the determination of the natural frequencies because the constraint applied by the sponge rubber varied each time the test was set up as the position and load on each of the blocks changed. This could cause a five per cent variation in the measured natural frequencies. However, the nodal patterns were changed very little by this effect.

Some symmetrical structures have two or more modes at the same frequency, the mode excited in practice being a combination of the two depending on the position and nature of the excitation. In these cases, it is impossible accurately to determine the mode shape. Modes of this type were therefore not used in the location scheme since this requires knowledge of the mode shape. The existence of these modes is discussed further in Section 5.3.

4.7 Test procedure

The support and excitation system used in all the tests reported here is shown in Fig. 5. With the aluminium plate described in Sections 6 and 7.1, an accelerometer was substituted for the strain gauge. This apparatus was placed in the constant temperature enclosure. Figure 6

shows the supporting electronic equipment. The signal from the oscillator was stable to ± 0.01 Hz over the frequency range of interest (50-2000 Hz).

The frequency and mode shape predictions for each structure to be tested were checked and the modes to be used for the non-destructive test were decided. Up to ten modes were usually used, the minimum being five. The actual number used depended on how many modes could readily be excited using the system described above. The natural frequencies of all the modes used could be determined to within at least 0.5 Hz and most could be found to within 0.2 Hz. With the aluminium plate described in Section 7.1, the natural frequencies could be resolved to at least 0.06 Hz.

The test procedure was then to measure the initial frequencies of the structure at least twice, leaving half-an-hour between the readings in order to check that the frequencies were reproducible and the temperature stable. The structure was then removed from the enclosure, damaged, and returned to the enclosure. After allowing time for the temperature to stabilise, the frequencies were again measured twice. The frequencies quoted in Tables 15 and 16 are therefore the mean of at least two readings. In cases where the extent of the damage was not obvious, an ultrasonic C-scan test was also carried out on the structure.

Occasionally, the frequency of one mode would increase slightly after damage. This was probably due to an error in the initial frequency readings and meant that the mode could not be used in the damage location routine. In two instances, a resonant peak became ill-defined after damage with several local maxima being found which made it impossible uniquely to determine the resonant frequency. This could be a useful indication that damage was present but, again, the mode could not be used in the location routine.

CHAPTER 5

INVESTIGATION OF THE ACCURACY OF THE FREQUENCY AND MODE PREDICTIONS

5.1 Introduction

This series of tests was designed to investigate the accuracy of the natural frequency and mode shape predictions made using the dynamic analysis described in Section 2.1. The tests were carried out on square aluminium and CFRP plates with a variety of ply configurations and on a trapezoidal, cross-ply CFRP plate. The experimental arrangement was the same as that described in Section 4.7, the plates being suspended on nylon thread. The vibration was excited by a moving coil loudspeaker and detected by a piezoelectric strain gauge bonded to the plate.

There have been few investigations of the natural modes of free-free anisotropic plates. Clary[35] investigated theoretically and experimentally the effect of fibre orientation on the first five flexural modes of rectangular, unidirectional, boron-epoxy panels. The agreement between theoretical and experimental natural frequencies was generally good, though there were large errors in some of the predictions for the thinner panels. Ashton[37] considered theoretically the effect of stacking sequence and degree of orthotropy on the first four flexural modes of square, free-free plates. The work described here was therefore the first experimental investigation into the natural modes of free-free multidirectional plates.

5.2 Material properties

The composite used in these tests was HT-S carbon fibre in DX210 epoxy resin. The plates were fabricated using nominally 60 per cent fibre volume fraction, 0.4 mm thick pre-preg sheets. The plates had either 7 or 8 layers and a side length of the order of 200 mm, giving a side length/thickness ratio of over 70. Details of the plates used are given in Table 1. The trapezoidal plate, No. 3A, was made from Plate 3 by cutting along a line from the mid-point of one side to the opposite corner.

The material properties used in the theoretical predictions are given in Table 2. The values for aluminium were generally accepted published values while the significant CFRP properties were measured. The longitudinal (E_x) and transverse (E_y) flexural Young's moduli were established using beam specimens cut from a unidirectional plate by measuring the first, free-free flexural natural frequencies of the beams. The longitudinal shear modulus, G_{xy}, was determined for a cylindrical specimen by

using the torsion pendulum described by Adams et al.[38]   The values of
the major (ν_{xy}) and transverse (ν_{yz}) Poisson's ratios were obtained from
data sheets.   It was not felt to be necessary to measure these as the
natural frequencies are insensitive to changes in Poisson's ratio.
Numerical tests have shown that the maximum frequency change in the modes
of interest in this study due to changing the value of ν_{xy} from 0.30 to
0.35 was of the order of 0.4 per cent.   The density for each plate was
computed from the mass of the plate and its dimensions.

5.3 Results

The theoretical and experimental frequencies are shown in Tables 3-8.
These have been expressed in non-dimensional form in order to facilitate
comparisons between plates of different dimensions.   The frequencies are
therefore expressed in terms of the parameter, ψ, defined such that

$$\psi = \frac{fa^2}{t} \sqrt{\frac{\rho}{E_y}}$$

The error in frequency prediction is given by

$$e = \frac{\psi_{exp} - \psi_{theor}}{\psi_{theor}}$$

The value of side length used in the calculation of ψ for the trapezoidal
plate, No. 3A, was the side length of plate 3 from which plate 3A was made.

The nodal line patterns corresponding to the mode numbers given in
the tables are shown in Figs. 7-12.   The aluminium plate (No. 1) and the
$\pm 45^\circ$ plate (No. 4) show instances of multiple eigenvalues.   This means
that, owing to symmetry, there are two possible mode shapes at the same
frequency.   These are referred to as A and B in the figures.   Experi-
mentally, if the plate is excited at this frequency, a linear combination
of these modes will, in general, be obtained, the precise nature of the
mode produced depending on the position and method of excitation and the
support positions.

5.4 Discussion

The results presented in Tables 3-8 show generally good agreement
between the predicted and measured frequencies, the worst error being
6.3 per cent.   The results of Clary[35] with 24 layer panels of similar
overall thickness to the plates used in this investigation show a worst
error of 14.4 per cent.   The average error obtained by Clary with the
24 layer panels was 4.4 per cent while the average error in the results
from the CFRP plates presented here was 2.8 per cent.   The results of the

tests on the trapezoidal plate demonstrate that the quality of the predictions is not dependent on the elements remaining undistorted.

The errors are probably largely due to thickness variations across the plates and property variations across a given plate and between the plates. A one per cent change in thickness would give a one per cent change in frequency, while a one per cent change in one of the elastic moduli would give up to a 0.5 per cent change in frequency, the magnitude of the change being dependent on the directions of the stresses in the given mode. The CFRP plates showed thickness variations of typically ± 5 per cent on the average values used in the predictions. The worst errors in the frequency predictions were in modes in which the material is stressed chiefly in shear. The torsional rigidity of cross-ply beam specimens cut from plates 3 and 4 was measured in the torsion pendulum described in Reference 38 and showed a ± 4 per cent variation on the mean value, indicating that the shear modulus varied significantly across the plates. The errors due to variations in dimensions and material properties could therefore readily account for the errors in the frequency predictions.

The variation in thickness across the aluminium plate was ± 1 per cent on the mean and it may be assumed that the material property variation across it was relatively small, though there may have been some anisotropy due to the rolling process. The results for this plate given in Table 3 show that the agreement between the theoretical and experimental frequencies is, on average, considerably better than for the CFRP plates, the worst error being 2.6 per cent. This suggests that the larger errors with the CFRP plates were caused by variations in the thickness and the material properties.

The number of elements used in the analysis affects the accuracy of the predictions. The theoretical frequencies quoted here were all calculated using a 6 x 6 mesh. The frequencies were also computed using a 5 x 5 mesh and the results were within 2 per cent of those obtained using the 6 x 6 mesh, indicating that the results are close to the "exact" solution. It is of interest to note that the use of 2 point integration in the formation of the element stiffness and mass matrices means that convergence is no longer necessarily from above, so the solution is not an upper bound on frequency as is normally the case with the finite element method. Convergence is, however, fast enough for this not to be a serious problem.

The nodal line patterns observed using sand were in good agreement with those predicted, except where the theory showed a multiple eigenvalue. In these cases, the pattern observed depended on the position of excitation. It was found to be possible to obtain the predicted mode shapes by clamping the plate at a point which lay on a nodal line of one of the possible modes but at which there was motion in the other mode. Vibration in one of the alternative modes was thus prevented.

The tests show that the dynamic characteristics of composite laminates vary considerably with the ply orientations. The lowest frequency tends to be one which stresses the material chiefly in shear. The lowest frequency parameter and the average of the first six frequency parameters for each of the CFRP plates are shown in Table 9. It can be seen that the lowest frequency of the $\pm 45°$ plate (No. 4) is over 50 per cent higher than those of the unidirectional plate (No. 2) and the cross ply plate (No. 3). The average of the first six frequencies of the unidirectional plate (No. 2) is 20 per cent lower than that of the other plates. The average frequency of the $\pm 45°$ plate is considerably higher than that of the other square plates. The nodal patterns shown in Figs. 7-12 show that the mode shapes are also strongly dependent on ply orientation. It is possible, therefore, for the designer to exercise considerable control over the dynamic response of a laminated composite structure simply by changing the ply orientation.

It was noted that the mode shape of the third mode of the $\pm 45°$ plate (No. 4) was different from that predicted by Ashton[37] for a similar plate. It appeared unlikely that this change was due to the slightly different material properties and ply orientation. Accordingly, the eight layer $\pm 45°$ plate considered by Ashton was analysed using the method described in Section 2.1. The frequency parameters for the first four modes are compared with the corresponding figures from Reference 37 in Table 10. The material properties and plate data used are given in Tables 1 and 2. The frequency parameter used in Reference 37 is defined in a different way to that used here, so the results quoted in Reference 37 have been converted to facilitate comparison. The nodal patterns predicted using the method of Section 2.1 are similar to those shown in Fig. 10. These agree with the predictions of Reference 37 apart from the third mode. The third mode of Reference 37 is shown as number 3T in Fig. 10. The experimental results from the $\pm 45°$ plate (No. 4) used in this investigation showed good agreement with the theoretical predictions made here. The predictions for the four layer $\pm 45°$ plate given in Reference 37 were

also checked using the analysis described in Section 2.1. The results are
shown in Table 10. In this case, the nodal pattern predictions are
similar though the methods do not agree on which mode has the lowest
frequency. The results for the 0° and $+ 45^o$ plates were also checked and
the agreement was found to be better than two per cent in frequency for the
0° plate and better than six per cent for the $+ 45^o$ plate. In both cases
the nodal pattern predictions were in good agreement. It appears,
therefore, that the mode shape predicted for the third mode of the eight
layer $\pm 45^o$ plate given by Ashton in Reference 37 is incorrect. Apart
from this, the results of Reference 37 are similar to those obtained here.

The plates used in these tests had ratios of side length to thickness
of the order of 70. In plates with high aspect ratios, even when they are
fabricated from a highly anisotropic material, transverse shear deformation
is not very significant in the lower natural modes. Shear deformation
becomes more significant in the higher modes as the ratio of wavelength to
thickness decreases. Therefore, the inclusion of transverse shear
deformation in the analysis does not make a large contribution to the
accuracy of the results quoted here. This has been demonstrated by
increasing the transverse shear stiffnesses by a factor of 10^3, thus making
the element effectively non-shear-flexible, and repeating the dynamic
analysis. The maximum frequency increase was about three per cent in the
most complex modes considered. Transverse shear effects would be more
significant in thicker plates or in, for example, a sandwich construction
using CFRP skins on a softer core.[39] Even with a sandwich construction,
however, the effects of transverse shear deformation are not likely to be
significant with the lower modes of panels of aspect ratio greater than 50.
Two honeycomb panels were used in the testing of the NDT technique but both
had aspect ratios of the order of 60 so the effect of transverse shear
deformation on the modes of interest was negligible.

5.5 Conclusions

The results show good agreement between the experimental natural
frequencies and nodal patterns and the theoretical predictions for all the
plates tested, the worst error in frequency being 6.3 per cent. The
accuracy obtained using the analysis of Section 2.1 appears to be as good
as is warranted by the uniformity of the material. These results have
been obtained using a fairly coarse mesh comprising 36 elements. The
element is readily generalisable to shells and will accommodate irregularly
shaped boundaries. It is also shear-flexible, which is an advantage in
such configurations as, for example, CFRP skins on a soft core, an appli-
cation in which fibre reinforced materials are commonly used. The results,

therefore, suggest that the element used is a good general purpose tool for the analysis of structures fabricated from composite materials.

The results show that the use of the analysis described in Section 2.1 readily satisfies the requirement of the damage location scheme which is that a reasonably accurate estimate of the mode shapes of the structure be obtained. This program was therefore used for the dynamic analysis of all the structures used in the investigation of the NDT technique. It is possible that a simpler element would have given sufficiently accurate results for the damage location scheme with the structures tested in this investigation. However, the element described in Section 2.1 has the advantage that it can be used to analyse any shell-type structure so the same program could be used with all two dimensional structures.

CHAPTER 6

EXPERIMENTAL INVESTIGATION OF THE TRANSIENT METHOD
OF FREQUENCY MEASUREMENT

6.1 Apparatus

The equipment used in the experimental investigation of the method
for improving the frequency resolution obtained from a transient test
described in Section 3.3 consisted of a transient capture unit which could
store 2048 samples on each of two channels using a 10 bit analogue-to-
digital converter at a pre-selected sample rate. These time points were
then output to a Prime 400 computer on which the fast Fourier transform,
the calculation of the response magnitude, and the estimation of the
natural frequencies were performed. It was only possible to carry out a
limited number of tests on the method because of the unreliability of the
transient capture unit and the computer interface.

6.2 Tests with a single frequency input

The first series of tests was carried out using the signal from a
high-stability, variable-frequency oscillator as input to the system in
order to investigate the accuracy obtainable with the available equipment
for a single frequency input whose amplitude was constant with time.
Five tests were carried out with different frequency inputs, the sample
rate in each case being 2 kHz, giving a theoretical maximum frequency of
1 kHz. The sample time to store 2048 points was therefore 1.024 seconds,
giving a spacing between the frequency points of 0.977 Hz. If the
computed input frequency had been taken to be that of the frequency point
at which the response function were a maximum, the uncertainty in the
value of the frequency obtained would have been approximately ± 0.5 Hz
(or ± 1/2 T). The results are set out in Table 11 and the response magni-
tude curve for the case of the input at 195.80 Hz is shown in Fig. 13.
This curve was formed by plotting the values of spectral density obtained
from the Fourier transform, the points being joined by straight lines. It
can be seen from Table 11 that the worst error was 0.06 Hz or approximately
0.06/T. This is about 16 times smaller than the spacing between the
frequency points produced by the transform.

6.3 Tests on an aluminium plate

A series of tests was also performed to determine the lower natural
frequencies of a free-free aluminium plate of dimensions 450 x 350 x 6 mm.
The support system was identical to that described in Section 4.7, the

plate being suspended on nylon thread passed through small holes near the plate edge and the response being detected by an accelerometer. Excitation was provided by an impulse from a hammer which had a force transducer bonded to the head. A typical time record of the output from the force transducer is shown in Fig. 14 and the corresponding spectrum over the frequency range of interest is shown in Fig. 15. In this test the transient capture unit was triggered by the output from the force transducer exceeding a pre-set level with the inclusion of a pre-trigger facility which stored the input to the unit for a fixed time before the trigger, thus enabling the leading edge of the force pulse to be recorded. It can be seen that the spectrum is sufficiently flat for it to be unnecessary to divide the response by the force in order to obtain the frequency response curve. Indeed, it would probably be less accurate to adopt this procedure since the local variations in the force spectrum are probably due to noise rather than to variations in the true level. The force was therefore not recorded in the main series of tests and the transient capture unit was triggered by the response exceeding a pre-set level.

Five tests were performed on this system. The sample rate used was again 2 kHz, giving a theoretical maximum frequency of 1 kHz. Anti-aliasing filters were set at 1 kHz which meant that the effects of aliasing were negligible in the frequency range of interest in this test, 0-500 Hz. A typical time record of the response is shown in Fig. 16 and the corresponding transform is given in Fig. 17. The computed values of the first six natural frequencies are given in Table 12. All the frequencies were corrected for changes in the ambient temperature by using a correction factor based on the temperature coefficients of modulus and expansion similar to that described in References 11 and 36. It can be seen that the largest error with respect to the mean values was 0.10 Hz, this being in the mode at 302 Hz. Fig. 17 shows that this mode had very low amplitude compared with the others so the signal to noise ratio was poor; it was also close to another mode which was excited strongly at 276 Hz. In spite of these factors, the worst accuracy achieved was approximately 0.1/T which is 10 times better than the spacing between the frequency points produced by the Fourier transform and the resolution obtained was better than this in the other modes.

Table 12 also shows the values of the corresponding natural frequencies obtained using steady-state excitation. The steady-state frequencies quoted are the mean of three readings and the maximum deviation

from the mean is also given in the table. The system used for this was the same as that described in Section 4.7, the exciting force being provided by a moving coil loudspeaker. It can be seen that the steady-state and transient frequencies are in good agreement, the worst error being 0.13 Hz in the first mode which was difficult to excite using the loudspeaker.

The modal damping ratios, c (proportion of critical damping), were determined approximately by exciting the structure at resonance using the loudspeaker, then switching off the excitation and recording the decaying response on a storage oscilloscope. The values obtained were typically of the order of 0.0003. The damping was too low to be measured accurately from the transient response with the short record time used, though the modal damping ratios were estimated from the transient data and were in reasonable agreement with the values obtained by the free-decay method.

6.4 Conclusions

The results show that it is possible to resolve the natural frequencies of a structure to within one-tenth of the spacing between the frequency points produced by the Fourier transform of the structural response to an impulse. This represents an improvement, in the worst case, by a factor of five over the resolution obtained if the resonant frequency is taken to be that of the frequency point at which the response magnitude is a maximum. This worst accuracy recorded was achieved on a mode which was only weakly excited by the impulse applied to the structure.

The results were obtained using an unsophisticated transient capture unit which employed 10 bit analogue-to-digital converters and at a low cost in terms of computer time and store. One of the limiting factors on the accuracy of the method is the error introduced in the analogue-to-digital conversion. This means that if higher frequency resolution were required it would be advantageous to use more accurate converters than the customary 10 or 12 bit. The results indicate that this would be more cost effective than, for example, doubling the store so that a longer record could be obtained and would be considerably less expensive in terms of computer time.

The resolution obtained in these tests would be adequate for the proposed non-destructive test and the computation requirements of the method are within the capabilities of a small mini-computer, so a unit to perform the data capture and extraction of the natural frequencies would be a fraction of the cost of, for example, the 'zoom' equipment referred to

in Section 3.3.   A very short test time can therefore be achieved at a
realistic cost for a wide variety of possible applications.

CHAPTER 7

INVESTIGATION OF THE NDT TECHNIQUE

The damage location charts for all the tests carried out are shown in Figs. 3 and 18-40. In each case, the dotted lines show the finite element mesh and the solid lines show the structure boundaries. The estimates of the severity of the damage applied, in terms of the size of a hole equivalent to the damage, computed by the method described in Section 2.7 are set out in Tables 13 and 14. The values given in Tables 13 and 14 for the measured size of the damage are the percentage of the area of the structure over which damage was visible. In the case of saw cut damage, the area was taken to be that of a circle whose diameter was the length of the cut. This is a reasonable approximation since the effect of the cut on the stress field in a direction perpendicular to the cut is similar to that of a hole. If the damage was not clearly visible, the affected area was taken to be that indicated by an ultrasonic C-scan test. The experimental procedure for all the tests was that described in Section 4.7.

7.1 Tests with simple forms of damage

The first series of tests was carried out on simple structures with readily quantifiable forms of damage in order to check the operation of the technique and the supporting analysis.

An aluminium plate of dimensions 450 x 350 x 6 mm was damaged by cutting a rectangular hole of size 25 x 19 mm at the site shown in Fig. 18, which also shows the location chart produced by the analysis set out in Section 2. It can be seen that the damage was successfully located within the constraints imposed by symmetry. The discrepancy shown in Table 13 between the actual area removed and that predicted by the location routine is probably due to the factors discussed in Section 2.7, i.e. the calculation is performed at the grid point which is predicted to be nearest to the damage site, which may not coincide with the true centre of the damage; the model of damage used does not take account of the mass of material removed by the hole, since this is usually negligible in comparison with the stiffness change, and the sensitivity analysis is only accurate for relatively small changes in the local stiffness.

The first test to be carried out on a CFRP component was on a square, unidirectional plate of dimensions 250 x 250 x 3 mm. This plate was damaged by cutting a square hole of side 21 mm at the site shown in Fig. 3. Again, four possible sites were indicated because of symmetry. The

discrepancy between the predicted and actual areas removed shown in
Table 13 is similar to that for the aluminium plate. This indicates the
order of accuracy which is to be expected from the routine which estimates
the magnitude of the damage.

Another unidirectional CFRP plate of similar dimensions to the first
plate was damaged with a series of saw cuts. The first was 20 mm long and
ran parallel to the fibre direction at the site shown in Fig. 19. The
second cut was at the same site and the same length but was made at right
angles to the first. The location chart for the two sets of damage
together is shown in Fig. 20. Another cut, approximately 45 mm long, was
then made at the orientation shown in Fig. 21 which also gives the output
from the damage location routine for the three sets of damage together.
The charts in Figs. 19, 20 and 21 show that the damage was located in each
case within the constraints imposed by symmetry, though with a small error
in the third instance. This was probably because the damage was then
fairly severe, so the model of damage at a point was no longer accurate.
The predicted equivalent areas removed, shown in Table 13, increase with
successive applications of damage and give an indication of the severity of
the damage. The predicted area increases between the first and second
cuts whereas the size of a hole surrounding the cuts remains constant
because the predicted area is the average of the size of hole required to
produce the observed frequency change in each mode. With a single cut,
the frequencies of modes in which the major stresses are parallel to the
cut are not changed significantly, so the size of hole is predicted to be
small.

The first multidirectional CFRP structure to be tested was a square,
cross-ply plate of similar dimensions to the unidirectional plates tested
previously. This was damaged by a saw cut of length 20 mm at the position
and orientation shown in Fig. 22. It can be seen from Fig. 22 that the
damage was correctly located. Again, four possible sites were indicated
because of symmetry. The saw cut was then extended until the total length
was 45 mm. The damage was again detected and correctly located, as shown
in Fig. 23. It can be seen from Table 13 that the predicted equivalent
areas removed give a reasonable indication of the severity of the damage,
bearing in mind the approximations made in the analysis.

This plate was then cut to a trapezoidal shape by removing the corner
containing the damage. Damage was again applied in the form of saw cuts,
the first being 25 mm long at the position and orientation shown in Fig. 24.
The structure was now asymmetrical, so the damage site is uniquely defined

on the location chart. The second cut was of similar size but was
approximately at right angles to the first at the same site. The location
chart for damage comprising the two cuts together is shown in Fig. 25 and
the frequency changes produced by the damage applied to this plate are set
out in Table 15. The order of magnitude of the changes is typical of that
obtained with all the types of damage investigated. One of the modes
tested showed a frequency increase after the first saw cut. This was
probably due to an error in the initial frequency measurements so this mode
was not used in the damage location analysis.

The frequency changes produced by the first cut were much smaller than
those produced by the second in spite of the fact that the cuts were of
similar length. The predicted equivalent area removed by the first cut
was 0.19 per cent of the plate area compared with the size of a hole
surrounding the cut which was 1.0 per cent of the plate area. This was
because the stress at the position of the saw cuts in the modes of interest
was mainly in a direction parallel to the first cut, which was close to,
and ran parallel to, the plate edge. Thus, a small hole at that site
would produce the same frequency changes as this cut. The value of the
equivalent area removed produced by the analysis of Section 2.7 must
therefore be viewed with caution if the damage is likely to be highly
directional.

If the technique described here were to be used as an in-service test
with measurements being made periodically, it would be important to be able
to detect and locate changes in the condition of the structure, not only
with respect to the virgin condition but also with respect to a stage where
some damage was present. In order to test the method under these condi-
tions, a location chart was produced using the frequency changes between
the first and second sets of damage. This is shown in Fig. 26. It can
be seen that the damage is again successfully located.

7.2 Tests with more realistic forms of damage

Three types of damage, crushing, local heating and impact, which are
more representative of those likely to be encountered with composite
components in service, have been investigated. It has not been possible
to examine the effect of fatigue or creep damage on the natural frequencies
because of the difficulty in inducing these on structures other than simple
specimens. Since this was a preliminary investigation into the non-
destructive testing method, it was felt that the effort required to perform
tests of this type was not warranted at this stage, though the method has
successfully been used to locate fatigue damage in one-dimensional

structures.[11,12]

The trapezoidal, cross-ply CFRP plate described in the previous section was damaged at the position shown in Fig. 27 by supporting it on a thick-walled 35 mm diameter tube, resting a 25 mm steel ball on the plate at the centre line of the tube and pressing the ball into the plate using a hydraulic press.   This caused a circular dent, approximately 15 mm in diameter, and a considerable amount of fibre breakage within this area. The location chart shown in Fig. 27 was produced from the frequency changes caused by the crushing with the ball bearing alone, that is using the frequencies obtained with the two saw cuts as the initial condition.

The predicted equivalent area removed corresponding to the location chart shown in Fig. 27 was 1.02 per cent of the plate area.   (The case given in Table 13 for crush damage plus two saw cuts corresponds to Fig. 35, not to Fig. 27.)   The area of the dent was approximately 0.5 per cent of the area of the plate and it is reasonable to assume that the actual damaged area would spread somewhat beyond this.   Thus, the predicted damaged area of 1.02 per cent was of a similar order, bearing in mind the assumptions and simplifications made, to the actual damaged area.

A square $\pm 45^\circ$ plate of dimensions 210 x 210 x 3 mm was damaged in the same fashion at the site shown in Fig. 28.   Again, the damage was correctly located though, in this case, four possible sites were indicated due to symmetry.   Good agreement is also shown between the predicted and measured equivalent areas removed given in Table 14.

Another square CFRP plate, in this case of dimensions 250 x 250 x 3 mm with plies oriented at $0,60,30,90,90,30,60,0^\circ$, was damaged by heating with a gas flame.   This produced a blister and some surface cracking in the area indicated on Fig. 29.   The location chart given in Fig. 29 shows that, in this instance, the damage was not correctly located but was predicted to be at one of the sites marked B rather than the correct site A.   In this test the damage was spread over a significant proportion of the area of the plate which meant that the model used of damage at a point was of doubtful validity.   In addition, the stresses in most modes are similar at sites A and B.   Indeed, if only 0 and 90° plies were used, the symmetry of the system would make it impossible to differentiate between the two sites.   These factors probably explain the poor definition on the location chart and the fact that the wrong pair of sites was predicted. This test illustrates the need for caution in interpreting the location chart in cases where the structure approximates fairly closely to a degree of symmetry which it does not, in fact, possess: that is, where a small

structures.[11,12]

The trapezoidal, cross-ply CFRP plate described in the previous section was damaged at the position shown in Fig. 27 by supporting it on a thick-walled 35 mm diameter tube, resting a 25 mm steel ball on the plate at the centre line of the tube and pressing the ball into the plate using a hydraulic press. This caused a circular dent, approximately 15 mm in diameter, and a considerable amount of fibre breakage within this area. The location chart shown in Fig. 27 was produced from the frequency changes caused by the crushing with the ball bearing alone, that is using the frequencies obtained with the two saw cuts as the initial condition.

The predicted equivalent area removed corresponding to the location chart shown in Fig. 27 was 1.02 per cent of the plate area. (The case given in Table 13 for crush damage plus two saw cuts corresponds to Fig. 35, not to Fig. 27.) The area of the dent was approximately 0.5 per cent of the area of the plate and it is reasonable to assume that the actual damaged area would spread somewhat beyond this. Thus, the predicted damaged area of 1.02 per cent was of a similar order, bearing in mind the assumptions and simplifications made, to the actual damaged area.

A square $\pm 45^{\circ}$ plate of dimensions 210 x 210 x 3 mm was damaged in the same fashion at the site shown in Fig. 28. Again, the damage was correctly located though, in this case, four possible sites were indicated due to symmetry. Good agreement is also shown between the predicted and measured equivalent areas removed given in Table 14.

Another square CFRP plate, in this case of dimensions 250 x 250 x 3 mm with plies oriented at $0,60,30,90,90,30,60,0^{\circ}$, was damaged by heating with a gas flame. This produced a blister and some surface cracking in the area indicated on Fig. 29. The location chart given in Fig. 29 shows that, in this instance, the damage was not correctly located but was predicted to be at one of the sites marked B rather than the correct site A. In this test the damage was spread over a significant proportion of the area of the plate which meant that the model used of damage at a point was of doubtful validity. In addition, the stresses in most modes are similar at sites A and B. Indeed, if only 0 and 90° plies were used, the symmetry of the system would make it impossible to differentiate between the two sites. These factors probably explain the poor definition on the location chart and the fact that the wrong pair of sites was predicted. This test illustrates the need for caution in interpreting the location chart in cases where the structure approximates fairly closely to a degree of symmetry which it does not, in fact, possess: that is, where a small

change in the geometry or ply orientations would increase the degree of
symmetry of the structure. In practice, this is unlikely to be a major
problem. The predicted equivalent area of damage given in Table 14 was
0.95 per cent of the plate area whereas the measured area was 6.7 per cent.
In fact, the predicted area is probably a reasonable estimate of the
severity of the damage because only the surface layers of the plate were
damaged by the flame so, although the blister covered 6.7 per cent of the
plate area, the damage was not equivalent to the removal of all the
material from this region.

The plate was then cut to trapezoidal shape so that the damaged area
was removed and was tested again, this time with impact damage. The plate
was supported on a thick walled, 35 mm tube and a 25 mm diameter steel ball
was rested on the plate at the centre line of the tube. The ball was then
struck with a hammer. The resulting damage was almost invisible apart
from a small dent and some slight surface cracking. It has been the
experience of the aerospace industry[40] that this type of damage can cause
a 50 per cent reduction in the strength of the laminate and is difficult to
detect other than by ultrasonic measurements which are not practicable for
the routine testing of large structures. It can be seen from Fig. 30 that
the damage was successfully located by the vibration measurements. In
this case, the structure was asymmetrical so it was possible to define the
damage site uniquely. Again, the predicted equivalent area removed, shown
in Table 14, was considerably lower than the area of damage indicated by
the ultrasonic C-scan test. This was probably because the damaged region
still contained a large proportion of undamaged material so the predicted
area is likely to be a better estimate of the severity of the damage.

7.3 Tests on honeycomb panels

Two structures were tested which are more representative of the ways
in which high quality fibre reinforced materials are used in industry. The
first of these was a 610 x 520 x 10 mm honeycomb panel with CFRP facings
which is used for floor panelling in aircraft. This was tested by pressing
a 25 mm diameter steel ball into one face so that this face was damaged but
the other face was unblemished and the damage was invisible from the remote
side. The results of this test are shown in Fig. 31. It can be seen
that the damage was again correctly located (within the limits imposed by
symmetry) in spite of the fact that the measured area of the damage was
only 0.12 per cent of the total area. The predicted equivalent area given
in Table 14 was 0.18 per cent and gives a reasonable estimate of the
severity of the damage.

The structure was then made asymmetrical by removing the corner con-taining the original damage and was tested again, this time by heating one face with a gas flame. This produced a large blister on one face, but again the damage was invisible from the remote side. Fig. 32 shows the location chart produced for this case. In this instance, the damage site was uniquely defined due to the asymmetry of the structure. Good agreement is shown between the predicted and measured areas removed given in Table 14.

The second structure obtained from the aerospace industry was a honey-comb panel which had CFRP facings with layers oriented at $0, 90, +45, -45^{\circ}$ and which had CFRP inserts along each edge with a total of 45, 10 mm holes drilled in them. The overall dimensions of the panel were 490 x 210 x 4 mm. The structure was modelled crudely for the dynamic analysis by ignoring the effect of the edge inserts and treating the component as a uniform panel. Damage was applied by crushing with a 25 mm steel ball in a hydraulic press, the first time with the opposite side supported on a flat plate so that only one face was damaged and the second time at the same site with the remote side supported on a thick walled 35 mm diameter tube, resulting in damage to both faces. The location chart for the first set of damage is shown in Fig. 33. It can be seen that the damage was predicted to be at one of the sites marked B rather than the correct site A, though the sites A are also shown to have a high probability of being damage sites. This result was caused by the fact that the structure approximates very closely to one in which the sites A and B would be indistinguishable by the vibration method due to symmetry. It is only the presence of the thin layers at $\pm 45^{\circ}$ which reduces the degree of symmetry. In this case, the damaged area was measured to be 0.1 per cent of the total, and the frequency changes were correspondingly small, as shown in Table 16. The wrong pair of sites was probably predicted because of small errors in the frequency changes due to their being the small differences in large quantities. This test again demonstrates the need for caution in interpreting the location chart with structures which approximate to a degree of symmetry which they do not possess. The two cases where this effect caused erroneous results were the only tests in which the damage was not correctly located within the constraints imposed by symmetry. The location chart for the second set of damage is shown in Fig. 34. In this instance, the damage was correctly predicted to be at one of the sites A. In view of the approximations made in the analysis, reasonable agreement is shown between the predicted and measured areas removed given in Table 14.

The natural frequency predictions made by the dynamic analysis were considerably less accurate with the sandwich panels than with the CFRP plates, the errors being of the order of 20 per cent with the first panel and 30 per cent with the more complex structure. This was probably due to uncertainty about the thickness of the CFRP skins and about their distance from the neutral axis, both of which have a large effect on the flexural stiffness. In the case of the more complex panel, the unsophisticated model used in the analysis also contributed to the poor accuracy of the frequency predictions. However, in both cases, the mode shape predictions were sufficiently accurate for the purposes of the damage location routine. This indicates that it is unnecessary to expend large amounts of effort and computer time in order to produce an accurate dynamic analysis of the structure. The basic requirement that the mode shapes be obtained reasonably accurately is readily met.

7.4   Tests with more than one damage site

In the damage location analysis described in Section 2, it is assumed that the damage is at one site only. It would be difficult to amend the method to take into account the possibility of two damage sites as the number of unknowns would then increase to four (two positions and two damage magnitudes) and this case would be fairly unusual in practice. Two tests were, however, carried out with damage at two sites.

The first involved the trapezoidal, cross-ply CFRP plate described in Sections 7.1 and 7.2. This was damaged with two saw cuts at one site and by crushing with a steel ball at another position. The location chart shown in Fig. 27 and discussed in Section 7.2 was for the crush damage using as the 'undamaged state' the frequencies measured after both saw cuts had been applied. This meant that, relative to the initial conditions, damage was at one site only. The chart shown in Fig. 35 is for the case of the saw cut and crush damage using the virgin frequencies as the initial conditions. The damage is therefore at two sites relative to the initial conditions: as expected, erroneous results were produced. The presence of damage was, however, still detected from the frequency changes. The routine which estimates the magnitude of the damage also assumes that the damage is at a single site defined by the grid point at which the location chart shows a value of 100. The value of 3.65 per cent for the equivalent area removed given in Table 13 for the case shown in Fig. 35 cannot therefore be assumed to be an accurate estimate of the severity of the damage. It does, however, give an indication of the amount of damage present.

The second test was carried out on a 240 x 240 x 3 mm unidirectional CFRP plate with one corner removed. A 10 mm hole was drilled at site A shown in Fig. 36 and was subsequently enlarged to 15 mm. Another hole was then drilled at site B, the size being increased from 10 mm to 15 mm and 20 mm. Some delamination occurred around site A so the extent of the damage could not be related accurately to the area removed by the holes, nor was it possible to define the exact position of the damage around site A. The location charts for each set of damage with respect to the virgin frequencies are shown in Figs. 36-40. The apparent errors in the predicted locations shown in Figs. 36 and 37 were probably due to the delamination which occurred in the fibre direction and which was more severe after the hole at A was enlarged. In the third case, that of a 15 mm hole at A and a 10 mm hole at B, the damage was again predicted to be close to site A as shown in Fig. 38. When both holes were of a similar size, Fig. 39 shows that the predicted site moved further away from site A and when the second hole became the larger of the two the computed location was again erroneous, although it had moved closer to site B, as indicated by Fig. 40. In fact, the magnitude of the damage at site A was probably still comparable with that at site B due to the delamination.

These tests indicated that, in situations where there are two damage sites, the results from the location routine are unreliable though, if the damage at one site is much more severe than that at the other, the major site will be predicted. However, even when the location routine gives erroneous results, the presence of damage is detected by the frequency changes. The predicted equivalent areas removed shown in Table 14 increase with increasing damage and give an indication of the severity of the damage even though the routine which estimates the magnitude of the defect also assumes a single site.

CHAPTER 8

CONCLUSIONS

It has been shown to be possible to detect, locate, and roughly to quantify damage in structures by using measurements of the structural natural frequencies. Tests have been successfully carried out on fibre-reinforced structures, including two obtained from the aerospace industry, with a variety of types of damage, including impact damage which was almost invisible but which is known to cause severe reductions in the strength of the laminate. The test technique is equally applicable to metallic components.

The proposed test requires access to only one point of the structure and is potentially very quick to perform. One set of frequencies is measured before the component is put into service and subsequent measurements are used to determine whether the structure is still sound. Alternatively, a set of frequencies measured at an intermediate stage can be used as the initial frequencies and the growth of damage from this state monitored.

The presence of damage is detected simply from changes in the natural frequencies without the need for any analysis. The location and estimation of the severity of the damage, however, requires a dynamic analysis of the structure to be carried out. Only one such analysis is required for each type of structure to be investigated and tests have shown that the model used need not be sophisticated since the technique requires that the mode shapes of the lower structural natural frequencies be adequately approximated - a criterion readily met by simple representations of complex structures. The results of the dynamic analysis may be stored on disc or tape and, along with the experimentally measured natural frequencies, form the input to the damage location program. This program could readily be adapted to run on a micro-computer. If diffuse rather than localised damage were present, due, for example, to environmental attack, the presence of damage would be detected from changes in the structural natural frequencies and it would be possible to monitor the progress of the degradation. The location routine could be adapted to test for overall degradation rather than localised damage. This would require the evaluation of the theoretical frequency changes owing to an overall reduction in the structural stiffness and the comparison of the error in assuming this structural state with the errors computed for damage at a point.

The method can be used to detect any form of damage which significantly reduces the stiffness of the structure in the direction of the major stresses induced by the type of vibration used. This means that a longitudinal crack in a straight bar would not be detected by the use of axial vibration but it would have a significant effect on the torsional modes. With shell structures, in most cases it is only practicable to use flexural vibration, so it would be difficult to detect, for example, interlaminar shear cracks in a laminated structure. Most other forms of damage would, however, be detected by measurements of the flexural modes.

The results indicate that damage equivalent to the removal of the order of 0.1 per cent of the area of a shell-type structure can be detected when the natural frequencies are measured to the accuracy obtained in this investigation (approximately ± 0.05 per cent). It would be difficult to achieve better reproducibility than this in practical situations since the limiting factor on the accuracy is probably the degree to which a constant temperature can be maintained, or changes be corrected for. In these tests, the air temperature was constant to ± 1 $^{\circ}$C and this would be difficult to improve upon in an industrial environment. If the test is to be used with composite materials, more work must be done on their time-dependent properties in order to develop a correction factor for the changes with time of the natural frequencies of structures fabricated from these materials.

The estimated severity of the damage in terms of the size of a hole equivalent to the damage shown in Tables 13 and 14 always increased with increasing damage, so the progress of the degradation could be monitored. In spite of the fact that the analysis used to produce the estimate was fairly unsophisticated and the accuracy of the prediction of the magnitude of the damage was less than that of the damage location, the agreement between the predicted and measured areas removed was generally good enough for the predicted area to give a potentially useful indication of the severity of the damage.

The finite element described by Zienkiewicz et al.[22,23] has been shown to give accurate frequency and nodal pattern predictions for structures fabricated from composite materials using a mesh comprising a fairly small number of elements. The element has the advantage that it can be readily generalised to accommodate curved shells and allows for transverse shear deformation. The results indicate that the element is a good general purpose tool for the analysis of fibre composite structures.

A method has been developed for improving the frequency resolution obtained with the transient testing technique described by White.[6,7] It has been shown to be possible to resolve the structural natural frequencies to within one-tenth of the spacing between the frequency points produced by the Fourier transform. This result represents an improvement by a factor of five over the commonly adopted technique and has been obtained using an unsophisticated transient capture unit at a low cost in terms of computer time and store.

REFERENCES

1. Adams, R. D., Flitcroft, J. E., Reynolds, W. N. and Hancox, N. L.,
    "Effects of shear damage on the torsional behaviour of carbon
    fibre reinforced plastics", J. Composite Materials, Vol. 7, 1973,
    pp. 68-74.

2. Adams, R. D., Walton, D., Flitcroft, J. E. and Short, D., "Vibration
    testing as a non-destructive test tool for composite materials",
    Composite Reliability Conference Proceedings, ASTM STP580, 1974.

3. Di Bendetto, A. T., Gauchel, J. V., Thomas, R. L. and Barlow, J. W.,
    "Non-destructive determination of fatigue crack damage in
    composites using vibration tests", Journal of Materials, Vol. 7,
    1972, pp. 211-215.

4. Schultz, A. B. and Warwick, D. N., "Vibration response: a non-
    destructive test for fatigue crack damage in filament reinforced
    composites", J. Composite Materials, Vol. 5, 1971, pp. 394-404.

5. Lifshitz, J. M. and Rotem, A., "Determination of reinforcement
    unbonding of composites by a vibration technique", J. Composite
    Materials, Vol. 3, 1969, pp. 412-423.

6. White, R. G., "Use of transient excitation in the dy namic analysis
    of structures", Jnl of Royal Aeronautical Society, Vol. 73, 1968,
    p. 1047.

7. White, R. G., "Evaluation of the dynamic characteristics of structures
    by transient testing", J. Sound and Vibration, Vol. 15, 1971,
    p. 147.

8. Spain, R. F., Schubring, N. W. and Diamond, M. J., "An electronic ear
    for certifying reliability", The Quality Engineer, Vol. 30, No. 1,
    pp. 15-20.

9. Hoffman, B., "Determination of material integrity of mechanical
    structures by vibration analysis", Materials Research and
    Standards, MTRSA, Vol. 12, 1972, pp. 17-20.

10. Reneker, D. H., Edelman, S., De Reggi, A. S. and Vanderhart, D. C.,
    "An NDT method using piezoelectric polymer transducers and
    computerised vibrational spectroscopy", NDT International,
    February 1978, pp. 15-16.

11. Adams, R. D., Cawley, P., Pye, C. J. and Stone, B. J., "A vibration
    technique for non-destructively assessing the integrity of
    structures", J. Mech. Eng. Science, Vol. 20, 1978, p. 93.

12. Cawley, P. and Pye, C. J., "Non-destructive testing of structures",
    B.Sc. thesis, University of Bristol, 1975.

13. Loland, O. and Mackenzie, A. C., "On the natural frequencies of
    damaged offshore oil platforms", Mech. Res. Comm., Vol. 1, 1974,
    pp. 353-354.

14. Loland, O., Begg, R. D. and Mackenzie, A. C., "The dynamic response
    of a fixed steel offshore oil platform", BSSM/RINA Conference,
    Edinburgh, Sept. 1975.

15. Loland, O., Mackenzie, A. C. and Begg, R. D., "Integrity monitoring of fixed steel offshore oil platforms", BSSM/RINA Conference, Edinburgh, Sept. 1975.

16. Loland, O. and Dodds, C. J., "Experiences in developing and operating integrity monitoring systems in the North Sea", OTC 2551, 1976.

17. Mayes, I. W. and Davies, W. G. R., "The vibrational behaviour of a rotating shaft system containing a transverse crack", Conference on Vibrations in Rotating Machinery, Cambridge, Sept. 1976, Paper C168/76 (I.Mech.E.).

18. Bishop, R. E. D. and Johnson, D. C., "The mechanics of vibration", Cambridge University Press, 1960.

19. Zienkiewicz, O. C., "The finite element method in engineering science", McGraw-Hill, 1971.

20. Bacon, D. G. C., "The dynamic properties of carbon and glass fibre reinforced plastic", Ph.D. thesis, University of Bristol, 1973.

21. Flitcroft, J. E., "The non-destructive testing of glass and carbon fibre reinforced plastics", Ph.D. thesis, University of Bristol, 1976.

22. Ahmad, S., Irons, B. M. and Zienkiewicz, O. C., "Analysis of thick and thin shell structures by curved finite elements", Int. J. Numerical Methods in Engineering, Vol. 2, 1970, p. 419.

23. Zienkiewicz, O. C., Taylor, R. L. and Too, J. M., "Reduced integration technique in general analysis of plates and shells", Int. J. Numerical Methods in Engineering, Vol. 3, 1971, p. 275.

24. Pagano, N. J., "Exact solutions for composite laminates in cylindrical bending", J. Composite Materials, Vol. 3, 1969, p. 398.

25. Mindlin, R. D., "Influence of rotatory inertia and shear on flexural motions of isotropic, elastic plates", J. Appl. Mech., Vol. 18, 1951, p. 31.

26. Sun, C. T. and Whitney, J. M., "Theories for the dynamic response of laminated plates", A.I.A.A. Journal, Vol. 11, 1973, p. 178.

27. Lekhnitskii, S. G., "Theory of elasticity of an anisotropic body", Holden-Day, 1963.

28. Zienkiewicz, O. C. and Hinton, E., "Reduced integration, function smoothing and non-conformity in finite element analysis (with special reference to thick plates)", J. Franklin Inst., Vol. 302, 1976, p. 443.

29. Anderson, R. G., "A finite element eigenvalue solution system", Ph.D. thesis, University of Wales, Swansea, 1968.

30. Irons, B. and Tuck, R., "A version of the Aitken accelerator for computer iteration", Int. J. Numerical Methods in Engineering, Vol. 1, 1969, p. 275.

31. Irons, B., "Structural eigenvalue problems: elimination of unwanted variables", A.I.A.A. Journal, Vol. 3, 1965, p. 961.

32. Kennedy, C. C. and Pancu, C. D. P., "Use of vectors in vibration measurement and analysis", J. Aeronautical Science, Vol. 14, 1947, pp. 603-625.

33. Clarkson, B. L. and Mercer, C. A., "Use of cross correlation in studying the response of lightly damped structures to random forces", A.I.A.A. Journal, Vol. 3, 1965, p. 2287.

34. Kandianis, F., "Frequency response of structures and the effect of noise on its estimates from the transient response", J. Sound and Vibration, Vol. 15, 1971, p. 203.

35. Clary, R. R., "Vibration characteristics of unidirectional filamentary composite material panels", Composite Materials: Testing and Design (second conference) ASTM STP497, 1972, p. 415.

36. Adams, R. D. and Coppendale, J., "Measurement of the elastic moduli of structural adhesives by a resonant bar technique", J. Mech. Eng. Science, Vol. 18, 1976, pp. 149-158.

37. Ashton, J. E., "Natural modes of free-free anisotropic plates", Shock and Vibration Bulletin, Vol. 39, 1969, p. 93.

38. Adams, R. D., Fox, M. A. O., Flood, R. J. L., Friend, R. J. and Hewitt, R. L., "The dynamic properties of unidirectional carbon and glass fibre-reinforced plastics in torsion and flexure", J. Composite Materials, Vol. 3, 1969, p. 594.

39. Adams, R. D. and Weinstein, A. S., "Flexural stiffness of sandwich beams", Trans. A.S.M.E., Jnl Eng. Maths. and Techn. paper no. 75-Mat-K.

40. Rhodes, M. D., Williams, J. G. and Starnes, J. H., "Effect of low velocity impact damage on the compressive strength of graphite-epoxy hat-stiffened panels", NASA TN D-8411, April 1977.

APPENDIX A

THE DERIVATION OF A MEAN ELASTICITY MATRIX
FOR A LAYERED MATERIAL

The strain energy of a structure at any instant is given by

$$S = \int_V \frac{1}{2} \underline{\sigma}^T \underline{\varepsilon} \; dV \quad , \tag{A1}$$

and stress and strain are related according to the equation

$$\underline{\sigma} = D \; \underline{\varepsilon} \quad . \tag{A2}$$

Thus, the strain energy is given by

$$S = \frac{1}{2} \int_V \underline{\varepsilon}^T D \underline{\varepsilon} \; dV \quad . \tag{A3}$$

It is required to derive a mean elasticity matrix for a structure
fabricated from n layers so that an average stress vector may be found.
This may be done by specifying that the strain energy of the structure
computed using the mean elasticity matrix according to Equation (A3) is
the same as that obtained by summing the strain energies of the individual
layers.   That is,

$$\frac{1}{2} \int_V \underline{\varepsilon}^T D^e \; \underline{\varepsilon} \; dV = \frac{1}{2} \sum_{k=1}^{n} \int_V \underline{\varepsilon}^T \; D^k \; \underline{\varepsilon} \; dV \tag{A4}$$

where D^e is the mean elasticity matrix and D^k is the elasticity matrix of
the kth layer, the integral on the right-hand side of the equation being
taken over the volume of the layer and that on the left being over the
volume of the structure.   Cartesion co-ordinates have been used in all
the work described here and, in this case, Equation (A4) becomes

$$\iiint \underline{\varepsilon}^T D^e \; \underline{\varepsilon} \; dx \; dy \; dz = \sum_{k=1}^{n} \iiint \underline{\varepsilon}^T D^k \; \underline{\varepsilon} \; dx \; dy \; dz \tag{A5}$$

The elasticity matrices are not dependent on x and y so Equation (A5)
reduces to

$$\int_t \underline{\varepsilon}^T D^e \; \underline{\varepsilon} \; dz = \sum_{k=1}^{n} \int_{h_{k-1}}^{h_k} \underline{\varepsilon}^T \; D^k \; \underline{\varepsilon} \; dz \tag{A6}$$

where h_k is the z co-ordinate of the top of the kth layer.

Flexural vibration has been used in the tests reported here, so it is
reasonable to assume a linear direct strain variation through the thickness
and a parabolic transverse shear strain variation.   The strain vector for
the element used here is therefore given by:

$$\underline{\varepsilon} = \begin{Bmatrix} \varepsilon_x \\ \varepsilon_y \\ \gamma_{yz} \\ \gamma_{zx} \\ \gamma_{xy} \end{Bmatrix} = \begin{Bmatrix} k_1 \, z \\ k_2 \, z \\ k_3 \, (1 - 4z^2/t^2) \\ k_4 \, (1 - 4z^2/t^2) \\ k_5 \, z \end{Bmatrix} \tag{A7}$$

where $k_1 \ldots k_5$ are functions of x and y.

Substituting Equation (A7) into Equation (A6) and equating similar terms gives

$$\left. \begin{aligned} D_{ij}^e &= \frac{4}{t^3} \sum_{k=1}^{n} D_{ij}^k \, (h_k^3 - h_{k-1}^3) & i,j = 1,2,5 \\ D_{ij}^e &= \frac{15}{8t} \sum_{k=1}^{n} D_{ij}^k \left[(h_k - h_{k-1}) - \frac{8}{3t^2} (h_k^3 - h_{k-1}^3) + \frac{16}{5t^4} (h_k^5 - h_{k-1}^5) \right] & i,j = 3,4 \quad . \end{aligned} \right\} \tag{A8}$$

All the structures used here had symmetrical ply configurations about the mid-plane. This means that

$$D_{13}^e = D_{14}^e = D_{23}^e = D_{24}^e = D_{35}^e = D_{45}^e = 0$$

The average elasticity matrix, D^e, defined by Equation (A8) has been used to compute the stress vectors for the layered materials used in these tests.

TABLE 1.   PLATE DATA

Plate number	Material	No. of layers	side length/mm	Thickness mm	Density kg/m³	ply orientation
1	Aluminium	—	398.5	6.29	2701	—
2	CFRP	7	252.5	2.78	1506	all 0°
3	CFRP	7	254.0	2.89	1507	90,0,0,90,0,0,90
4	CFRP	8	207.0	3.27	1513	+45,-45,-45,+45,-45,-45,+45,
5	CFRP	8	229.0	3.16	1532	0,60,30,90,90,30,60,0
3A	As 3 but cut to trapezoidal shape					
plates used to check predictions of Ref. 37	*	8	350.0	4.0	1500.0	+45,-45,+45,-45,-45,+45,-45,+45
	*	4	350.0	4.0	1500.0	+45,-45,-45,+45

*The material properties used do not relate to a real material.

TABLE 2.   MATERIAL PROPERTIES

Material	$\dfrac{E_x}{GN/m^2}$	$\dfrac{E_y}{GN/m^2}$	$\dfrac{G_{xy}}{GN/m^2}$	ν_{xy}	ν_{yz}
Aluminium	70.3	70.3	26.2	0.34	0.34
CFRP	112.5	7.89	4.48	0.30	0.30
Properties used in checking predictions of Ref. 37	100.0	10.0	5.0	0.30	0.30

TABLE 3.   RESULTS FOR PLATE NO. 1 (ALUMINIUM)

Mode	ψ_{exp}	ψ_{theor}	% error
1	0.634	0.639	-0.8
2	0.961	0.936	+2.6
3	1.19	1.19	-0.4
4	1.66	1.65	+0.3
5	2.96	3.00	-1.5
6	3.02	3.05	-1.0

TABLE 4.   RESULTS FOR PLATE NO. 2 (unidirectional CFRP)

Mode	ψ_{exp}	ψ_{theor}	% error
1	0.79	0.79	0
2	1.02	1.03	-1.0
3	1.84	1.92	-4.2
4	2.81	2.86	-1.8
5	3.60	3.77	-4.5
6	3.98	3.90	+2.1

TABLE 5.   RESULTS FOR PLATE NO. 3 (cross-ply CFRP)

Mode	ψ_{exp}	ψ_{theor}	% error
1	0.76	0.81	-6.2
2	2.42	2.48	-2.4
3	2.92	2.97	-1.7
4	3.13	3.18	-1.6
5	3.51	3.57	-1.7
6	5.09	5.23	-2.7

TABLE 6.   RESULTS FOR PLATE NO. 4 ($\pm$ 45° CFRP)

Mode	ψ_{exp}	ψ_{theor}	% error
1	1.27	1.23	+3.3
2	1.84	1.88	-2.1
3	2.47	2.57	-3.9
4	3.91	4.07	-3.9
5	5.35	5.66	-5.5
6	5.81	6.01	-3.3

TABLE 7.   RESULTS FOR PLATE NO. 5 $(0,60,30,90,90,30,60,0^{\circ}$ CFRP)

Mode	ψ_{exp}	ψ_{theor}	% error
1	1.01	0.95	+6.3
2	1.95	2.01	+3.0
3	2.48	2.52	-1.6
4	3.21	3.23	-0.6
5	4.05	4.01	+1.0
6	4.63	4.75	-2.5

TABLE 8.   RESULTS FOR PLATE NO. 3A (trapezoidal cross-ply CFRP)

Mode	ψ_{exp}	ψ_{theor}	% error
1	1.02	1.07	-4.7
2	2.55	2.60	-1.9
3	3.06	3.14	-2.5
4	4.06	4.09	-0.7
5	5.72	5.92	-3.4
6	6.77	7.03	-3.7

TABLE 9.   THE VARIATION OF THE NATURAL FREQUENCY PARAMETER WITH
PLY ORIENTATION

Plate No.	Lowest ψ	Average ψ for first six modes
2	0.79	2.38
3	0.81	3.04
4	1.23	3.57
5	0.95	2.91
3A	1.07	3.98

TABLE 10.   COMPARISON OF RESULTS FOR $\pm$ 45° PLATES WITH THOSE OF REFERENCE 37

Mode	8 layer plate		4 layer plate	
	ψ	ψ from Ref. 37	ψ	ψ from Ref. 37
1	1.15	1.27	1.14	1.23
2	1.52	1.53	1.20	1.21
3	2.26	2.54*	2.37	2.46
4	3.36	3.43	2.69	2.74

*   Different mode shape

TABLE 11

Results of the Single Frequency Input Tests

Frequencies/Hz		
Input	Computed	Error
195.80	195.78	− 0.02
250.50	250.49	− 0.01
500.00	500.03	+ 0.03
750.00	750.05	+ 0.05
800.10	800.04	− 0.06

TABLE 12

Results of Tests on Aluminium Plate

Mode	Mean of transient tests	Maximum deviation from mean	Mean of steady state tests	Maximum deviation from mean	Steady state − transient frequency
1	124.06	0.05	124.19	0.01	0.13
2	158.65	0.04	158.71	0.01	0.06
3	276.61	0.03	276.61	0.05	0.00
4	302.40	0.10	302.42	0.01	0.02
5	359.16	0.09	359.13	0.04	− 0.03
6	466.96	0.05	466.95	0.06	− 0.01

$1/T = 0.977$ Hz

TABLE 13   THE ESTIMATED SEVERITY OF DAMAGE (INITIAL TESTS)

Structure	Type of damage	Equivalent area removed (% of total)		Figure showing relevant location chart
		Predicted	Measured	
aluminium plate	hole	0.47	0.31	18
square, unidirectional CFRP plate	hole	1.04	0.69	3
square, unidirectional CFRP plate	1 saw cut	0.35	0.5†	19
	2 saw cuts	0.76	0.5†	20
	3 saw cuts	1.42	2.5†	21
square, cross-ply CFRP plate	20 mm saw cut	0.39	0.5†	22
	45 mm saw cut	1.62	2.5†	23
trapezoidal, cross-ply CFRP plate	1 saw cut	0.19	1.0†	24
	2 saw cuts	2.17	1.6†	25
	2 saw cuts + crushing	3.65	2.6†	35

†With saw cut damage, the measured area was taken to be that of a circle surrounding the cut(s).

TABLE 14   THE ESTIMATED SEVERITY OF DAMAGE (LATER TESTS)

Structure	Type of damage	Equivalent area removed (% of total)		Figure showing relevant location chart
		Predicted	Measured	
square ±45° CFRP plate	crushing	1.10	1.0	28
square 0,60,30,90° CFRP plate	local heating	0.95	6.7	29
trapezoidal 0,60,30,90° CFRP plate	impact	0.41	3.7	30
sandwich panel	crushing	0.18	0.12	31
sandwich panel with one corner removed	local heating	3.10	3.2	32
sandwich panel with CFRP edge inserts	crushing on one face crushing on both faces	0.13 0.20	0.10 0.30	33 34
unidirectional, trapezoidal CFRP plate	10 mm hole at A 15 mm hole at A 15 mm hole at A + 10 mm hole at B 15 mm hole at A + 15 mm hole at B 15 mm hole at A + 20 mm hole at B	0.38* 1.78* 2.40* 2.93* 4.72*	0.16 0.37 0.53 0.74 1.03	36 37 38 39 40

*Delamination occurred around site A so the predicted areas removed cannot be directly related to the sizes of the holes.

TABLE 15   RESULTS FROM TRAPEZOIDAL, CROSS-PLY, CFRP PLATE

Damage	Undamaged Frequencies/Hz									
	104.32	260.98	312.74	415.29	584.48	693.24	794.70	936.50	1062.25	1150.93
	Frequency Reductions from Virgin Condition/Hz									
First saw cut	0.06	0.39	0.29	0.14	-0.07	0.14	2.70	0.62	0.20	0.28
Second saw cut	0.85	5.46	4.50	2.08	1.78	4.32	5.29	3.70	1.20	1.68
Crush damage	1.24	5.66	5.91	3.44	3.93	4.38	9.02	6.90	10.41	6.51

TABLE 16   RESULTS FROM SANDWICH PANEL WITH CFRP EDGE INSERTS

Damage	Undamaged frequencies/Hz						
	187.08	2.3.99	343.16	370.22	433.77	447.24	575.13
	Frequency reductions/Hz						
Crushing on one side	0.10	0.24	0.23	0.33	0.25	0.12	0.38
Crushing on both sides	0.20	0.60	0.43	0.51	0.55	0.39	0.63
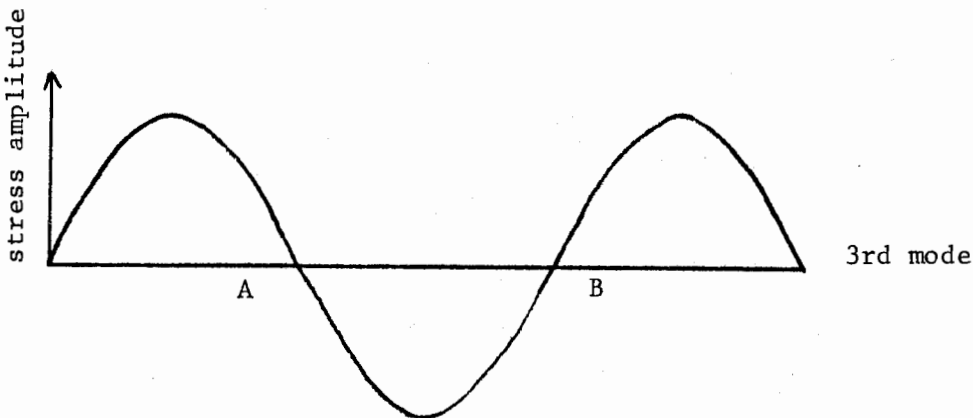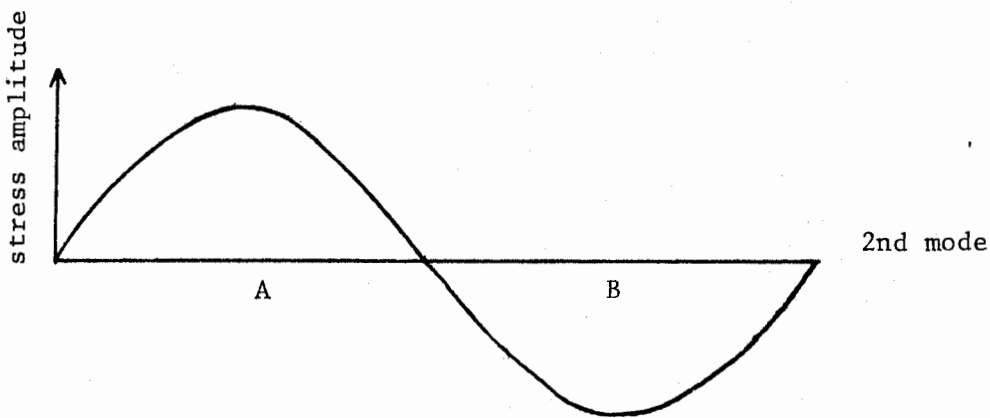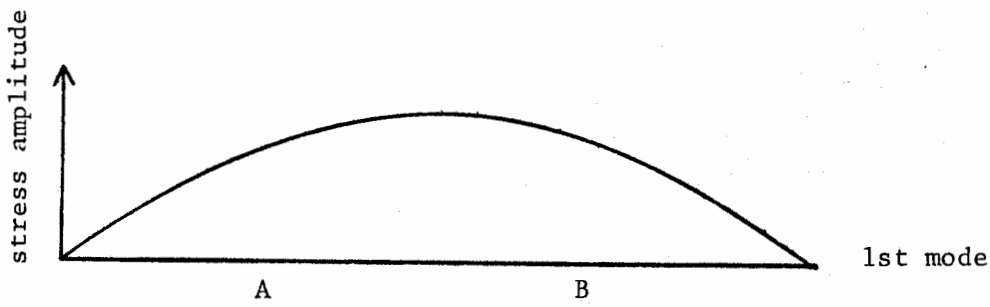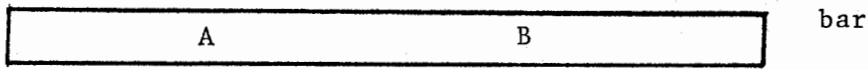
Fig. 1   Sketch of stress distribution in first three axial modes of
a free-free bar.
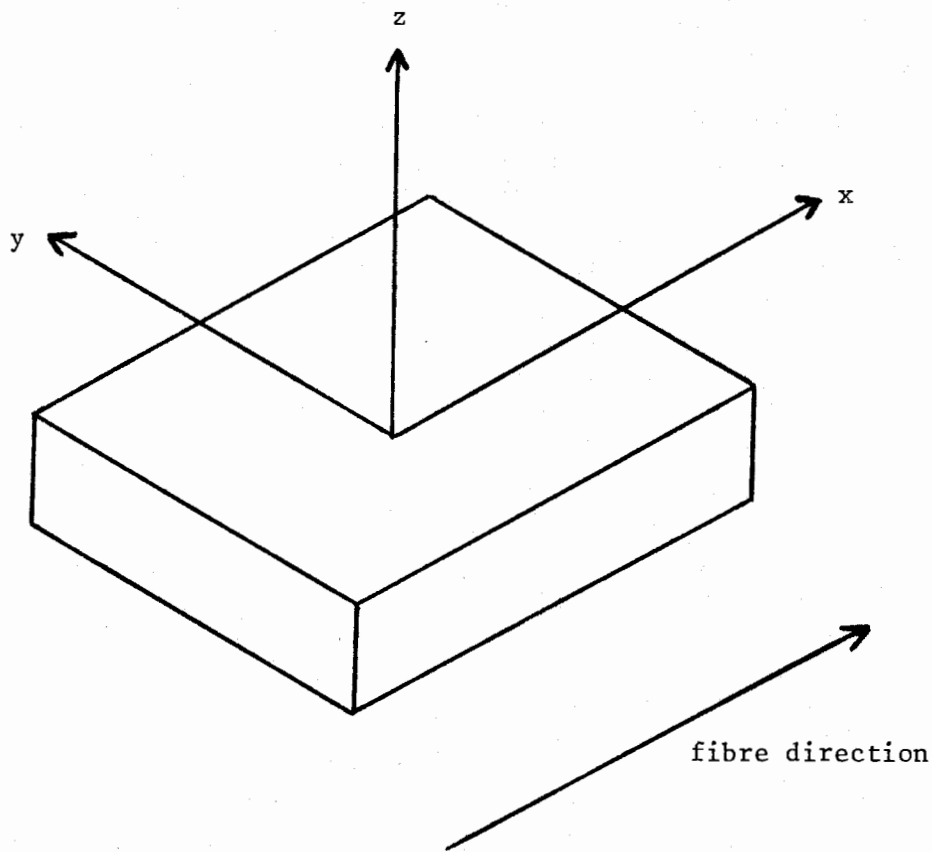
Fig. 2   Co-ordinate system for unidirectional fibre reinforced
         material.

21 mm square hole

2	2	2	2	1	1	1	1	2	2	2	2
4	4	6	5	5	5	5	5	5	6	4	4
11	10	21	19	10	7	7	10	19	21	10	11
19	24	100	74	13	2	2	13	74	100	24	19
13	15	14	13	5	2	2	5	13	14	15	13
2	2	2	2	1	1	1	1	2	2	2	2
2	2	2	2	1	1	1	1	2	2	2	2
13	15	14	13	5	2	2	5	13	14	15	13
19	24	100	74	13	2	2	13	74	100	24	19
11	10	21	19	10	7	7	10	19	21	10	11
4	4	6	5	5	5	5	5	5	6	4	4
2	2	2	2	1	1	1	1	2	2	2	2

fibre direction

— — — — — finite element mesh

——————— plate boundaries
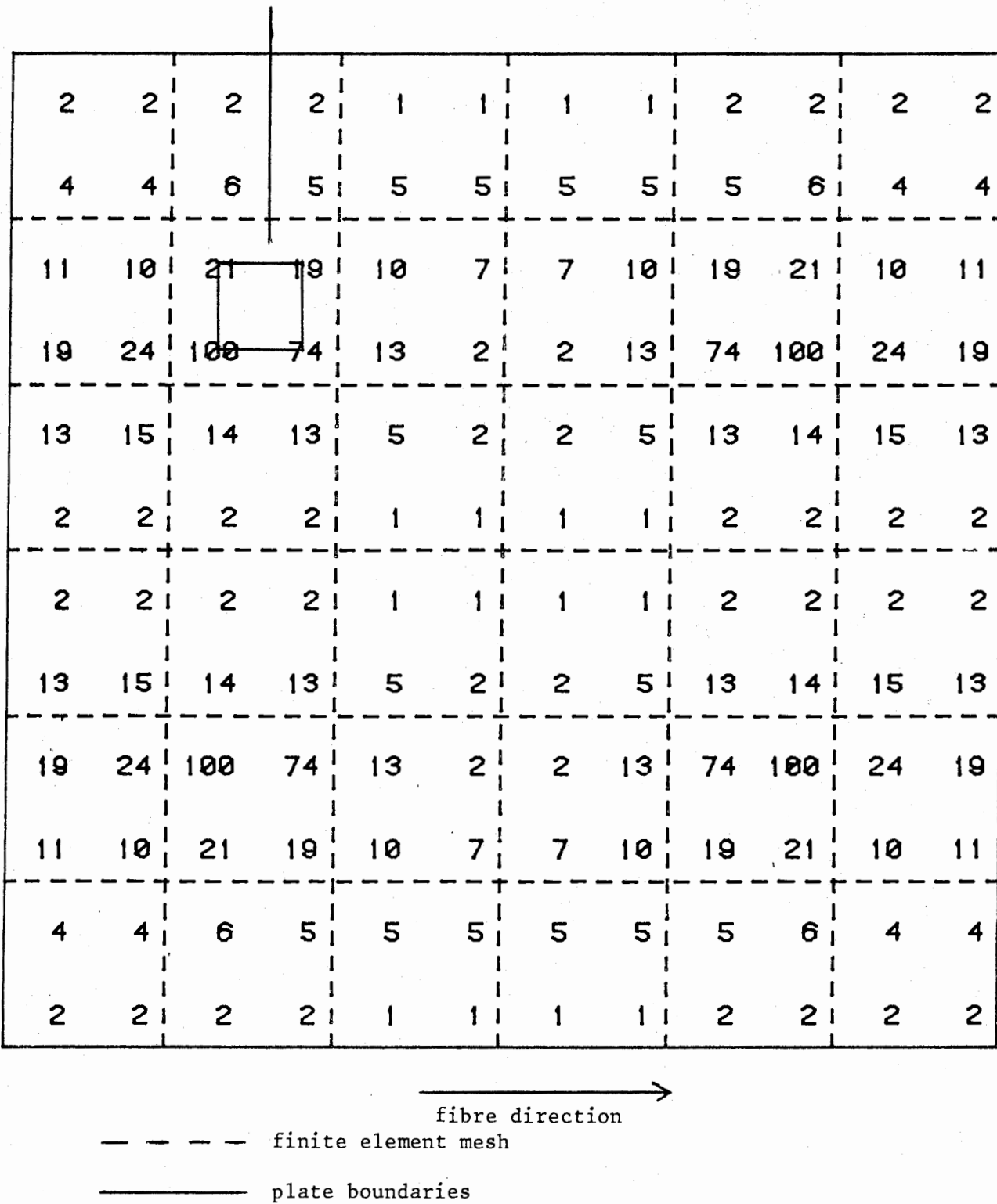
Fig. 3   Location chart for unidirectional CFRP plate with hole.
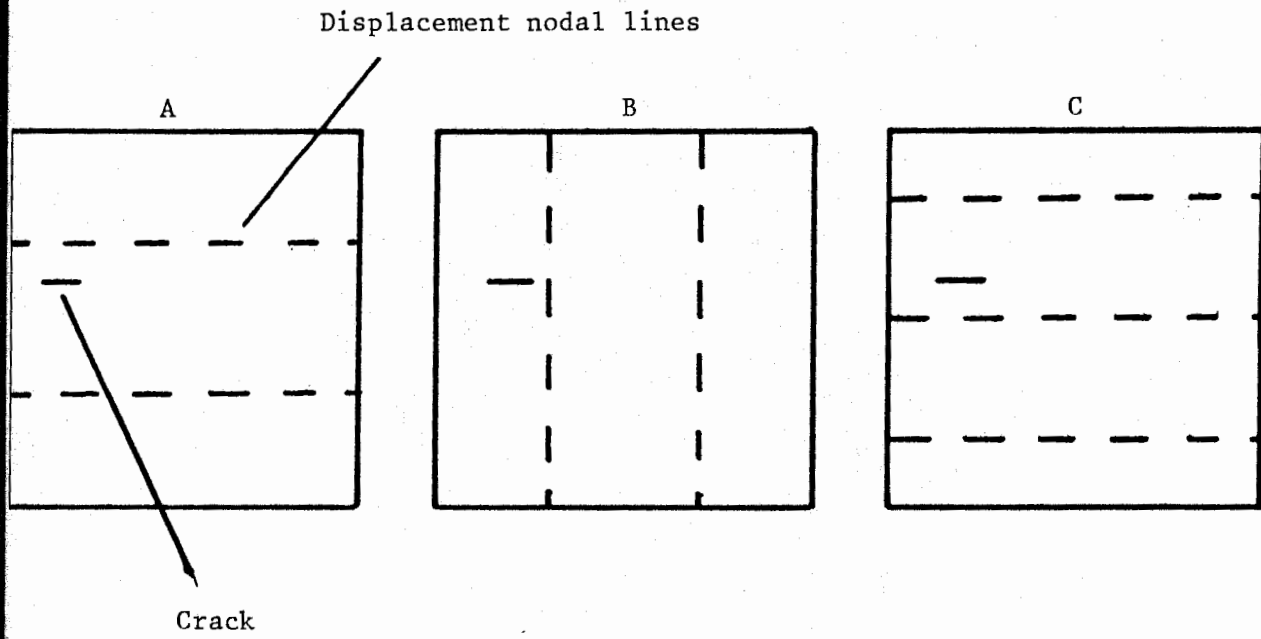
Fig. 4   Illustration of the problem of directional damage.
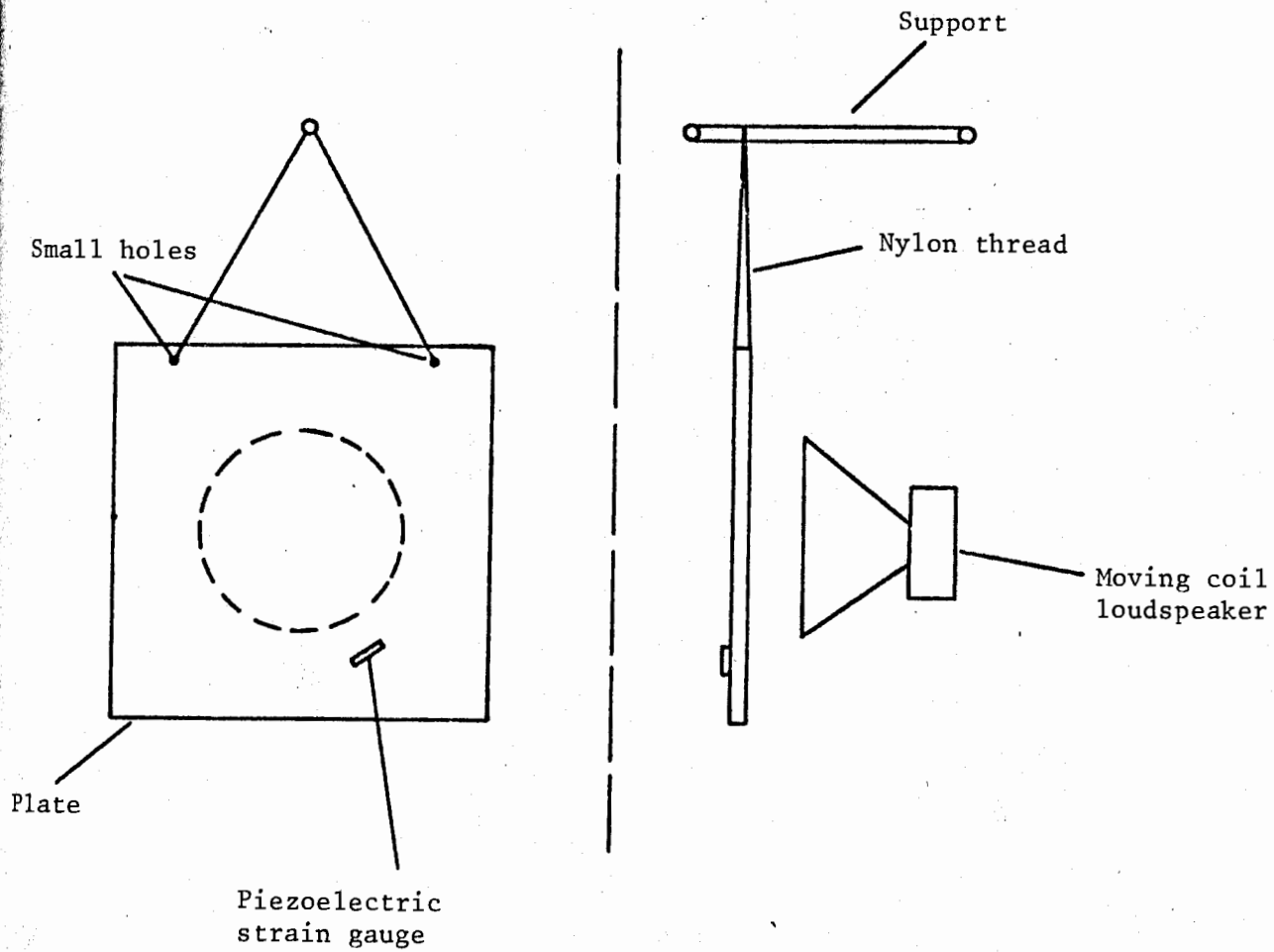
Fig. 5   Diagram of excitation system.
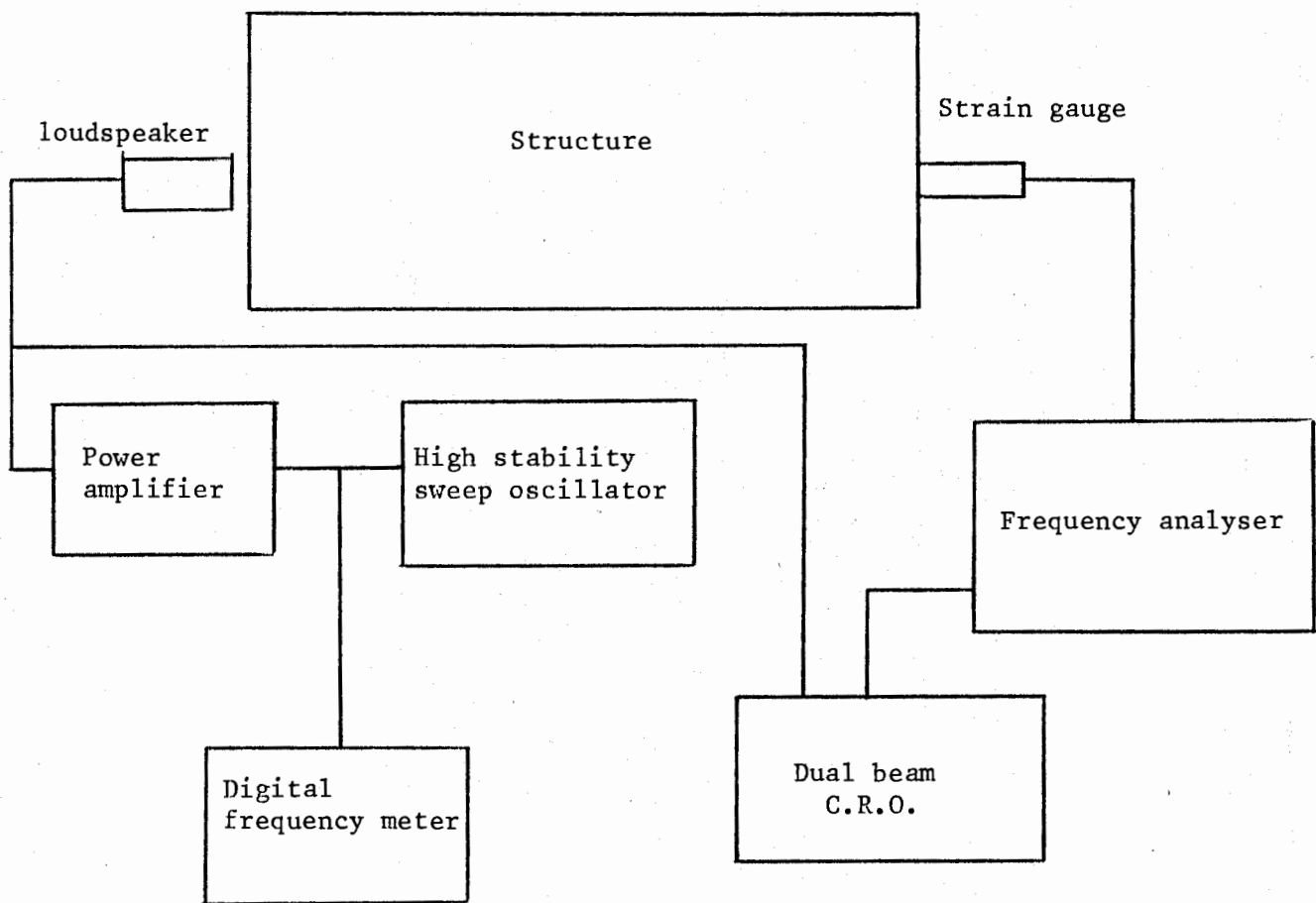
Fig. 6   Block diagram of electronic apparatus.
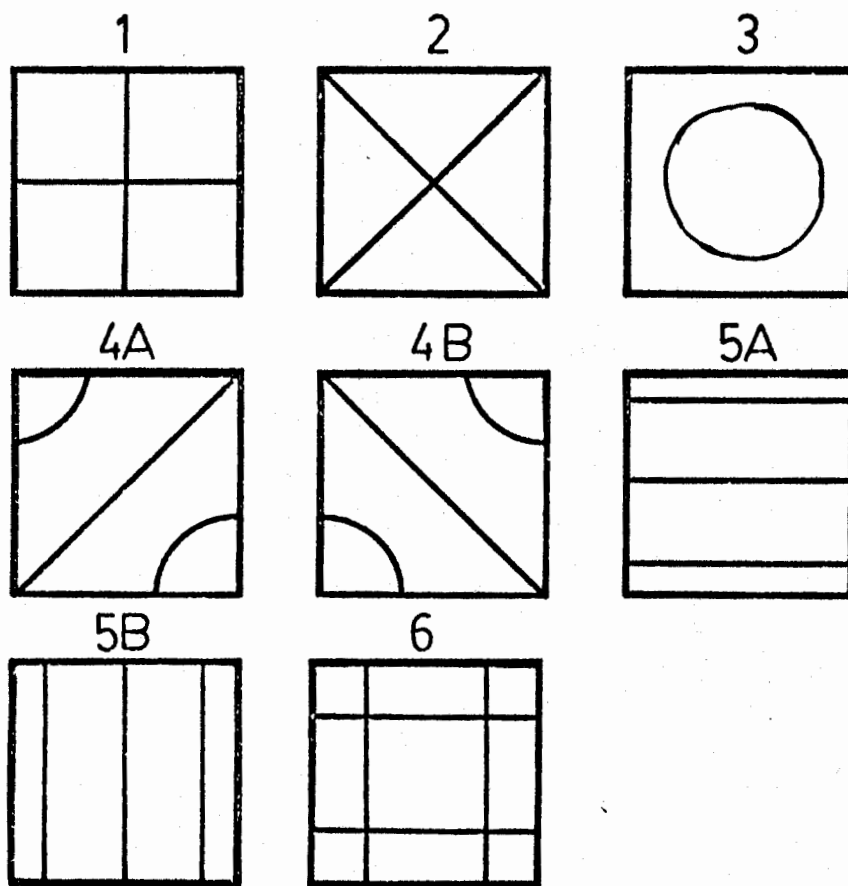
Fig. 7   Nodal patterns of Plate 1 (Aluminium).

1   2   3

4   5   6

Fibre direction
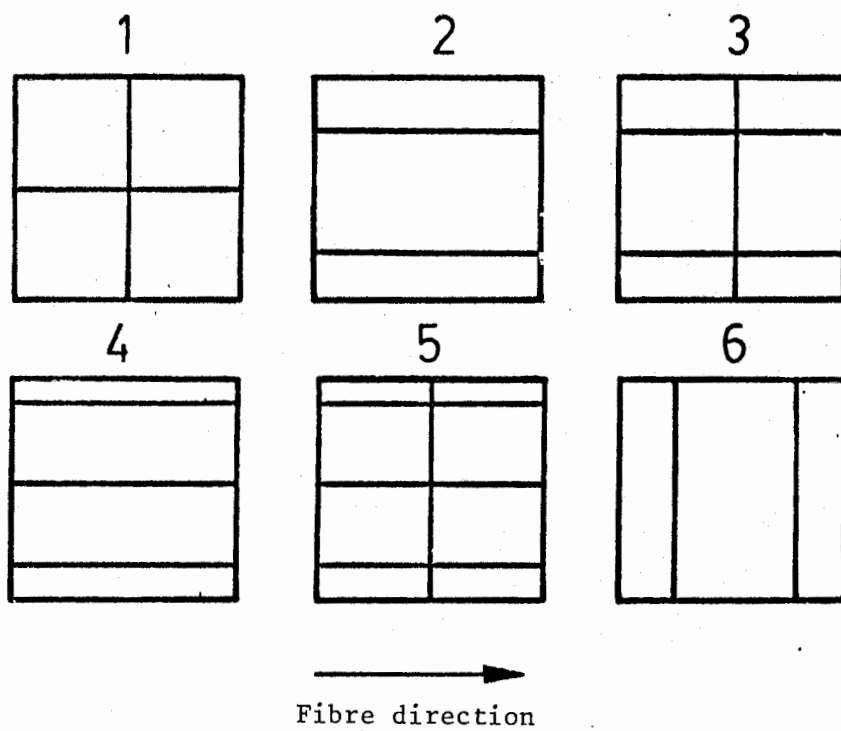
Fig. 8   Nodal patterns of Plate 2 (unidirectional CFRP).

Direction of outer fibres
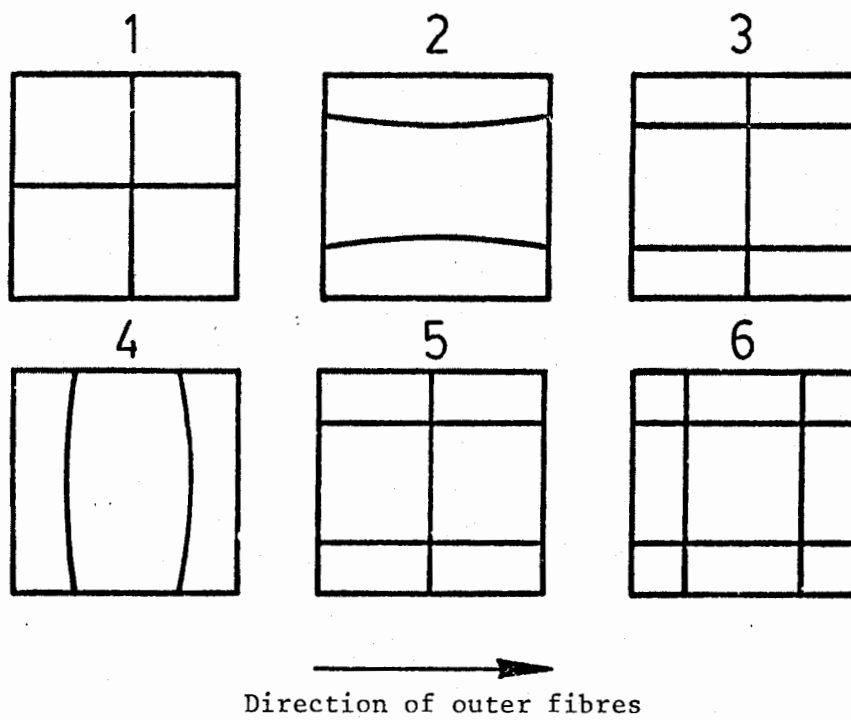
Fig. 9   Nodal patterns of Plate 3 `(0, 90° CFRP)
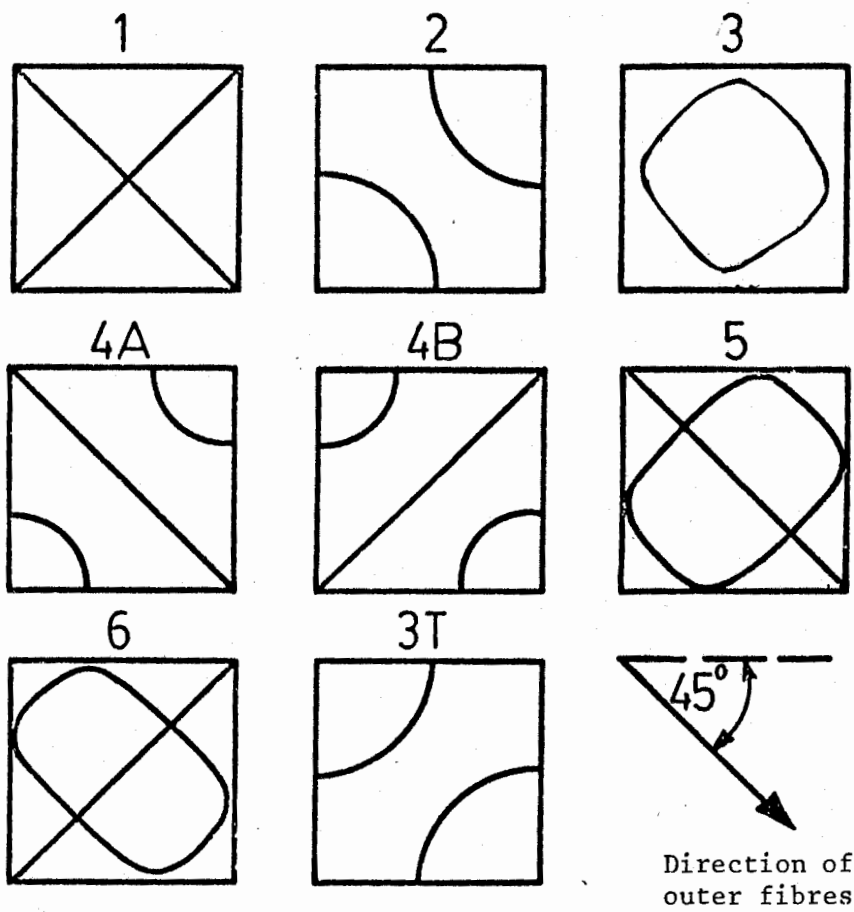
Fig. 10   Nodal patterns of Plate 4 (± 45° CFRP).

Direction of outer fibres
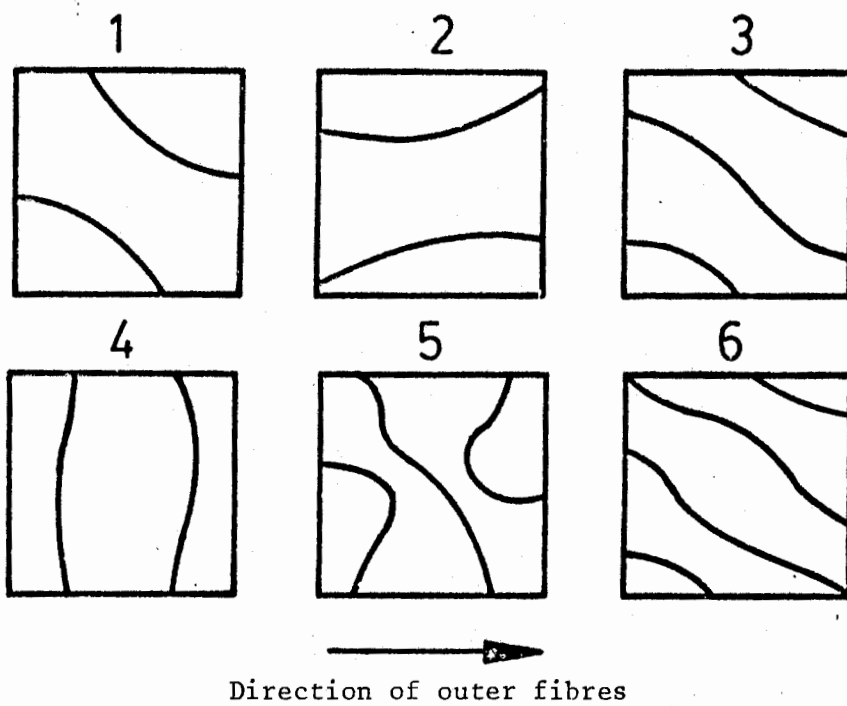
Fig. 11   Nodal patterns of Plate 5 (0,60,30,90,90,30,60,0$^{\mathrm{o}}$ CFRP).

Direction of outer fibres
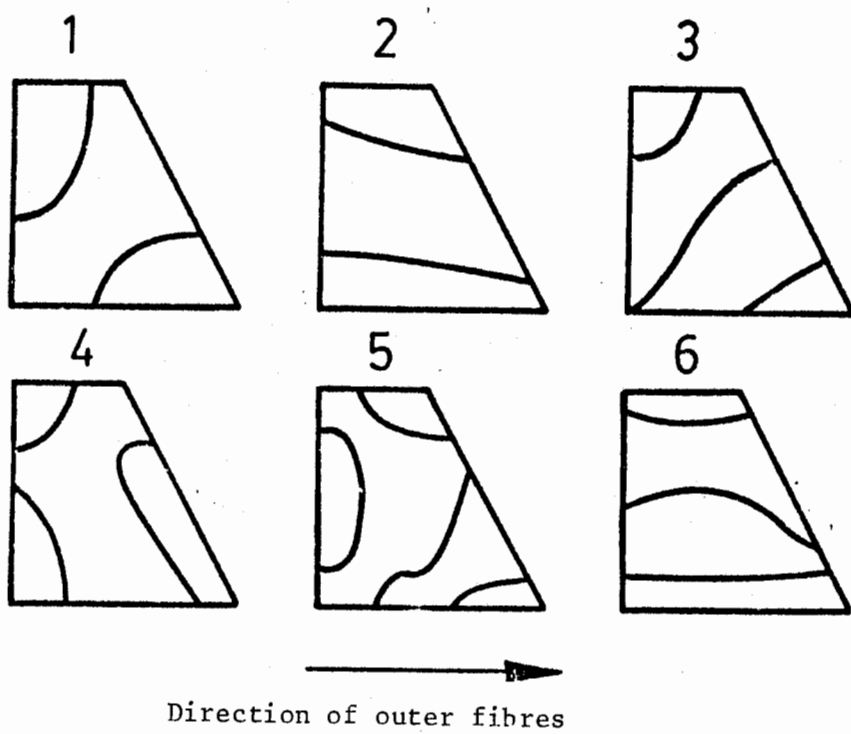
Fig. 12   Nodal patterns of Plate 3A (0, 90° CFRP).
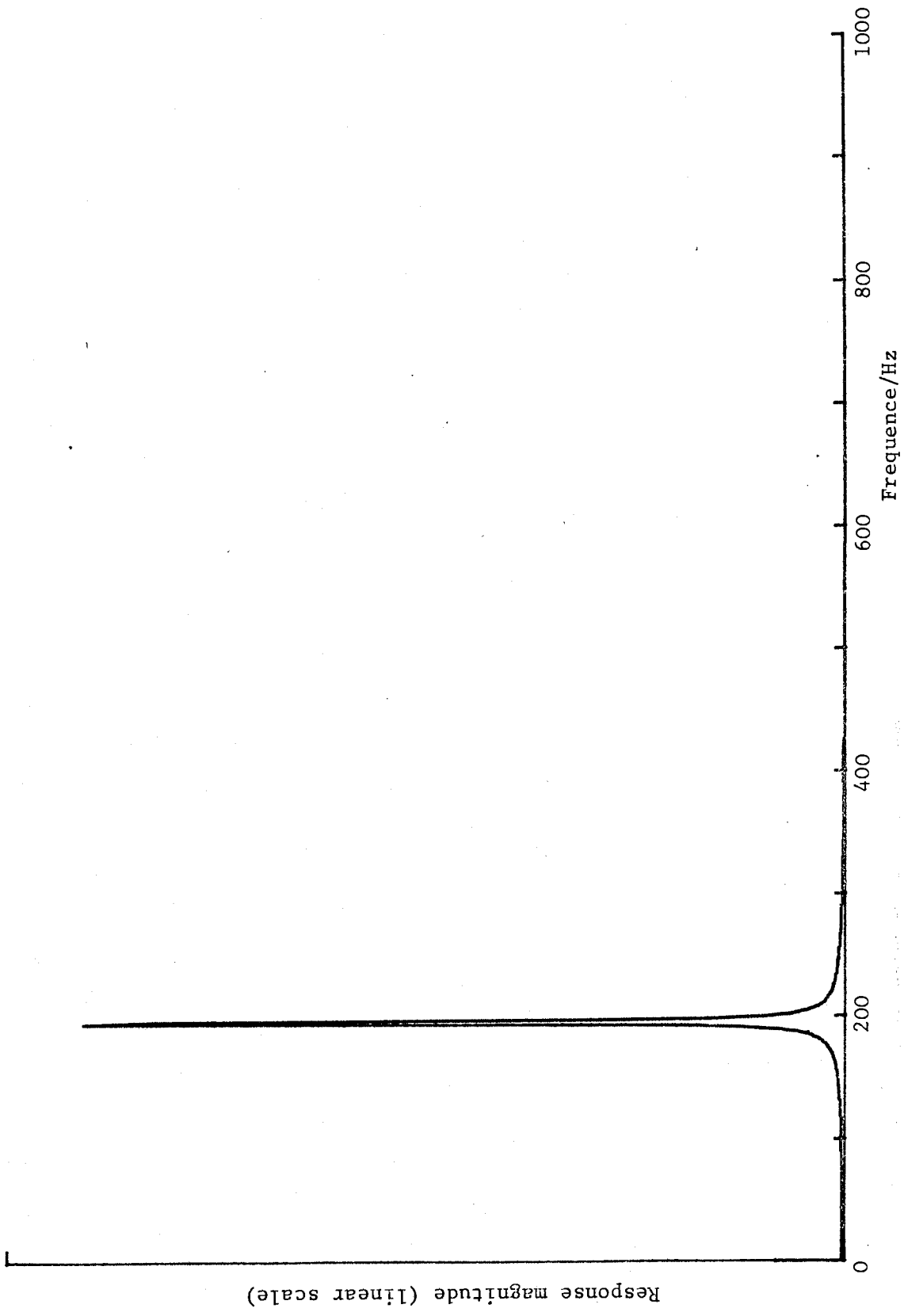
Fig. 13   The frequency response curve for a single frequency input at 195.80 Hz.

Time/Seconds

1.024

0

Force (linear scale)
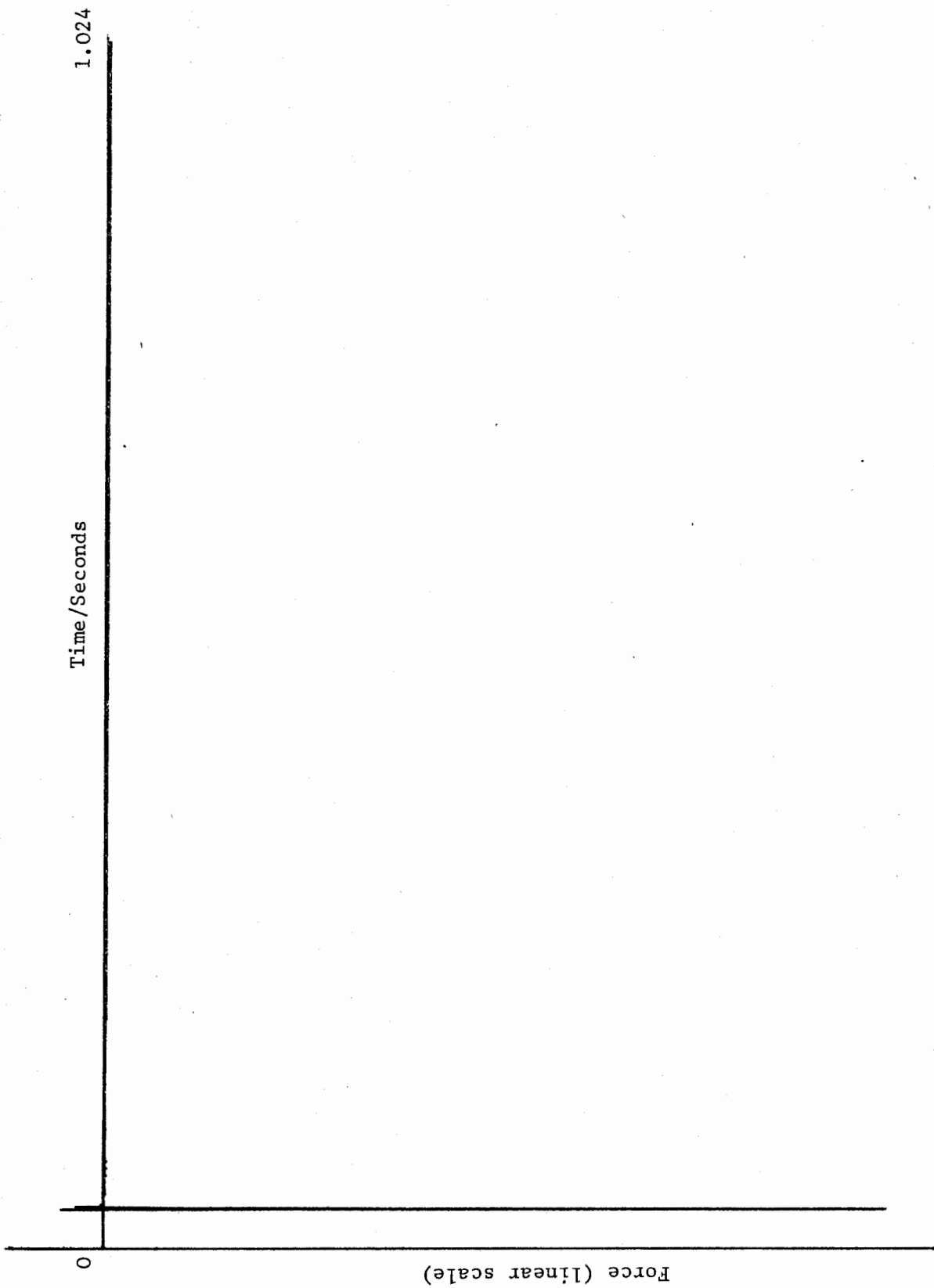
Fig. 14   Time record of force input from hammer on aluminium plate.

Force (linear scale)

Frequency/Hz

0   100   200   300   400   500
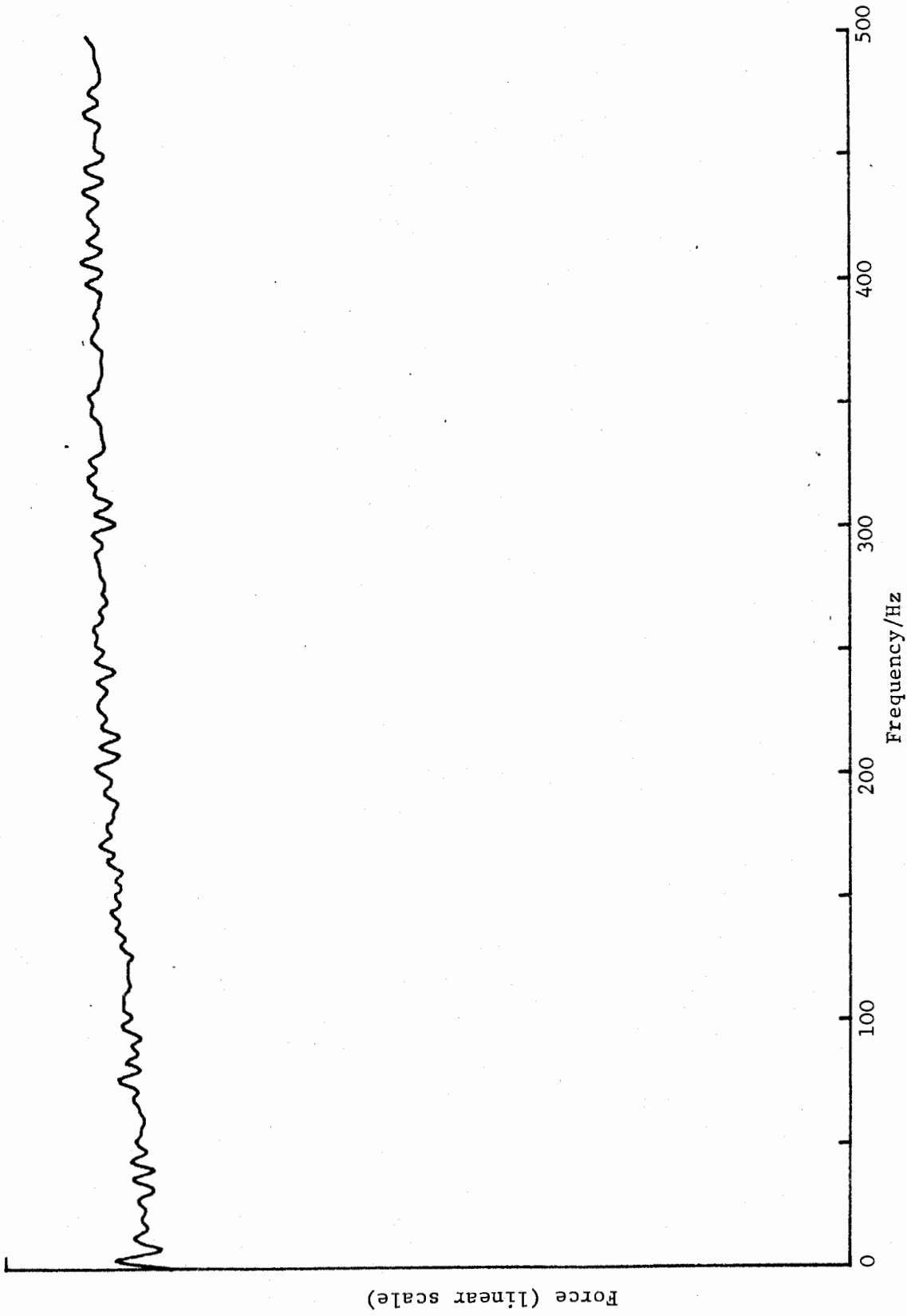
Fig. 15   The frequency content of the force input.
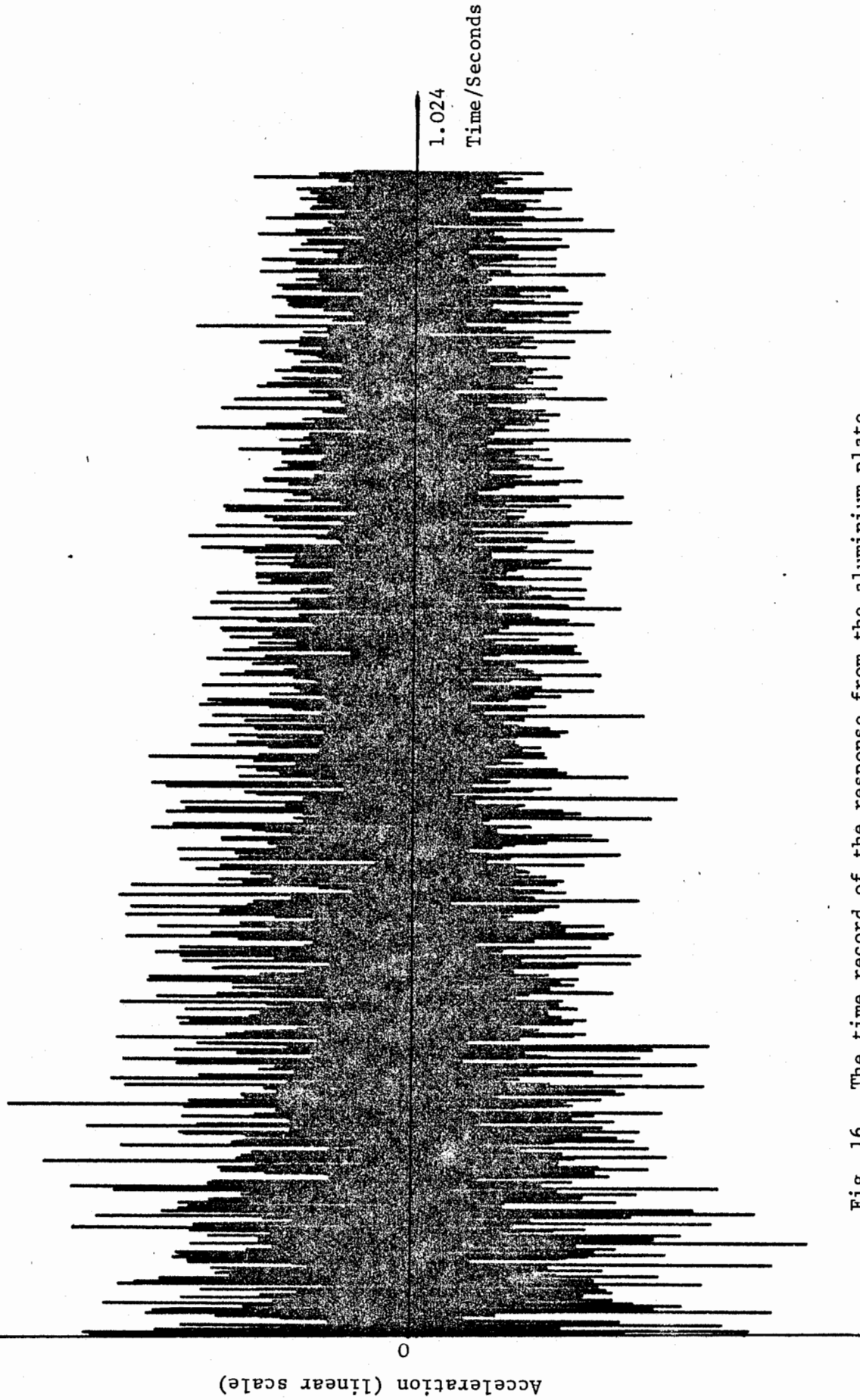
Fig. 16   The time record of the response from the aluminium plate.
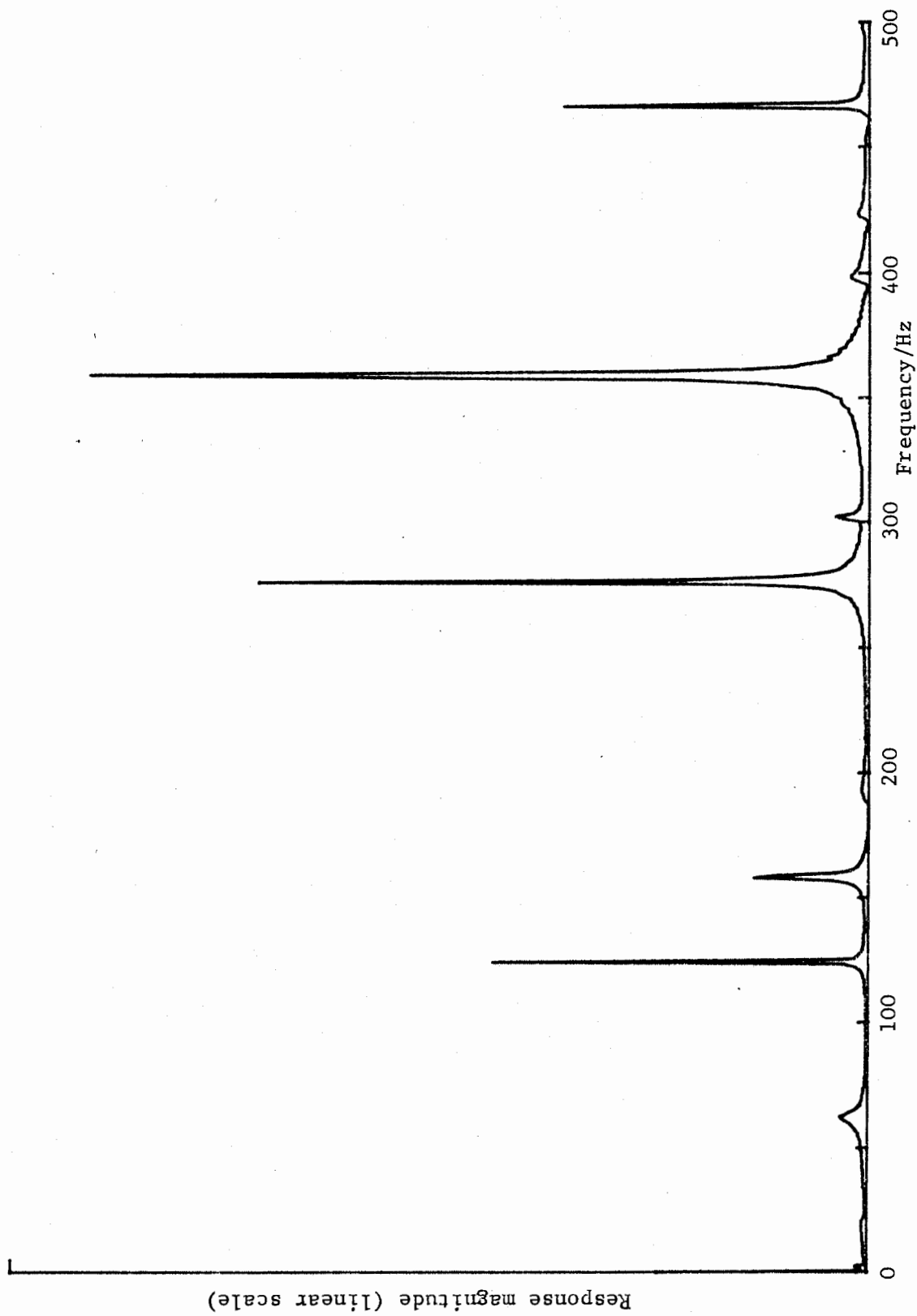
Fig. 17   The frequency response of the aluminium plate.

25 x 19 mm hole

2	2	2	3	3	3	3	3	3	2	2	2
1	2	4	5	6	6	6	6	5	4	2	1
2	2	4	4	20	19	19	20	4	4	2	2
2	2	4	5	57	100	100	57	5	4	2	2
2	2	4	4	10	4	4	10	4	4	2	2
2	2	4	4	11	3	3	11	4	4	2	2
2	2	4	4	11	3	3	11	4	4	2	2
2	2	4	4	10	4	4	10	4	4	2	2
2	2	4	5	57	100	100	57	5	4	2	2
2	2	4	4	20	19	19	20	4	4	2	2
1	2	4	5	6	6	6	6	5	4	2	1
2	2	2	3	3	3	3	3	3	2	2	2

_ _ _ _ _ _   finite element mesh

‾‾‾‾‾‾‾   plate boundaries

Fig. 18   Location chart for aluminium plate with hole.

17	15	7	4	2	2	2	2	4	7	15	17
20	21	15	11	12	10	10	12	11	15	21	20
11	10	15	15	37	36	36	37	15	15	10	11
11	12	16	16	25	9	9	25	16	16	12	11
26	51	100	39	21	7	7	21	39	100	51	26
15	30	38	18	11	8	8	11	18	38	30	15
15	30	38	18	11	8	8	11	18	38	30	15
26	51	100	39	21	7	7	21	39	100	51	26
11	12	16	16	25	9	9	25	16	16	12	11
11	10	15	15	37	36	36	37	15	15	10	11
20	21	15	11	12	10	10	12	11	15	21	20
17	15	7	4	2	2	2	2	4	7	15	17

saw cut

fibre direction →

Fig. 19   Location chart for unidirectional CFRP plate with saw cut.

8	9	8	5	3	3	3	3	5	8	9	8
6	9	14	11	10	9	9	10	11	14	9	6
11	18	18	15	13	10	10	13	15	18	18	11
11	27	33	28	28	26	26	28	28	33	27	11
11	61	100	48	26	15	15	26	48	100	61	11
6	12	21	26	21	12	12	21	26	21	12	6
6	12	21	26	21	12	12	21	26	21	12	6
11	61	100	48	26	15	15	26	48	100	61	11
11	27	33	28	28	26	26	28	28	33	27	11
11	18	18	15	13	10	10	13	15	18	18	11
6	9	14	11	10	9	9	10	11	14	9	6
8	9	8	5	3	3	3	3	5	8	9	8

saw cuts

fibre direction

Fig. 20   Location chart for unidirectional CFRP plate with two saw cuts.
Virgin frequencies taken as undamaged values.

16	14	15	10	8	7	7	8	10	15	14	16
13	19	22	15	12	11	11	12	15	22	19	13
17	36	31	21	9	6	6	9	21	31	36	17
10	27	33	29	16	6	6	16	29	33	27	10
8	23	29	66	38	15	15	38	66	29	23	8
10	18	31	100	57	22	22	57	100	31	18	10
10	18	31	100	57	22	22	57	100	31	18	10
8	23	29	66	38	15	15	38	66	29	23	8
10	27	33	29	16	6	6	16	29	33	27	10
17	36	31	21	9	6	6	9	21	31	36	17
13	19	22	15	12	11	11	12	15	22	19	13
16	14	15	10	8	7	7	8	10	15	14	16

fibre direction →

saw cuts

Fig. 21 Location chart for unidirectional CFRP plate with three saw cuts. Virgin frequencies taken as undamaged values.

saw cut

14	12	14	10	8	3	3	8	10	14	12	14
27	40	46	24	12	3	3	12	24	46	40	27
30	65	100	42	15	3	3	15	42	100	65	30
18	33	45	33	14	2	2	14	33	45	33	18
9	14	16	15	11	3	3	11	15	16	14	9
1	1	1	2	2	2	2	2	2	1	1	1
1	1	1	2	2	2	2	2	2	1	1	1
9	14	16	15	11	3	3	11	15	16	14	9
18	33	45	33	14	2	2	14	33	45	33	18
30	65	100	42	15	3	3	15	42	100	65	30
27	40	46	24	12	3	3	12	24	46	40	27
14	12	14	10	8	3	3	8	10	14	12	14

Fig. 22   Location chart for cross-ply CFRP plate with saw cut.

extended saw cut

23	18	19	12	8	2	2	8	12	19	18	23
33	100	74	28	12	2	2	12	28	74	100	33
26	68	84	43	14	2	2	14	43	84	68	26
21	47	51	31	12	1	1	12	31	51	47	21
11	17	17	15	9	2	2	9	15	17	17	11
1	1	1	2	2	1	1	2	2	1	1	1
1	1	1	2	2	1	1	2	2	1	1	1
11	17	17	15	9	2	2	9	15	17	17	11
21	47	51	31	12	1	1	12	31	51	47	21
26	68	84	43	14	2	2	14	43	84	68	26
33	100	74	28	12	2	2	12	28	74	100	33
23	18	19	12	8	2	2	8	12	19	18	23

Fig. 23   Location chart for cross-ply CFRP plate with extended saw cut.

Fig. 24   Location chart for cross-ply, trapezoidal CFRP plate
           with saw cut.

saw cuts

Fig. 25   Location chart for cross-ply, trapezoidal CFRP plate with
two saw cuts.   Virgin frequencies taken as undamaged values.
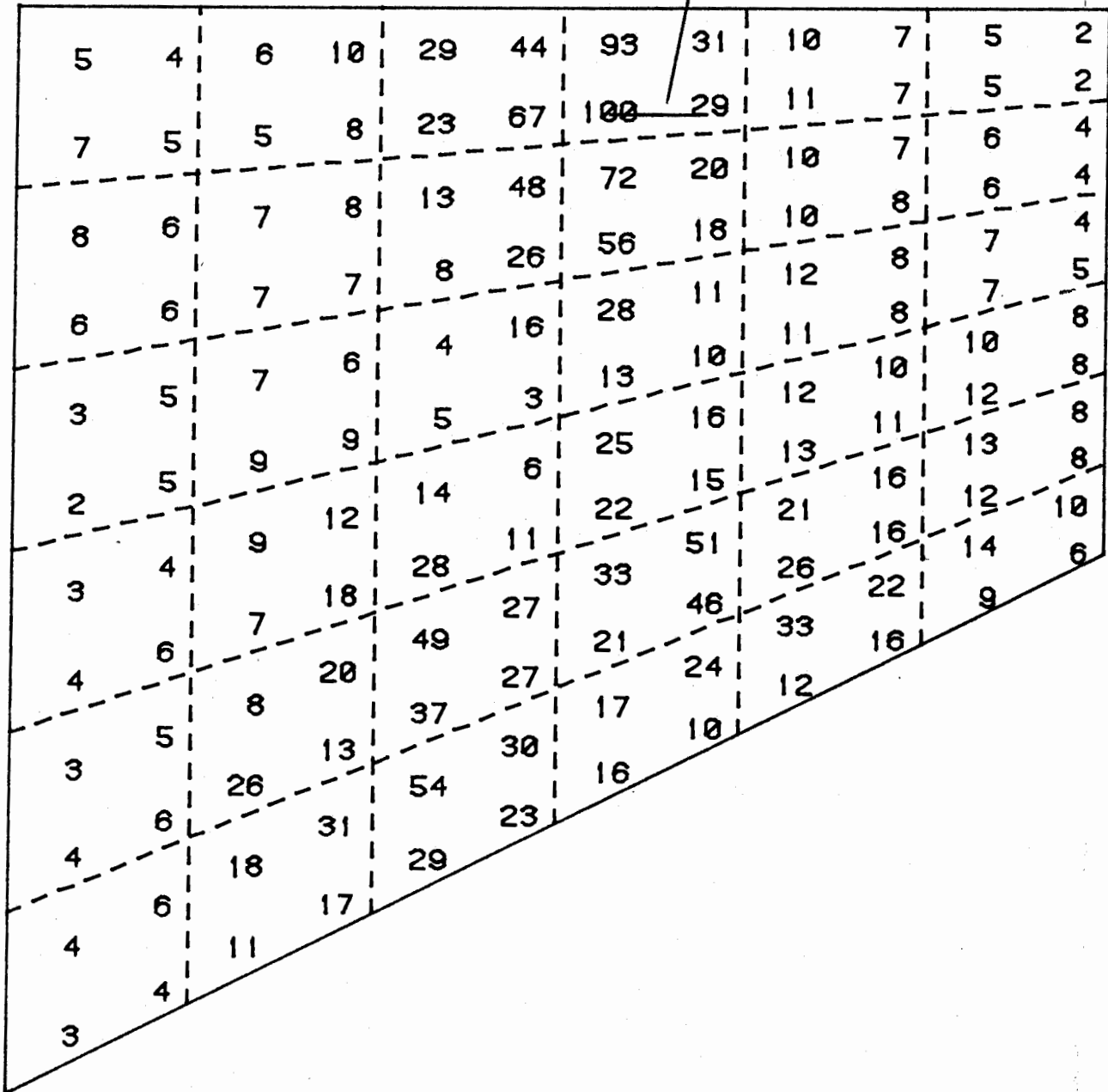
2nd saw cut

1st saw cut

```
 1    2 |  4    6 | 13   51 |100/  20 |  8    5 |  6    2
                                                    5    1
 1    2 |  3    8 | 23   56 | 79  36 | 14    7 |  8    3
                            35   31 | 31   13 |  7    3
 1    2 |  3    7 | 26   43 | 16   11 | 14    7 |  4    2
                        9   15 |              3 |  4    2
 1    2 |  3    4 |    2    5 |  8    4 |  5    3 |  5    3
                    3       5 |      3 |  3    4 |  6    4
 2    2 |  4    3 |  2    1 |  5    5 |  4    4 |  9    5
              5 |          4 |  6      |  4   10 | 14    6
 2    3 |  7      |  4      |  7    4 |  8   13 | 13    6
          8 |  6 |  7 |      10 |  11 |      15 |  8    4
 2    4 |  8    7 |  7      | 17   15 |  20   12
 2    3 |  4      | 12   17 | 17   21 | 12
          3 |  8 | 20   23 | 22   12
 1    2 |    7 | 22   23
 1    2 |  5   11 | 19
          7 |
 1    2 |  4      7
 1    2 |  4
 1      |  2
    1 |
 1
```

Fig. 26   Location chart for trapezoidal cross-ply CFRP plate with
two saw cuts.   Frequencies after first cut taken as
undamaged values.
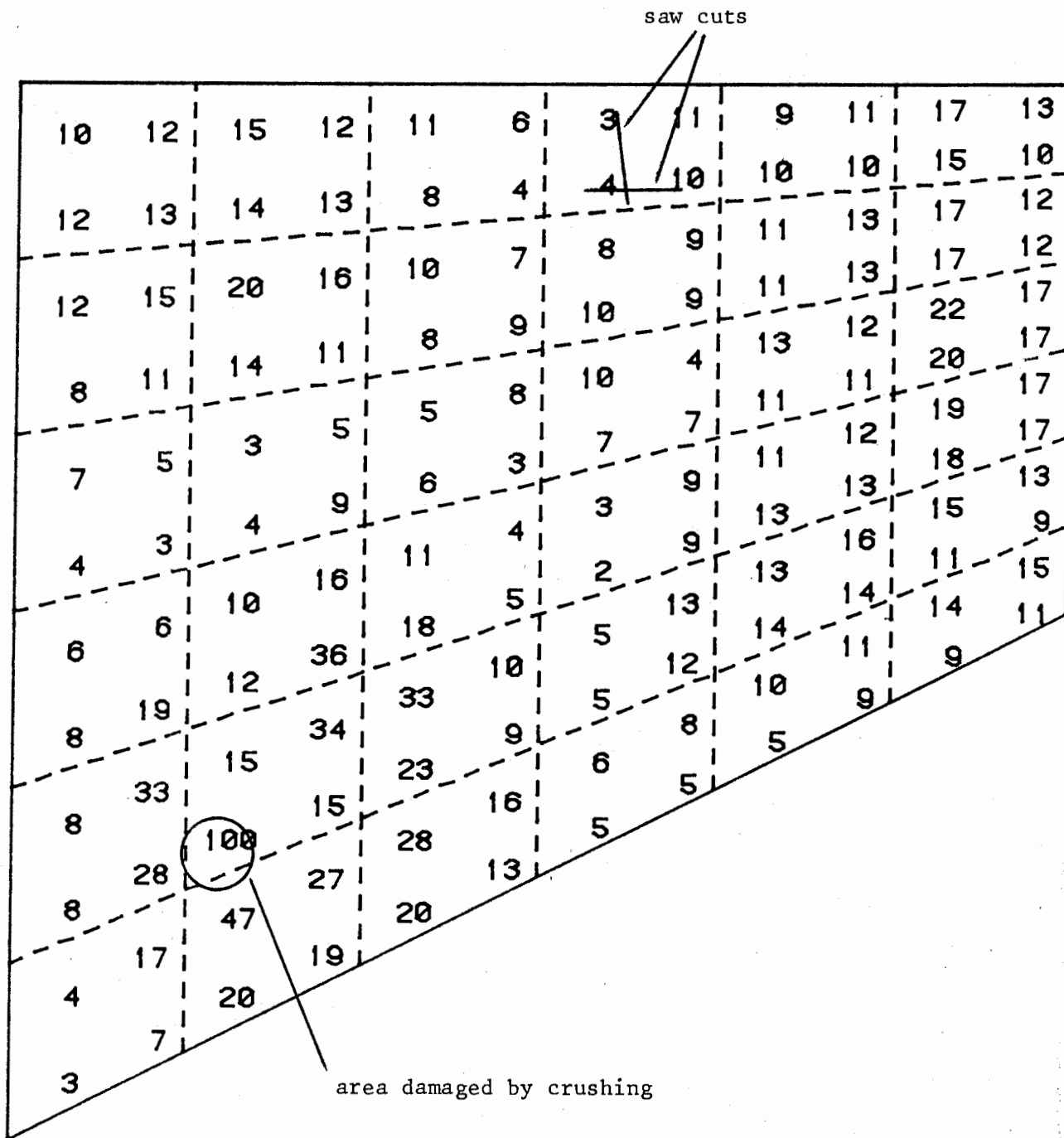
Fig. 27   Location chart for trapezoidal, cross-ply CFRP plate with
           saw cuts and crush damage.   Frequencies after saw cuts taken
           as undamaged values.

area damaged by crushing

14	15	21	28	21	5	5	21	28	21	15	14
15	13	32	43	32	3	3	32	43	32	13	15
21	32	100	71	34	2	2	34	71	100	32	21
28	43	71	67	16	4	4	16	67	71	43	28
22	32	34	16	1	16	16	1	16	34	32	22
5	3	2	4	16	7	7	16	4	2	3	5
5	3	2	4	16	7	7	16	4	2	3	5
22	32	34	16	1	16	16	1	16	34	32	22
28	43	71	67	16	4	4	16	67	71	43	28
21	32	100	71	34	2	2	34	71	100	32	21
15	13	32	43	32	3	3	32	43	32	13	15
14	15	21	28	21	5	5	21	28	21	15	14

Fig. 28   Location chart for ± 45° CFRP plate with crush damage.

48	79	43	16	9	7	9	16	30	44	21	18
38	69	67	A 33	27	9	8	35	100 B	54	34	20
13	23	39	41	13	12	7	10	55	76	75	33
17	8	15	24	30	17	10	28	33	24	25	19
14	21	11	7	10	14	15	31	25	13	6	3
16	26	33	11	6	13	20	13	9	10	12	10
10	12	10	9	13	20	13	6	11	33	26	16
3	6	13	25	31	15	14	10	7	11	21	14
19	25	24	33	28	10	17	30	24	15	8	17
33	75	76	55	10	7	12	13	41	39	23	13
20	34	54 B	100	35	8	9	27	A 33	67	69	38
18	21	44	30	16	9	7	9	16	43	79	48

area of blister

Fig. 29   Location chart for $0,60,30,90,90,60,30,0^{\circ}$ CFRP plate damaged by local heating.

| 1	2	3	3	5	4	2	3	5	8	13	7
2	2	3	4	7	9	3	4	7	16	15	7
3	6	6	7	13	11	4	4	5	13	13	7
3	9	11	10	18	10	4	3	6	11	8	5
4	15	22	9	8	4	3	4	7	7	8	3
5	28	36	9	3	1	2	4	7	6	6	3
8	74	82	11	2	1	5	8	12	8	4	2
19	100	43	12	3	3	7	12	14	9	3	2
29	70	19	8	7	11	14	19	11	6	3	1
42	34	12	11	15	13	15	21	11	8	3	1
19	15	11	12	13	10	6	12	9	7	4	2
12	12	11	15	15	8	2	10	8	10	7	3

area of damage indicated by C-scan

Fig. 30   Location chart for trapezoidal 0,60,30,90,90,30,60,0^o CFRP plate damaged by impact.

area damaged by crushing

3	8	13	13	11	2	2	11	13	13	8	3
3	8	28	36	19	3	3	19	36	28	8	3
7	18	100	53	24	2	2	24	53	100	18	7
5	13	31	33	24	4	4	24	33	31	13	5
2	9	10	9	9	5	5	9	9	10	9	2
2	7	4	2	2	4	4	2	2	4	7	2
2	7	4	2	2	4	4	2	2	4	7	2
2	9	10	9	9	5	5	9	9	10	9	2
5	13	31	33	24	4	4	24	33	31	13	5
7	18	100	53	24	2	2	24	53	100	18	7
3	8	28	36	19	3	3	19	36	28	8	3
3	8	13	13	11	2	2	11	13	13	8	3

Fig. 31   Location chart for sandwich panel with crush damage.
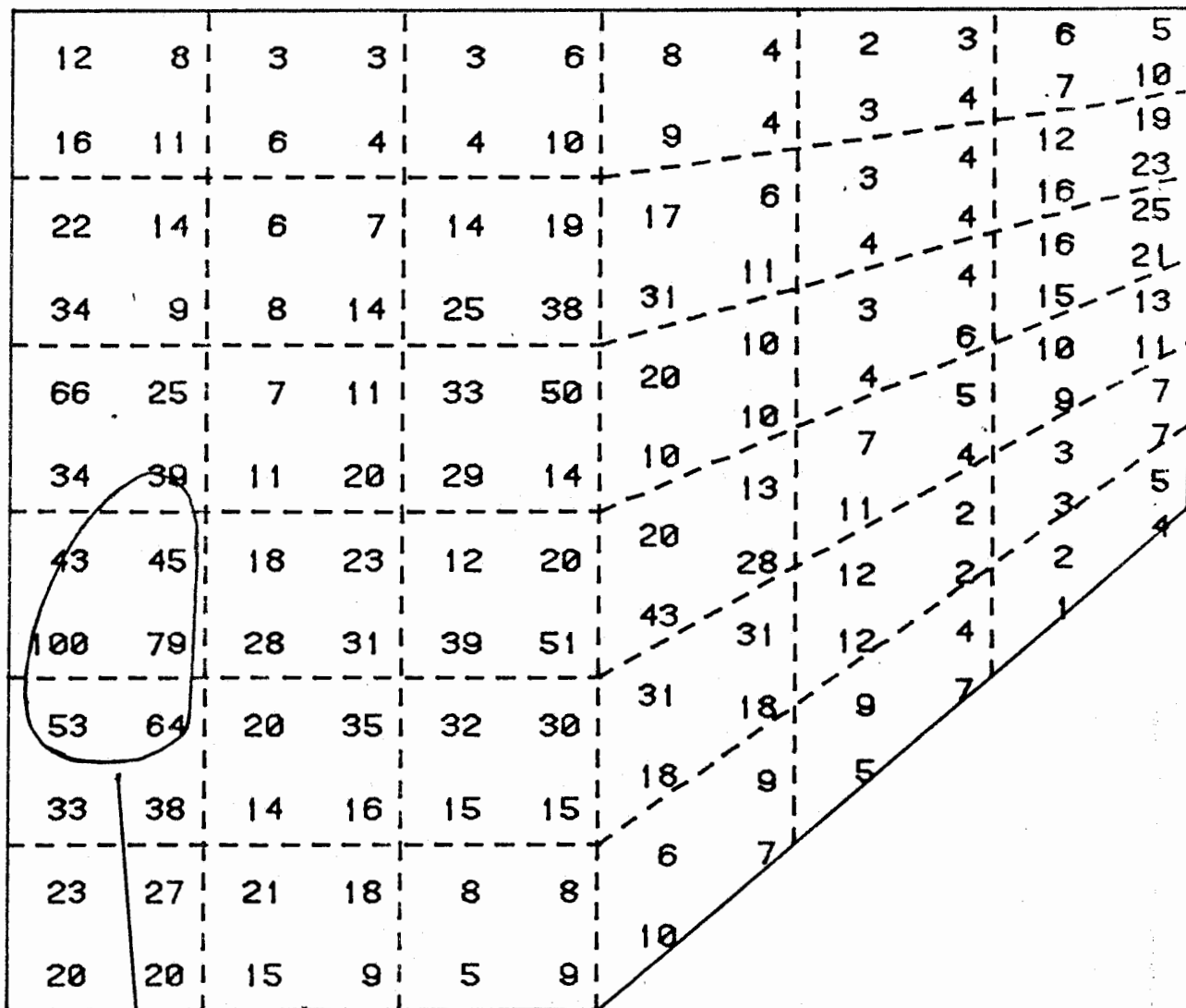
area of blister

Fig. 32   Location chart for sandwich panel damaged by local heating.

damaged area

8	5	6	7	4	2	3	6	5	6	6	7
7	7	8	14	12	3	3	13	15	7	8	10
11	12	11	28	12	3	8	14	30	7	13	12
10	13	13	50 O 80		3	7	100^B	14	8	14	9
9	13	9	14	27	3	5	45	10	10	13	8
8	13	7	6	12	2	3	21	6	9	13	6
6	13	9	6	21	3	2	12	6	7	13	8
8	13	10	10	45	5	3	27	14	9	13	9
9	14	8	14 $_B$100		7	3	80$_A$	50	13	13	10
12	13	7	30	14	8	3	12	28	11	12	11
10	8	7	15	13	3	3	12	14	8	7	7
7	6	6	5	6	3	2	4	7	6	5	8

Fig. 33   Location chart for sandwich panel with CFRP edge inserts damaged on one face by crushing.

damaged area

3	2	3	2	1	1	2	2	2	3	3	2
2	3	4	5	3	1	2	4	6	3	3	2
3	5	6	7	3	1	3	4	17	4	5	3
2	6	7	100	9	1	2	17	7	4	6	2
2	6	5	8	6	1	1	10	4	6	5	2
2	6	4	3	3	1	1	6	3	5	5	2
2	5	5	3	6	1	1	3	3	4	6	2
2	5	6	4	10	1	1	6	8	5	6	2
2	6	4	7	17	2	1	9	100	7	6	2
3	5	4	17	4	3	1	3	7	6	5	3
2	3	3	6	4	2	1	3	5	4	3	2
2	3	3	2	2	2	1	1	2	3	2	3

Fig. 34   Location chart for sandwich panel with CFRP edge inserts damaged on both faces by crushing.

saw cuts

area damaged by crushing

Fig. 35   Location chart for trapezoidal, cross-ply CFRP plate with
saw cut and crush damage.   Virgin frequencies taken as
undamaged values.
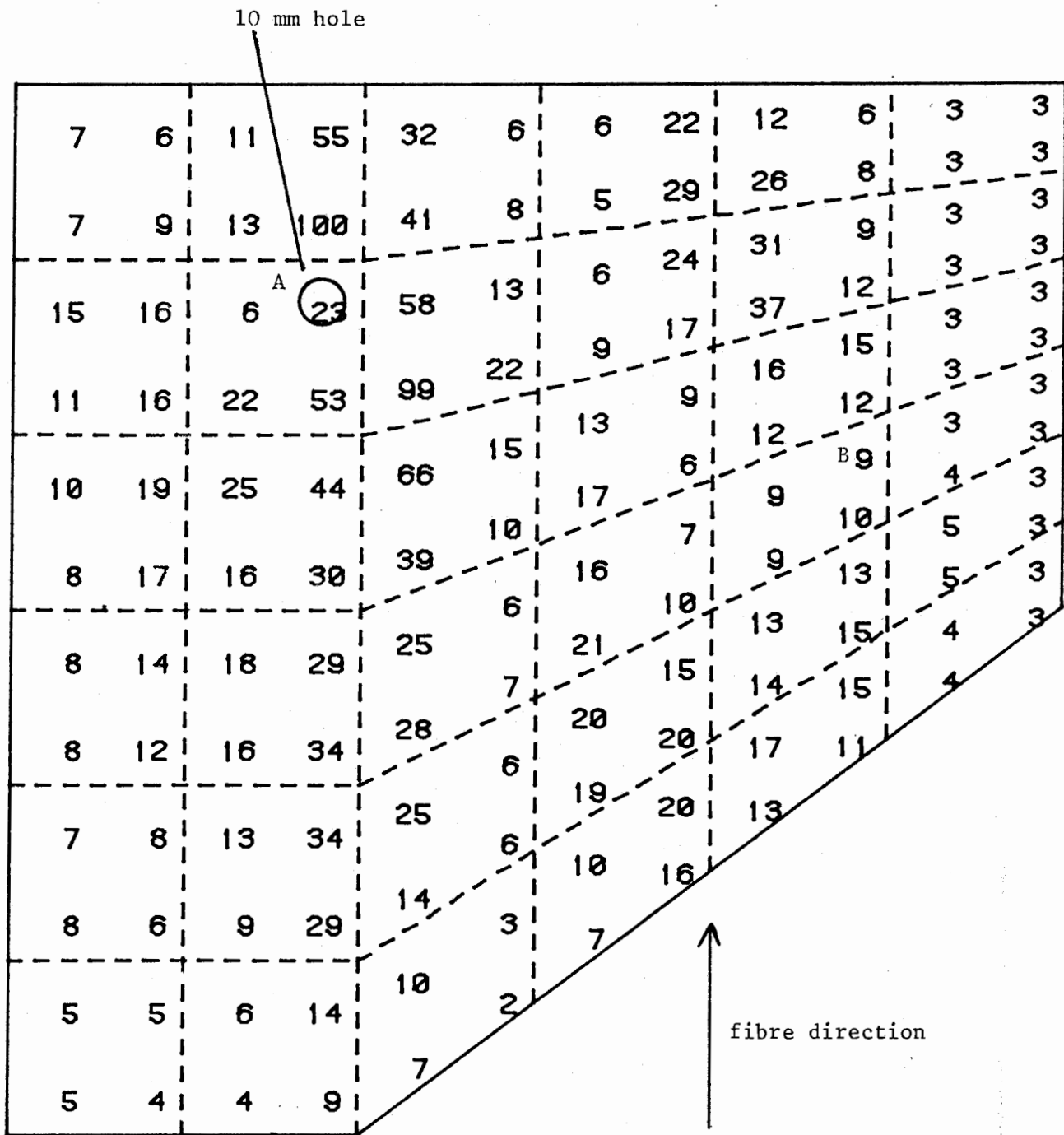
Fig. 36   Location chart for unidirectional CFRP plate with 10 mm hole
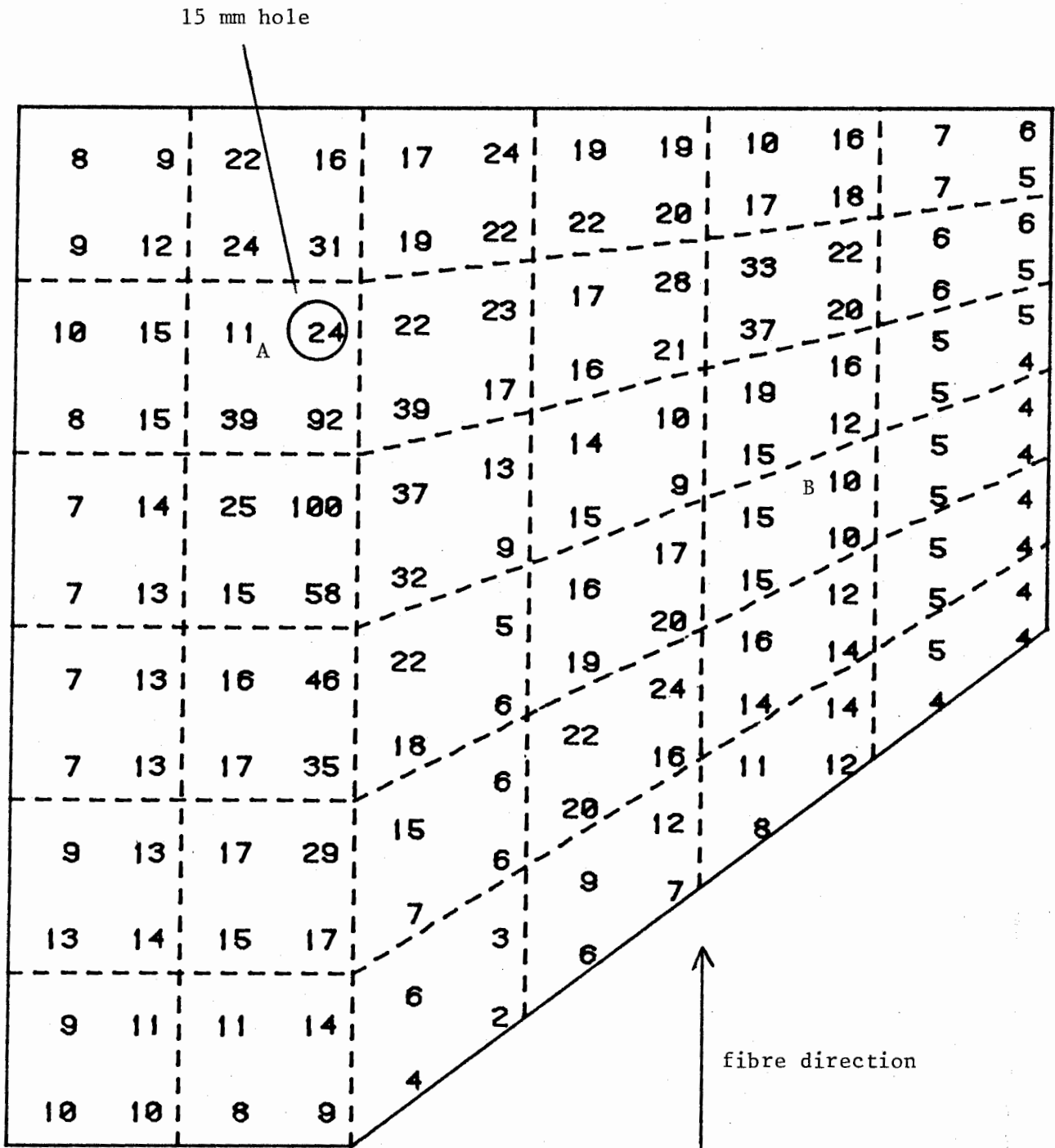   at site A.

Fig. 37   Location chart for unidirectional CFRP plate with 15 mm hole
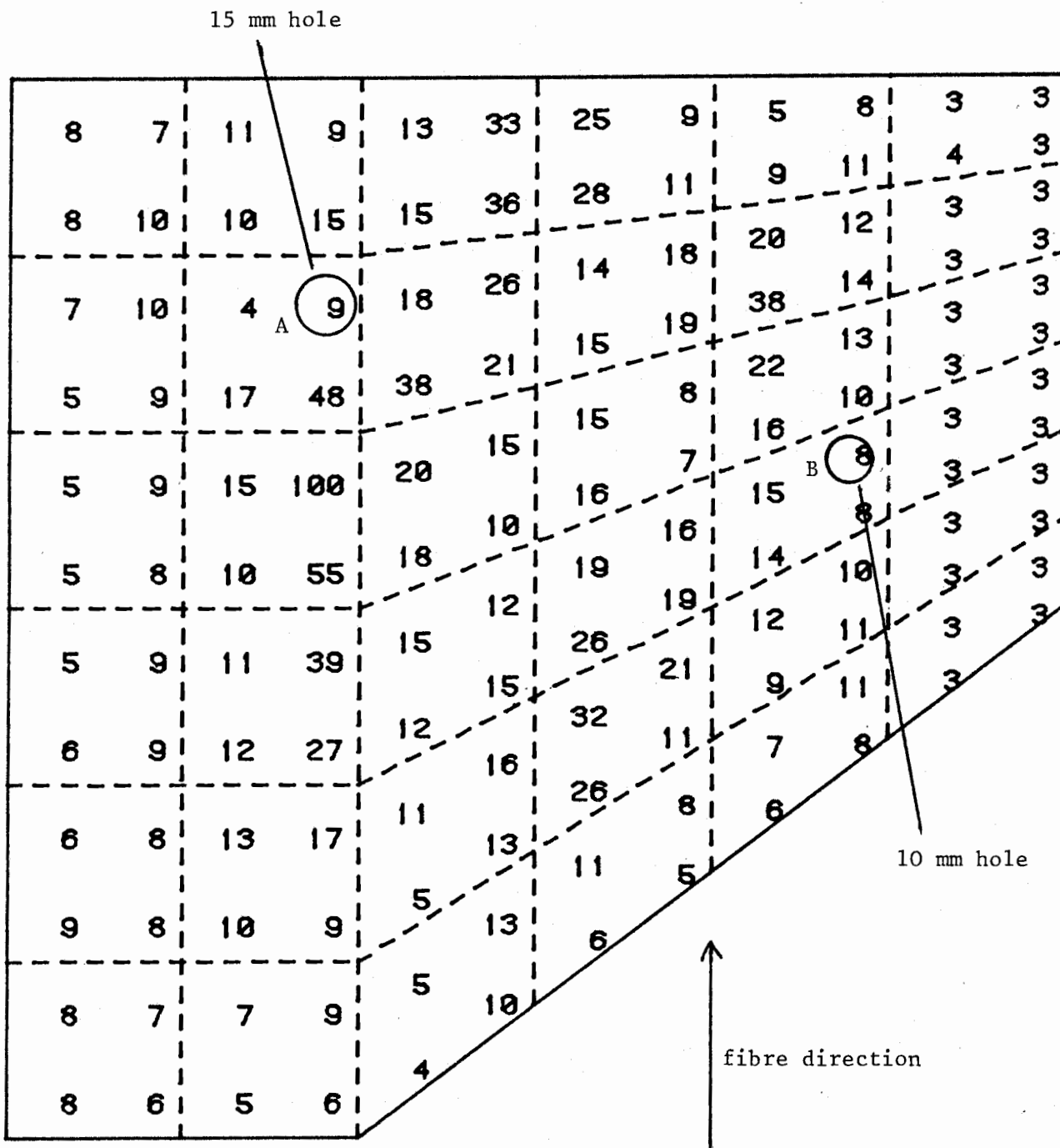   at site A.

Fig. 38   Location chart for unidirectional CFRP plate with 15 mm hole
           at site A and 10 mm hole at B.   Virgin frequencies taken as
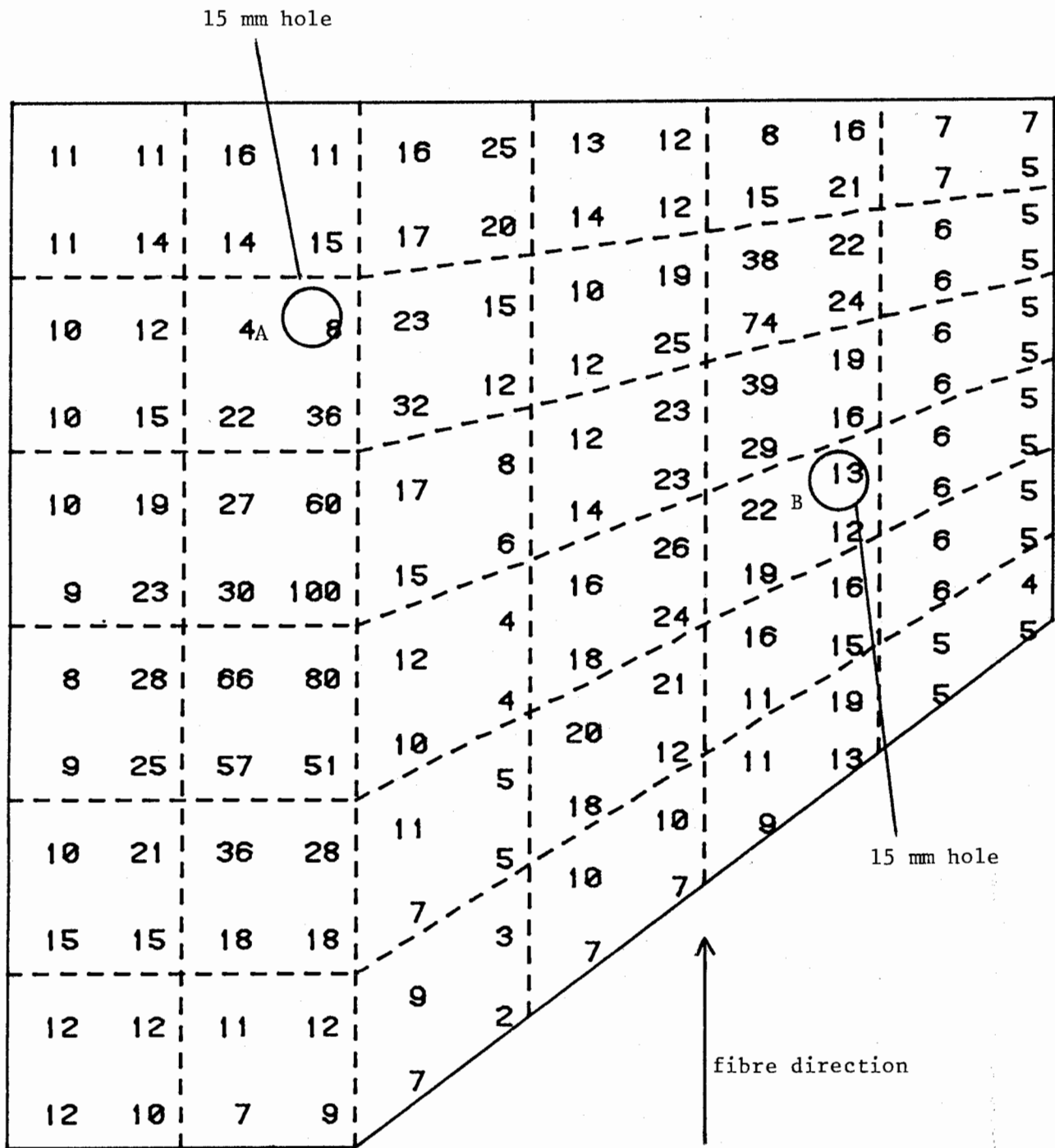   undamaged values.

15 mm hole

15 mm hole

fibre direction

Fig. 39   Location chart for unidirectional CFRP plate with 15 mm
holes at sites A and B.   Virgin frequencies taken as
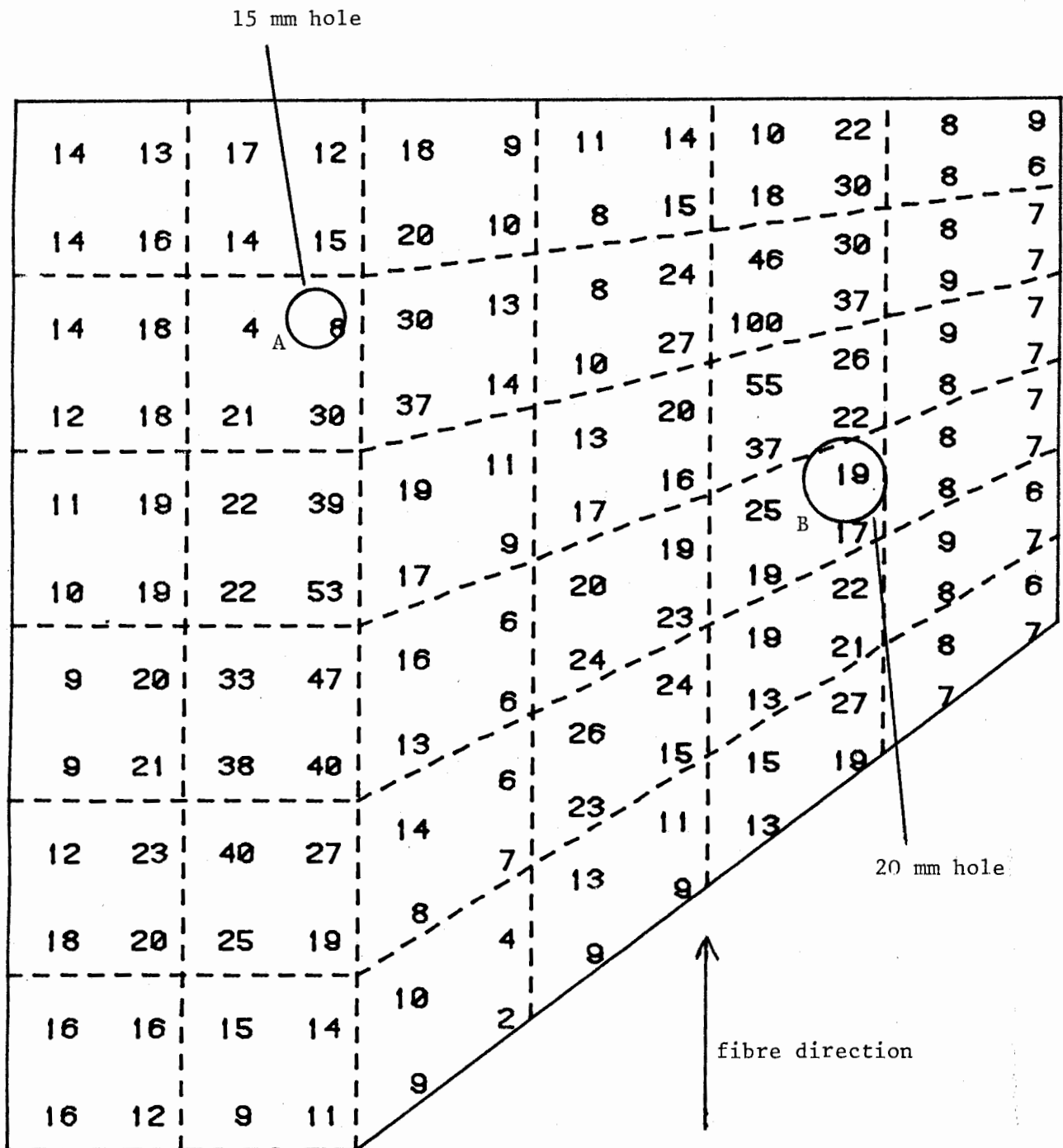undamaged values.

Fig. 40   Location chart for unidirectional CFRP plate with 15 mm
           hole at site A and 20 mm hole at B.   Virgin frequencies
           taken as undamaged values.